MODELLING OF SOME BIOLOGICAL PHENOMENA VIA FRACTIONAL DIFFERENTIAL EQUATIONS

Abhijit Shit

Department of Mathematics
Indian Institute of Technology Guwahati
Guwahati - 781 039, India

January 2025

Modelling of Some Biological Phenomena via Fractional Differential Equations

A thesis submitted to
Indian Institute of Technology Guwahati
for the award of the degree

of

Doctor of Philosophy

by

Abhijit Shit

Roll No.: 196123001

Under the guidance of

Dr. Swaroop Nandan Bora

Department of Mathematics
Indian Institute of Technology Guwahati
Guwahati - 781 039, India

January 2025

Dedicated to my parents

Smt. Shikha Shit

&

Shri Joydeb Shit

DECLARATION

I do hereby declare that the thesis entitled **Modelling of Some Biological Phenomena via Fractional Differential Equations** is accomplished under the supervision of **Dr. Swaroop Nandan Bora**, Professor, Department of Mathematics, Indian Institute of Technology Guwahati for the award of the degree of Doctor of Philosophy and this work has not been submitted elsewhere for a degree.

Date: 12 / 01 / 2025
Place: Guwahati

Abhijit Shit
Roll No.: 196123001
Department of Mathematics
Indian Institute of Technology Guwahati
Guwahati - 781 039, Assam, India

CERTIFICATE

This is to certify that the work contained in this thesis entitled **Modelling of Some Biological Phenomena via Fractional Differential Equations** has been carried out by **Mr. Abhijit Shit**, a student in the **Department of Mathematics**, **Indian Institute of Technology Guwahati**, under my supervision for the award of the degree of **Doctor of Philosophy** and this work has not been submitted elsewhere for a degree.

Date: 12 / 01 / 2025
Place: Guwahati

Dr. Swaroop Nandan Bora
Professor
Department of Mathematics
Indian Institute of Technology Guwahati
Guwahati - 781 039, Assam, India

Acknowledgements

It is said that there are the stars that guide the sailors to their coveted destinations. Likewise, my voyage of PhD would have never been accomplished without the gracious presence of these wonderful people, who glitter in my life as bright as the stars in the sky. Rendering this occasion, I want to express my heartfelt gratitude to them for being an inevitable part of my PhD journey.

First and foremost, I would like to express my sincere gratitude to my benevolent supervisor, Dr. Swaroop Nandan Bora, for always being a ray of hope amidst the darkest night. His immense support and constant guidance have helped me circumvent all the difficulties I came across throughout the course of my PhD journey. His encouragement and guidance not only paved the way for my development as a researcher but also changed my personality, ability and nature in many ways. His gracious presence has always been a constant source of motivation, not merely to become a prolific researcher but a good human being too. His sound moral and ethical principles, and his endeavour to be impeccable in every aspect will always be my source of inspiration.

I would like to use this opportunity to express my gratitude to the members of my doctorate committee Prof. Bhupen Deka, Prof. Jiten Chandra Kalita, and Dr. Sweta Tiwari, for their insightful comments and innovative ideas, which have helped improving the calibre of my study at different points in this journey. I owe special thanks to Dr. Satyajit Pramanik for some sound and fruitful discussions which at times helped me find the ray after the dark tunnel.

I express my heartfelt gratitude to all of Mathematics Department faculty members at IIT Guwahati who taught me during my M.Sc. and PhD, especially Prof. Rajen Kumar Sinha, Prof. Anupam Saikia, Prof. M. Guru Prem Prasad, Prof. Gautam K. Das, Dr. Anjan K. Chakrabarty. I would also like to thank every member of the department staff for their technical assistance and official cooperation throughout my PhD journey.

I sincerely acknowledge the Ministry of Education, Govt. of India for providing financial assistantship during the period of my PhD programme.

I would like to express my courteous appreciation to seniors for sharing their research expertise and hard-earned experiences. Special thanks to my seniors Dr. Jogen, Dr. Shantiram, Dr. Abhijit, Dr. Nilay, Dr. Kuldeep, Dr. Ajit, Dr. Raman, Dr. Gouranga, Dr. Mrityunjoy, and Mr. Puspendu for their invaluable advices both on academic and non-academic matters. My friends and juniors have always been constant companions in academic as well as non-academic well beings. I convey my heartfelt accolade to my

school friends: Sani, Debashis, Milan, Sourav; IITG friends: Shiva, Matap, Aniruddha, Sandip, Sagar, Mijanur, Shilpi (Biswas), Khyodeno; juniors: Shilpi (Jain), Sunil, Mahesh, Nabanita, Sohini for being a part of my PhD journey. There are many more, but it is difficult for me to express everyone's part here. I convey my sincere apology to them.

I wish to express my deepest gratitude to my beloved parents for their unconditional love, encouragement and understanding. I do believe that, without their blessings and constant support, this work probably would have not seen the light of the day.

Finally, I remain ever grateful to the Almighty God for His blessings.

Date: 12 / 01 / 2025
Place: Guwahati

Abhijit Shit
Roll No.: 196123001
Department of Mathematics
Indian Institute of Technology Guwahati
Guwahati - 781 039, Assam, India

Abstract

The study of integer-order differential equations has always been in the limelight for its importance and usefulness in the mathematical modelling of a large number of physical phenomena. Most of them are tackled by considering either ordinary differential equations or partial differential equations of integer order. Researchers have nowadays found that modelling real-world problems through fractional-order governing equations captures various phenomena in a more realistic way, which the models governed by integer-order ones lack. Notwithstanding the fact that not sufficient studies have been conducted in the area of fractional-order differential equations from an application point of view, it is fair to note that modelling physical phenomena by considering such equations has acquired more attention at present in comparison to earlier times. It is a well-known fact that fractional differential equations are studied through the framework of fractional calculus which generalizes the concepts of differentiation and integration in a more erudite and general manner with the consideration of real orders in place of integer orders. Such a consideration can be realized through a number of ways of representation of the derivatives and integrals of real order instead of integer order, for example, Riemann-Liouville, Caputo, Hilfer, ψ-Hilfer, and so forth.

This thesis mainly focuses on the applicability of the fractional model in some problems arising in the biological science. Here, we use the conventional Caputo derivative for the mathematical formulation of the chosen problems. We try to obtain analytical solutions by means of integral transform since an analytical solution is capable of elucidating the behaviour of the solution explicitly for a vast range of values for the chosen parameters and the arbitrary constants. We also validate our solution with the existing literature and present some interesting attributes which the integer-order models failed.

In the beginning, we come up with the conventional fractional generalization of the ESR test model, where we incorporate the uniform average blood velocity, which was not considered in the earlier models. This inclusion not only makes the model much more realistic but also leads to some interesting results which outperform the existing works. Later, we also incorporate the concentration gradient of the blood nutrients in the previous model. This incorporation too helps us come up with some further impactful attributes, and for this case also, this model outperforms the earlier model.

Next, we deal with the modelling for mass transport in the brain cells. Here, we formulate the integer-order model for the mass transport by considering solutions for two layers. While fitting the experimental data to this integer-order model, we find that this model is unable to provide much accuracy as expected. This motivates us to render the

fractional approach, which successfully helps in circumventing the issue and coming up with a compact model, which promises to be impactful for the future research in this direction.

In another problem, we invoke the fractional-order model for modelling the blood flow in a stenosed artery under MHD effect through a porous medium, thereby substituting the conventional integer-order model. We come up with a solution which is capable of providing some interesting velocity profiles corresponding to different orders of the derivative. The external magnetic field intensity, together with the fractional-order of the derivative, helps in providing an efficient model in the treatment of the stenosed artery in human body.

The last problem of this thesis investigates the ion diffusion in the extracellular microenvironment of the rat cerebellum through a fractional-order modelling. Here, we find some loopholes in the integer-order model while approximating the experimental data by the analytical solution. This motivates us revisit the modelling under the light of the fractional differential equation. Fortunately, we succeed in coming up with a better-suited model which takes care of all the shortcomings of the integer-order model. Henceforth, being able to approximate a large class of experimental data and prescribe the best suitable value for the fractional-order derivative, it certainly helps us establish the reliability of the proposed fractional-order model.

भारतीय प्रौद्योगिकी संस्थान गुवाहाटी
Indian Institute of Technology Guwahati

List of Figures

List of Tables

Contents

1 Introduction

"In every mathematical investigation, the question will arise whether we can apply our mathematical results to the real world."

V. I. Arnold

1.1 Overview

1.1.1 Fractional calculus

It is a well-accepted fact that differential equations form the basis of most of the physical phenomena since they can elucidate the phenomena in a more profound and prolific manner. When we deal with problems in our real-life scenario where continuous change is taking place, there comes the role of differential equation, which is widely known for measuring the rate of change. Most of the phenomena can be captured by differential equations, whether they are ordinary differential equations or partial differential equations. Differential equation is one of those branches which is not only used in the mathematical field merely as a tool or a topic of analysis but also has a huge impact on modelling a numerous phenomena occurring in widely spread areas of biological science, physical science, chemical science and many other applied branches of science. An equation which consists of the derivatives of one or more dependent variables with respect to one or more independent variables along with the dependent and independent variables is called a differential equation. In this thesis, we utilize the generalization of the derivatives termed as $\frac{d^\alpha C}{dx^\alpha}$, $\frac{\partial^\alpha C}{\partial x^\alpha}$ and $\frac{\partial^\alpha C}{\partial t^\alpha}$, where $\alpha \in \mathbb{R}^+$, which we refer as fractional derivatives. Actually, these derivatives came into picture to facilitate some queries. When Leibniz first introduced the idea of a symbolic method and used the symbol $\frac{d^n y}{dx^n} = D^n y$ for the n-th derivative, where n is a non-negative integer, L'Hospital asked Leibniz about the possibility of n being a fraction. "What if $n = \frac{1}{2}$? " In 1695, Leibniz replied, "It will lead to a paradox." But he added prophetically, "From this apparent paradox, one day useful consequences will be

drawn." Later, the question became: "Can the meaning of derivatives of integer-order $D^n y$ be extended to have some meaning where n is any number - rational, irrational or complex?" The latter question was answered affirmatively and this led to a new horizon that is now well-known as the fractional calculus, and we often mention it as the differentiation and integration of arbitrary order.

The history of fractional calculus hence dates back to the end of seventeenth century and it has been developed progressively till now. Here are some of the mathematicians who helped flourishing this field of fractional calculus by their remarkable imprints: Euler (1730), Lagrange (1772), Laplace (1812), Lacroix (1819), Fourier (1822), Abel (1823), Liouville (1832), Grünwald (1867), Letnikov (1868), Heaviside (1892), Weyl (1917), Erdélyi (1939), Kober (1940), Riesz (1949), etc. In June 1974, the first conference on Fractional Calculus and its Applications was organized by B. Ross at the University of New Haven, Connecticut. As for the first monograph, the credit is ascribed to Oldham and Spanier [47], who published a book in 1974 devoted to fractional calculus. A number of additional books have appeared since then, with titles explicitly devoted to fractional calculus (or fractional differential equations) and its applications, for example, Miller and Ross (1993) [43], Samko et al. (1993) [52], Carpinteri and Mainardi (1997) [40], Podlubny (1999) [48], Hilfer (2000) [25], Kilbas et al. (2006) [34], Das (2011) [12], and others, and the list is expected to grow in the forthcoming years.

Although fractional calculus has a long history, but from the application point of view, it fell into oblivion for many years since it was not considered useful for solving problems in physics and engineering. This was due to its high complexity and the lack of an acceptable physical and geometric interpretation. In 2002, Podlubny [48] proposed an explanation of fractional phenomena. He proposed both a geometrical interpretation of the Riemann-Liouville fractional integral and a physical interpretation for the Riemann-Liouville and Caputo fractional derivatives. Of late, ψ-Hilfer derivative seems to have received the focus in a good number of researches involving fractional differential equations. In 2018, da Sousa and de Oliveira [9] came up with a handful of fractional derivatives and integrals in view of fractional integral with respect to a different function and by incorporating the ψ-Hilfer derivative. Later on, they also came up with a Leibniz-type rule to take care of the operator for ψ-Hilfer fractional derivative in a couple of ways—first, dealing with the operator of ψ-Riemann-Liouville fractional derivative and then the other one dealing with the operator of ψ-Hilfer fractional derivative [9, 10]. These seminal works have not only made a substantial contribution to the generalization of certain results but have also shown a promising future aspiration which certainly holds motivation for the researchers in this field.

In the last few decades, there has been an explosion of research activities on the application of fractional calculus to very diverse scientific fields ranging from modelling

TH-3553_196123001

biological phenomenon, physics of diffusion and advection phenomena to control systems to finance and economics. Scientists have discovered that many phenomena, not completely understood before, have complex microscopic behaviours, and that their macroscopic dynamics cannot be modelled precisely via integer-order derivatives. In particular, it has been found that most of the processes associated with complex systems have nonlocal dynamics involving long-term memory effects, which is precisely the property that characterizes fractional derivative operators. In order to appreciate the potentialities of fractional calculus in a better way from an application point of view, some examples of complex system from mathematical biology, modelled by fractional differential equations are given below.

1.1.2 Mathematical biology

In the field of mathematical biology and bioengineering, there is an ongoing need to develop efficient and high fidelity material models to approximate a large class of experimental data taken from the laboratory. For this purpose, fractional calculus is used to develop fractional-order convection-diffusion equations, which could be useful for modelling biological phenomena. In the work of da Sousa et al. [8, 11], it is asserted that a description based on fractional-order differential equations potentially has superior accuracy and gives the possibility of correlating the hierarchical structure of biological phenomena in a better way than the integer-order ones.

In terms of reality, the world has witnessed many life-threatening disasters from its inception, for instance, the Corona virus pandemic very recently, which has been threatening the mankind repeatedly. Scientists have been trying their best to come up with solutions to these problems to cope in this world. Apart from these, there are plenty of frightful diseases like AIDS, hepatitis (caused by the hepatitis delta virus), cancer, and so forth, which lack suitable solutions to date−both medically and mathematically. Scientists, doctors, mathematicians, and many others are trying to come up with suitable solutions to reducing these threats to the human race. As such, mathematical modelling for such problems is nowadays attracting sufficient focus. In 2018, Zubik-Kowal [67] came up with a solution to the disease caused by the hepatitis delta virus, where the simulation involved an appropriate differential equation. They were able to settle some relevant questions through the model with respect to this disease. In the same year, Tannenbaum et al. [61] presented a mathematical model, taking care of the growth of tumour cells in the human body, by considering partial differential equations. They developed an efficient algorithm that showed fast clinical applications. Since the above-mentioned diseases have unfortunately seen rapid growth these days, the mathematical model describing those problems has been investigated again and again extensively, which highlights the relevance and importance of mathematical models for real-world problems. Most importantly, the

equations that form the backbones of these models are nothing but differential equations, which not only govern the process but also help in drawing important recommendations to find measures for tackling important real-world problems. Many such problems have found suitable modelling through fractional differential equations.

1.2 Preliminaries

Here, we quickly revisit some well-known functions and results which have tremendous use in the study of fractional differential equations and their applications. Since, we intend to apply the fractional calculus to some biological phenomena, hence, we also have a quick review on some aspects of fluid dynamics and biology.

1.2.1 Special functions

- **Gamma function**

  The Gamma function $\Gamma(z)$ is defined by the integral

  $$\Gamma(z) = \int_0^\infty e^{-t} t^{z-1} dt, \quad \mathrm{Re}(z) > 0.$$

  When $z = n$, where n is a positive integer, then the Gamma function is related to the factorial function by

  $$\Gamma(n) = (n-1)!. \tag{1.1}$$

  The Gamma function satisfies the recursive property

  $$\Gamma(z+1) = z\Gamma(z).$$

  For a specific value of z, an exact value of $\Gamma(z)$ exists. For positive integers, $\Gamma(.)$ is defined by (1.1). The Gamma function evaluated at $z = \frac{1}{2}$ is

  $$\Gamma\left(\frac{1}{2}\right) = \sqrt{\pi}.$$

- **Mittag-Leffler function**

  The exponential function e^z plays an important role in integer-order differential equation as well as in fractional differential equation. It was introduced by G. M. Mittag-Leffler in 1903. A one-parameter Mittag-Leffler function is defined by the series expansion

  $$E_\alpha(z) = \sum_{k=0}^{\infty} \frac{z^k}{\Gamma(\alpha k + 1)}.$$

A two-parameter Mittag-Leffler function is defined by the series expansion

$$E_{\alpha,\beta}(z) = \sum_{k=0}^{\infty} \frac{z^k}{\Gamma(\alpha k + \beta)}.$$

It follows from the above definition that

$$E_{1,1}(z) = \sum_{k=0}^{\infty} \frac{z^k}{\Gamma(k+1)} = \sum_{k=0}^{\infty} \frac{z^k}{k!} = e^z.$$

- **Wright function**

  The Wright function plays a pivotal role in the solutions of linear fractional partial differential equation, for example, fractional diffusion or wave equation.
  This function is related to Mittag-Leffler function of two parameters $E_{\alpha,\beta}(z)$ and was first introduced by E. M. Wright, and is defined as follows:

$$W(z;\alpha,\beta) = \sum_{k=0}^{\infty} \frac{z^k}{k!\Gamma(\alpha k + \beta)}.$$

- **Bessel function**

  The Bessel functions of the first kind, denoted by $J_\beta(x)$, are the solutions of Bessel's differential equation

$$x^2 \frac{d^2y}{dx^2} + x\frac{dy}{dx} + (x^2 - \beta^2)y = 0,$$

  where β need not necessarily be an integer. Bessel function of first kind is defined by

$$J_\beta(x) = \sum_{k=0}^{\infty} \frac{(-1)^k}{k!\Gamma(k+\beta+1)} \left(\frac{x}{2}\right)^{2k+\beta}.$$

  The general solution of Bessel's equation can be written as

$$y(x) = c_1 J_\beta(x) + c_2 J_{-\beta}(x),$$

  where β is not an integer.

  However, the solution of Bessel's equation for β being an integer, i.e., $\beta = n$, takes the form

$$y(x) = c_1 J_n(x) + c_2 Y_n(x),$$

  where $Y_n(x)$ is called the Bessel function of second kind. Furthermore, there are Bessel functions of third kind and modified Bessel functions too, but they do not appear to be noteworthy for our works in the thesis.

Most of the definitions and results used in this section have been taken from the books by Podlubny [48], Debnath and Bhatta [14].

1.2.2 Some well-known derivative and integral formulas

(a) Riemann-Liouville fractional integral and derivative

Let $\Omega = [a,b];\ -\infty < a < b < \infty$ be a finite interval on the real axis. The Riemann-Liouville fractional integrals of a function f defined on Ω, I^{α}_{a+} and I^{α}_{b-} of order $\alpha \in \mathbb{C}$, $\mathrm{Re}(\alpha) > 0$, are defined by

$$(I^{\alpha}_{a+}f)(x) = \frac{1}{\Gamma(\alpha)} \int_a^x \frac{f(t)dt}{(x-t)^{1-\alpha}}; \qquad x > a,\ \mathrm{Re}(\alpha) > 0, \tag{1.2}$$

and

$$(I^{\alpha}_{b-}f)(x) = \frac{1}{\Gamma(\alpha)} \int_x^b \frac{f(t)dt}{(x-t)^{1-\alpha}}; \qquad x < b,\ \mathrm{Re}(\alpha) > 0. \tag{1.3}$$

These integrals (1.2) and (1.3) are, respectively, called the left- and right-sided Riemann-Liouville fractional integrals.

The Riemann-Liouville fractional derivatives $D^{\alpha}_{a+}(f)$ and $D^{\alpha}_{b-}(f)$ of order $\alpha \in \mathbb{C}$, $\mathrm{Re}(\alpha) > 0$, are defined by

$$\begin{aligned}(D^{\alpha}_{a+}f)(x) &= \left(\frac{d}{dx}\right)^n (I^{n-\alpha}_{a+})(x) \\ &= \frac{1}{\Gamma(n-\alpha)} \left(\frac{d}{dx}\right)^n \int_a^x \frac{f(t)dt}{(x-t)^{\alpha-n+1}}; \qquad x > a,\ n = \lceil \mathrm{Re}(\alpha) \rceil + 1,\end{aligned}$$

and

$$\begin{aligned}(D^{\alpha}_{b-}f)(x) &= \left(-\frac{d}{dx}\right)^n (I^{n-\alpha}_{b-})(x) \\ &= \frac{1}{\Gamma(n-\alpha)} \left(-\frac{d}{dx}\right)^n \int_x^b \frac{f(t)dt}{(x-t)^{\alpha-n+1}}; \qquad x < b,\ n = \lceil \mathrm{Re}(\alpha) \rceil + 1.\end{aligned}$$

(b) Caputo fractional derivative

The left- and right-sided Caputo fractional derivatives with order $\alpha \in \mathbb{C}$, $\mathrm{Re}(\alpha) > 0$, $n = \lceil \mathrm{Re}(\alpha) \rceil + 1$ of a function $f(x) \in AC^n[a,b]$ (the space of functions which have absolutely continuous derivatives up to $(n-1)$-th order on $[a,b]$) are defined as

$$\left({}^{C}D^{\alpha}_{a+}f\right)(x) = \frac{1}{\Gamma(n-\alpha)} \int_a^x \frac{f^{(n)}(t)dt}{(x-t)^{\alpha-n+1}}; \qquad x > a, \tag{1.4}$$

and

$$\left({}^{C}D^{\alpha}_{b-}f\right)(x)=\frac{1}{\Gamma(n-\alpha)}\int_{x}^{b}\frac{f^{(n)}(t)dt}{(x-t)^{\alpha-n+1}};\qquad x<b. \tag{1.5}$$

In particular, for $\alpha\in(0,1]$ and $a=0$, we have

$$\left({}^{C}D^{\alpha}_{0+}f\right)(x)=\begin{cases}\dfrac{1}{\Gamma(1-\alpha)}\displaystyle\int_{0}^{x}\frac{f'(t)dt}{(x-t)^{\alpha}}; & x>0,\quad 0<\alpha<1,\\ \dfrac{df}{dt}(t); & \alpha=1.\end{cases} \tag{1.6}$$

.

(c) ψ-Riemann-Liouville fractional integrals:-

Let $[a,b](-\infty\le a<b\le\infty)$ be a finite or an infinite interval on $\mathbb{R}$ and $\alpha\in(0,1)$. Further, let $\psi(t)$ be an increasing and positive continuous function on $[a,b]$ with a continuous derivative $\psi'(t)\neq 0$ on (a,b). The left- and right-sided ψ-Riemann-Liouville fractional integrals of a function g with respect to the function ψ on $[a,b]$ are defined as follows (da Sousa et al. [9, 10]):

$$\mathcal{I}^{\alpha;\psi}_{a+,t}g(t)=\frac{1}{\Gamma(\alpha)}\int_{a}^{t}\psi'(x)[\psi(t)-\psi(x)]^{\alpha-1}g(x)dx, \tag{1.7}$$

and

$$\mathcal{I}^{\alpha;\psi}_{b-,t}g(t)=\frac{1}{\Gamma(\alpha)}\int_{t}^{b}\psi'(x)[\psi(t)-\psi(x)]^{\alpha-1}g(x)dx. \tag{1.8}$$

In particular, if we take $\psi(t)=t$ in Eqs. (1.7) and (1.8), then we obtain left- and right-sided Riemann-Liouville fractional integrals as

$$\mathcal{I}^{\alpha}_{a+,t}g(t)=\frac{1}{\Gamma(\alpha)}\int_{a}^{t}(t-x)^{\alpha-1}g(x)dx, \tag{1.9}$$

and

$$\mathcal{I}^{\alpha}_{b-,t}g(t)=\frac{1}{\Gamma(\alpha)}\int_{t}^{b}(t-x)^{\alpha-1}g(x)dx. \tag{1.10}$$

(d) ψ-Hilfer fractional derivatives:-

Let $[a,b](-\infty\le a<b\le\infty)$ be a finite or an infinite interval on $\mathbb{R}$ and $\alpha\in(n-1,n)$, with $n\in\mathbb{N}$. Also, let g and $\psi\in C^{n}([a,b],\mathbb{R})$, with ψ being increasing and $\psi'(t)\neq 0$ on (a,b). The left- and right-sided ψ-Hilfer fractional derivatives of order α and type β, where $0\le\beta\le 1$, are defined by the following (da Sousa et al. [9, 10]):

$${}^{H}\mathbb{D}^{\alpha,\beta;\psi}_{a+,t}g(t)=\mathcal{I}^{\beta(n-\alpha);\psi}_{a+,t}\left(\frac{1}{\psi'(t)}\frac{d}{dt}\right)\mathcal{I}^{(1-\beta)(n-\alpha);\psi}_{a+,t}g(t), \tag{1.11}$$

and

$$ {}^{H}\mathbb{D}^{\alpha,\beta;\psi}_{b-,t}g(t) = \mathcal{I}^{\beta(n-\alpha);\psi}_{b-,t}\left(\frac{1}{\psi'(t)}\frac{d}{dt}\right)\mathcal{I}^{(1-\beta)(n-\alpha);\psi}_{b-,t}g(t). \tag{1.12} $$

In particular, if we choose $\psi(t) = t$ and consider the limit $\beta \to 1$ in Eqs. (1.11) and (1.12), we get the left- and right-sided Caputo fractional derivatives, respectively, as

$$ \mathcal{D}^{\alpha}_{a+,t}g(t) = \mathcal{I}^{(n-\alpha)}_{a+,t}\left(\frac{d}{dt}\right)g(t), \tag{1.13} $$

and

$$ \mathcal{D}^{\alpha}_{b-,t}g(t) = \mathcal{I}^{(n-\alpha)}_{b-,t}\left(\frac{d}{dt}\right)g(t), \tag{1.14} $$

with $0 < \alpha \leq 1$.

(e) Laplace transform

The Laplace transform of a function g of a single variable $t > 0$ is defined as follows:

$$ \mathcal{L}\{g(t)\} = \int_0^{\infty} e^{-st}g(t)dt = \bar{g}(s), $$

where s is the transformed variable with $\mathrm{Re}(s) > 0$. Note that g has to be piecewise continuous and of exponential order.

Similarly, the Laplace transform of a function of two variables $g(x,t)$ for $x \in \mathbb{R}$, $t > 0$, with respect to t is defined by

$$ \mathcal{L}\{g(x,t)\} = \int_0^{\infty} e^{-st}g(x,t)dt = \bar{g}(x,s). $$

(f) Laplace transform of Caputo fractional derivative

Following Abramowitz and Stegun [1], the Laplace transform of the Caputo fractional derivative of order α for $\alpha \in (n-1,n)$, $n \in \mathbb{N}$ of a function $g(t) \in AC^n[0,\infty)$, is given by

$$ \mathcal{L}\{\mathcal{D}^{\alpha}_{0+,t}\ g(t)\}(s) = s^{\alpha}G(s) - \sum_{k=0}^{n-1} s^{\alpha-k-1}g^{(k)}(0), \tag{1.15} $$

where $g^{(k)}(0) = \lim_{k\to 0} D^k g(t)$ with $D \equiv \frac{d}{dt}$ as the usual differential operator and $G(s)$ is the Laplace transform of $g(t)$.

In particular if $\alpha \in (0,1]$ then Eq. (1.15) takes the following form:

$$ \mathcal{L}\{\mathcal{D}^{\alpha}_{0+,t}\ g(t)\}(s) = s^{\alpha}G(s) - s^{\alpha-1}g(0). \tag{1.16} $$

(g) Advantage of using Caputo fractional derivative

From Eq. (1.15), it is quite evident that the Laplace transform of Caputo fractional derivative includes the initial conditions appearing in the form of classical integer-order derivatives, which are quite familiar for their well-established physical significance which can be considered one important advantage in utilizing Caputo derivative in the problem formulation. On the contrary, the Laplace transform of Riemann-Liouville fractional derivative involves fractional-order for the initial conditions which are difficult to deal with. This justifies the selection of Caputo derivative over other types of fractional derivatives for most of the problems and so is the case with the problems in this thesis.

1.2.3 Basic definitions of fluid dynamics and mathematical biology (in the context of our thesis)

Fluid dynamics is a sub-discipline of fluid mechanics where we study the effect of forces on the motion of fluid (liquids and gases).

Fluid:-

A fluid is a substance that continuously deforms under an applied shear stress, however small it is. This continuous deformation under the application of shear stress constitutes a flow. The tangential stress in a fluid body depends on the velocity of deformation and vanishes as this velocity approaches zero.

Types of fluid:-

- **Incompressible fluid**:- A fluid whose volume or density does not change with pressure is known as an incompressible fluid.
  For example: oil, honey etc.

- **Compressible fluid**:- A type of fluid that changes its volume under varying pressure and that results in altering in its density, is called a compressible fluid.
  For example: gas, vapour, steam etc.

- **Viscous fluid**:- A viscous fluid is a genuine fluid that flows with some resistance in the opposite direction of its flow. The resistance is called viscosity, and the fluid is viscous.
  For example: water, oil, honey etc.

- **Inviscid fluid**:- A fluid which has no internal friction or, in scientific terms, viscosity, is an inviscid fluid. This means that the fluid has no resistance to shape change and any force exerted on it is instantly transferred to all parts of the fluid. They do not exist in real world; but the assumption holds true in many cases.

- **Ideal fluid**:- A fluid which is incompressible and has no viscosity is known as an ideal fluid. Ideal fluid does not exist in real world; it is an assumption which holds true in many cases.
- **Real fluid**:- A fluid which possesses some viscosity is known as a real fluid.
  For example: water, kerosene, petrol etc.
- **Newtonian fluid**:- A real fluid which obeys the Newton's law of viscosity (i.e., shear stress is directly proportional to shear strain rate) is known as a Newtonian fluid.
  For example: water, air, emulsions etc.
- **Non-Newtonian fluid**:- A real fluid which does not obey the Newton's law of viscosity is known as a Non-Newtonian fluid.
  For example: rubber, suspension of starch in water.

Types of fluid flow:-
Fluid flow can be classified in the following categories:

- **Steady and unsteady flow:-** A steady flow is defined as a flow in which the various hydro-dynamics parameters and fluid properties at any point do not change with time while the flow in which any of these parameters changes with time is known as an unsteady flow.
- **Compressible and incompressible flow:-** A fluid flow is said to be compressible if the fluid density varies with the variation in pressure or temperature while if the density remains invariant under variation of pressure and temperature, then the flow is said to be incompressible.
- **Laminar and turbulent flow**:- A fluid flow is said to be laminar if each particle of the fluid follows the path of its preceding particle. For example: the flow of blood through the arteries and veins of the human body.

  A turbulent flow is a fluid flow in which the fluid undergoes irregular fluctuations, or mixing, in contrast to laminar flow. For example: flow of river water.

Since one of our objectives is to apply fractional differential equations to the problems arising in biology (related to blood flow), we deem it pertinent to discuss in brief a couple of important equations of fluid dynamics. The fundamental set of equations of fluid dynamics contains the equation of continuity and equation for conservation of momentum.

1. **Equation of continuity (conservation of mass)**:- The law of conservation of mass states that mass can neither be created nor be destroyed. Mathematically, it can be written as

$$\frac{\Delta m}{\Delta t} = 0,$$

where m is the mass of the system.

The *equation of continuity of a compressible fluid* is written as

$$\frac{\partial \rho}{\partial t} + \nabla.(\rho \vec{U}) = 0,$$

where $\vec{U}$ is the velocity vector and ρ is the density of the fluid.

2. **Conservation of linear momentum equation**:- In Newtonian mechanics, the conservation of momentum is defined by Newton's second law of motion. According to this law "The rate of change of momentum of a fluid particle is proportional to the impressed action and takes place in the direction of the impressed action." If the impressed action is $\vec{F}$, then the equation of linear momentum is

$$\frac{d}{dt}(m\vec{U}) = \sum \vec{F}.$$

Some aspects of biology:-

- **Viscosity**:- Viscosity refers to the resistance to the flow exerted by the fluid. It is a measure of the internal friction within a fluid that opposes motion when subjected to a force or shear stress. In simpler terms, viscosity determines how easily a fluid flows or how "thick" or "sticky" it is.
- **Porosity**:- Porosity or void fraction is a measure of the void (i.e., "empty") spaces in a material, and is a fraction of the volume of voids over the total volume, between 0 and 1, or as a percentage between 0% and 100%. Depending upon the pore size (diameter of the pores), porosity can be categorized into three types.
  - ➦ **Microporosity**:- Microporosity refers to those pores having diameter smaller than 2 nm, and the medium is known as microporous medium. Microporosity can be defined differently in other contexts. For example, in the context of porous aggregations such as soil, stenosis, micropores are defined as cavities with sizes less than 30 μm. For the problems in our thesis, we deal with a microporous medium.
  - ➦ **Mesoporosity**:- The pores whose diameter is greater than 2 nm and less than 50 nm, correspond to mesoporosity, and the medium is referred as mesoporous medium.
  - ➦ **Macroporosity**:- The term macroporosity refers to the pores whose diameter is greater than 50 nm, and the medium is called macroporous medium.
- **Tortuosity**:- Tortuosity is defined as the average hindrance of a complex medium relative to obstacle-free medium.

- **Artery**:- An artery is a blood vessel in humans and most other animals that takes oxygenated blood away from the heart in the systemic circulation to one or more parts of the body. Exceptions that carry deoxygenated blood are the pulmonary arteries in the pulmonary circulation that carry blood to the lungs for oxygenation.
- **Capillary**:- Blood flows from the heart through arteries, which branch and narrow into arterioles, and then branch further into capillaries where nutrients and wastes are exchanged. Capillaries are microvessels and the smallest blood vessels in the body.
- **Stenosis**:- Stenosis is the abnormal narrowing of a blood vessel or other tubular organ or structure such as foramina and canals caused by fatty deposits or cholesterol flex, which get sedimented in the inner wall of the blood vessels.
- **Interstitial space**:- The interstitial space that lies between blood vessels and cells provides the fluid and structural environment surrounding those cells. Under most conditions in most tissues, the fluid from the vascular space continually filters from the microvessels into the interstitial space.

1.2.4 Fractional differential equations

Nowadays, the subject of fractional differential equations is gaining much importance and attention than earlier. The so-called fractional differential equations are specified by generalizing the standard integer-order derivative to arbitrary order. Due to the effective memory function of fractional derivative, fractional differential equations have been widely used to describe many physical phenomena such as seepage flow in porous media and in fluid dynamic traffic model. For more interesting theoretical results and scientific applications of fractional differential equations, we refer to the monographs of Podlubny [48], Kilbas et al. [34], Miller and Ross [43] and some recent developments on this field in the articles of da Sousa et al. [9, 10].

With the advent of fractional calculus and fractional differential equations and their potential use in appropriate applications, researchers have been able to model complex systems by considering fractional-order differential equations as replacements of classical integer-order ones. It is noticed that these fractional models are more efficient in providing better descriptions of the phenomena in a more realistic way and also in helping to draw more accurate information on the underlying physical aspects. In this context, fractional differential equations have commanded significant attention owing to their important applications in different branches of science, particularly in the fields of biology and medicine.

Based on the nature of the derivative (ordinary or partial), fractional differential equations are classified into two sub-classes.

- **Fractional ordinary differential equations**:-
  The fractional ordinary differential equations have the following general form:

$$F(x, y(x), D^{\alpha_1} y(x), D^{\alpha_2} y(x), \cdots, D^{\alpha_n} y(x)) = g(x),$$

  where F and g are given functions and D^{α_k} are the operators of fractional differentiation with $\mathrm{Re}(\alpha_k) > 0$ or complex α_k with $\mathrm{Re}(\alpha_k) > 0$, $k = 1, 2, 3, \cdots, n$.

  For example: consider the initial value problem

$$D_0^{\alpha} y(x) = g(x),$$

  for a given function g with $y(0) = y_0$ and $x > 0$.

- **Fractional partial differential equations**:-
  When we generalize the partial derivative to arbitrary order in the corresponding partial differential equation, the resulting differential equation is then known as a fractional partial differential equation.

  For example: consider the following fractional heat equation:

$$D_{0+}^{\alpha} u(x,t) = \frac{1}{\pi^2} \frac{\partial^2 u}{\partial x^2}(x,t) \quad x > 0, t > 0,$$

  with the following initial and boundary values

$$\begin{aligned} &u(0,t) = 0, \quad \frac{\partial u}{\partial x}(0,t) = \pi \mathbb{E}_{\alpha}(-\alpha t), && t > 0, \\ &u(x,0) = \sin(\pi x), && x > 0, \end{aligned}$$

  where $0 < \alpha \leq 1$.

1.3 Literature survey

Our thesis aims at providing and authenticating fractional models for some biological phenomena which are usually modelled by integer-order differential equations. Prior to taking up the problems, we have carried out an extensive survey of a number of biological phenomena. Consequently, we pick up a number of problems pertaining to different aspects. Below, we present the literature survey topic-wise in order to have a methodical and clear insights into the already accomplished works.

1.3.1 Erythrocyte Sedimentation Rate (ESR) test

The ESR (Erythrocyte Sedimentation Rate) test has been extensively used for different types of clinical diagnosis. The history of the ESR test dates back to the ancient Greek era and hence it can probably be considered as one of the oldest medical tools for diagnosis (Kushner [37]). However, this test became popular only towards the end of the 19th and early 20th century when it found its place as a non-specific test for diagnosing and monitoring inflammation (Grzybowski and Sak [21], Bedell and Bush [3]). Looking at the recent developments, it can be seen that the ESR test is also used as a good biomarker in order to detect abnormal and deformed erythrocytes (in other words, red blood cells (RBCs)) (Darras et al. [13]). Inspite of the fact that the ESR test is used frequently in medical science, physical mechanisms governing the sedimentation of erythrocytes have not seen much progresses in the last century. At present time, owing to the development of more sophisticated methods, the ESR test is not much in demand despite of the fact that it is a quick and cost-effective test. Whatsoever, even now the ESR test is considered a suitable diagnostic tool for patients having ailments due to suspected giant cell arthritis, rheumatics polymyalgia, rheumatoid arthritis and some other ailments (Brigden [4]).

Polish physician E. F. Biernacki, in 1897, came up with a blood test that was capable of accurately diagnosing the acute phase of inflammatory diseases as well as acting as a follow-up for body inflammation, which is actually known as the Erythrocyte Sedimentation Rate (ESR) as discussed above (Kucharz [35], Kucharz and Edmund [36], Grzybowski and Sak [22]). In the early part of the 19th century, Robin Fahraeus and A. Westergren, while carrying out pregnancy and tuberculosis tests, developed a test which bore resemblance to ESR test and was named the Fåhraeus-Westergren test (Westergren [64, 65], Fåhraeus [15]). In this direction, looking into the mathematical aspects, Sharma et al. [56] formulated a mathematical model with conventional partial derivative (integer-order) terms to study the nutrient concentration in blood which was considered an important factor that directly influenced ESR, which is also called VHS, hemosedimentation velocity. da Sousa et al. [7], in the second half of 2017, presented a mathematical model in which a time-fractional derivative replaced the integer-order derivative. Furthermore, recently da Sousa et al. [11] have accomplished a validation of the fractional-order model for ESR by considering practical data.

1.3.2 Mass transport in brain cells

Diffusion of molecules in any biological tissue, especially in the brain, is of utmost importance in the widely-spread areas ranging from biological processes to the treatment procedures like drug delivery to biological tissues to magnetic resonance imaging (MRI). Human tissues are considered a porous medium, with the knowledge that these are made

up of dispersed cells separated by connective voids through which nutrients and other minerals get transported to each cell in the tissues. The mass transport in the local environment of the tissues is very sensitive and gets affected by the packing geometry of the cells and their membrane permeability that controls the transportation of nutrients across the membranes. The diffusion-reaction process in a complicated geometry, at a microscopic level, is an immensely difficult process. Plenty of research has been conducted in this direction, e.g., Puri et al. [49], Meidani and Hasan [42].

Sharan and Popel [55] developed a mathematical model for oxygen transport in brain microcirculation in the presence of blood substitutes. Vafai et al. [33] numerically analyzed the role of various diffusion parameters of brain tissues like tortuosity, porosity and extracellular space in their water diffusion model. Later on, a mathematical model describing effective tortuosity and effective diffusion in the extracellular space of the brain was studied by Harbe et al. [26]. A mathematical model describing oxygen transport in peripheral nerve tissue using Krogh cylinder symmetry was presented by Jain and Sharma [57]. Huang et al. [31] found an exact solution for one-dimensional solute transport in heterogeneous porous media with scale-dependent dispersion.

1.3.3 Fractional model for blood flow in a stenosed artery under MHD effect through a porous medium

It is quite well-known that blood also exhibits biomagnetic characteristics like any other biomagnetic fluid. The matured red blood cells in human blood contain highly concentrated hemoglobin molecules (oxides of iron), which are one of the main reasons behind the magnetic nature of blood. The state of oxygenation state directly affects the blood magnetic property (Sharma et al. [58], Jain et al. [30]). Considerable amount of research has been carried out in studying the blood flow in arteries by treating blood to be sometimes a Newtonian, sometimes a non-Newtonian fluid. As most of the physical phenomena are connected with a porous medium, it is of utmost importance to investigate the magnetic field effect on the fluid in the porous medium - both theoretically and practically.

The mathematical framework of biofluid, analogous to that of the ferrohydrodynamics, was first developed by Haik et al. [23]. They neglected the induced electric field effect and considered only the magnetic field effect (applied from an external source) on the fluid. Many researchers have investigated blood flow in the light of magnetohydrodynamics, which, with the help of electrical conducting fluids, includes the Lorenz force caused by the induced currents and ignores the magnetization effect (Varshney et al. [63]).

1.3.4 Fractional model for ion diffusion in the extracellular microenvironment of the rat cerebellum

The diffusion of ions in the microenvironments of the brain cell is of paramount gravity in the context of analysing the physiology of neuronal populations. An ion, which moves in the interstitial spaces between capillaries or cells can be referred as the most general instance for the diffusion phenomenon in the microenvironments of the brain cell. As long as the ion sustains its low concentration in an aqueous or a free medium, its movement obeys the Fickian diffusion laws which reflect the microscopic behaviour of Brownian motion of the ions at a macroscopic level. This Brownian motion is defined as the collection of all the paths traced by the random walks resulted by the collisions of the ions and the solvent molecules of the medium. The diffusion process in a complex medium may have restrictions owing to several factors. The fundamental ones are the inevitable aftermaths caused by the complex geometry of the medium. In addition, uptake, binding or structural deformation with respect to the time caused by some particular properties of a certain medium can be mentioned as the secondary ones. The extracellular milieu of a neuron consists of neuroactive compounds, metabolic substrates and different ions that can have remarkable effect on the short-term and long-term neuronal phenomenon. Hence, the diffusion of these extracellular substances in the microenvironments of the brain cell can be inferred as an important factor. Brain cell microenvironment consists of the microscopic inorganic ions which are one of the most common chemical particles, and their study has caught more importance than earlier times since ion-selective micropipette helps depicting meaningful differences during neuronal phenomena (Nicholson and Phillips [44], Somjen [60]).

Many studies have been carried out in this direction concerning the ion diffusion in brain tissue; the radio tracer is being utilized in most of them. These methods were developed from the ones used in muscles (Harris and Burn [24], Keynes [32]). But they do not present sufficient accuracy in spatio-temporal analysis and, therefore, have most generally ended up with certain issues, for example, the extracellular space volume.

To come up with a solution to incorporate the implicit analysis of the previous works, Nicholson and Phillips [44] undertook the study of ion transport in the extracellular microenvironments of the rat cerebellum.

1.4 Motivation

It is a well-known fact that most of the physical phenomena can be modelled using integer-order differential equations as the governing equations. Of late, however, it has been realized that fractional-order differential equations represent physical phenomena in a more appropriate way as compared to integer-order differential equations. Although not many

researchers have come forward in utilizing fractional-order differential equations, it can still be observed that modelling through such equations has received more importance than before. In various mathematical modelling of biological problems, researchers have found that there are some attributes which the integer-order models lack. The difference is quite vivid when they tried to validate their model by fitting the experimental data to their models. As the fractional models are renowned for their special ability in capturing the experimental data in a more accurate manner and depicting the biological phenomena more profoundly in most instances, we intend to apply the same methodology to investigate some biological phenomena where integer-order models were found not capable of meeting the expectations of the researchers.

It is worthwhile mentioning that, in this thesis, our effort is restricted to application-based fractional differential equations only; it does not make any attempt to analyze the qualitative nature of the equations. In other words, we do not touch upon explicitly the theoretical analysis like uniqueness, stability and convergence of the solutions at present and wish to study them in the sooner future. However, although we put aside these analyses for the time being, but it can be observed that the uniqueness of solution can be achieved for the model solutions by means of the linearity of the Caputo derivative (since our all models are linear only), and the convergence can be followed from the graphical analysis. As the explicit solutions for the models are at our disposal, finding some estimates for the model parameters seems not that much difficult for examining the stability.

1.5 Organization of the thesis

The thesis is arranged in the following manner:

- Chapter 2 presents a new solution to the time-fractional ESR model, taking into account the non-zero uniform average blood velocity. We not only obtain an analytic solution to the generalized model of Sharma et al. [56] and da Sousa et al. [7], but also present some new results which establish that the developed fractional-order model is a better-suited one through which prediction of the ESR rate can take place more accurately. The same is established through graphs and tables which point toward a more practical ESR model. Furthermore, through numerical experiments, the appropriate values of the uniform blood velocity and the order of the fractional derivative are recommended.

- In Chapter 3, a new insight is presented into the solution of the erythrocyte sedimentation rate (ESR) model, based on fractional derivative with respect to time, with non-zero uniform velocity of blood by incorporating the concentration gradient of the blood nutrients. An analytical solution is acquired for the modified ESR

fractional model in addition to presenting some new interesting results. The best possible suitable range for the concentration gradient is found for the model whose use will be helpful in approximating the clinical data from laboratory tests in a profound and accurate manner, and also in diagnosing the ESR rate more accurately. Further, an appropriate range is proposed for the uniform velocity of blood as well as the fractional order of the time derivative to construct the feasible model. In addition, it is also shown what value of the fractional order gives a closer resemblance to the clinical data. Validation and verification of the obtained results against earlier results demonstrate the effectiveness of the proposed model.

- Chapter 4 elucidates the process of mass transport to brain tissues in a mathematical framework by considering two concepts of porosity and tortuosity in the model. Henceforth, the analytical solutions to the mass transport model are also obtained to find the response functions by means of which the transport process becomes quite explicit. For a better insight into the transport process, a graphical analysis is also taken into account. The newly-developed fractional version not only presents better-suited analytical solutions to the model but additionally the graphs also show the matching of the solutions for both integer-order and fractional models. Based on the approximation for four sets of experimental data made by the analytical solution through means of graphical and numerical results, the fractional model also leads to the selection of the best possible values for the fractional order. We also establish the credibility of the fractional-order model in approximating a wide class of experimental data taken form the laboratory.

- Chapter 5 presents a fractional approach as a substitute to the integer-order model, describing the MHD effect of blood flow in a stenosed artery. We not only obtain an analytical solution for the fractional governing equation but also present an expression for the wall-shear stress. After the successful verification of our model with existing literature, we analyze the obtained plots by using the analytic expression. We exhibit how the fractional model is helpful in controlling the blood flow through a stenosed artery. We also show that the external magnetic field, along with the fractional order of the governing equation, plays a pivotal role in the solution of the problem involving the treatment of stenosis.

- In Chapter 6, we discuss a generalized version of the ion transport model presented by Nicholson and Phillips [44], which illustrates the diffusion process in the extracellular microenvironment of the rat cerebellum. We obtain a fractional-order model by generalizing the integer-order derivative to study the transport process. The analytical solution appears to be of utmost importance in approximating the experimental data existing in the literature. We carry out graphical and tabular

analysis, comparing our result with the existing ones which shows our model to be a better-suited one. We also prescribe the best possible value for the fractional derivative to reach the best match with the experimental data.

- Chapter 7 summarizes the results obtained in the previous chapters and gives some direction for future study based on the results obtained in this thesis.

2

ESR fractional model with non-zero uniform average blood velocity

This chapter proposes and discusses a new solution corresponding to the time-fractional ESR model, taking into account the non-zero uniform average blood velocity. We not only obtain an analytic solution to the generalized model of Sharma et al. [56] and da Sousa et al. [7], but also present some new results which establish that the developed fractional-order model is a better-suited one through which prediction of the ESR can take place more accurately. The same is established through graphs and tables which point toward a more practical ESR model. Furthermore, through numerical experiments, the appropriate values of the uniform blood velocity and the order of the fractional derivative are recommended.

2.1 Fractional ESR model

In this section, we present the most generalized mathematical model of ESR test devised by Sharma et al. [56] by replacing the integer-order linear partial differential equation by a fractional-order equation to examine the ESR test in order to look at the behaviour of the concentration of nutrients in blood cells which explicitly influences ESR to a large extent. This time-fractional model is to be developed for erythrocyte sedimentation rates by utilizing the available methods to solve the governing fractional-order partial differential equation. We are going to adopt Caputo time-fractional derivative so as to illustrate that the developed model presents the generalization of the integer-order model.

Following Sharma et al. [56], let $C(x,t)$ be the blood concentration of nutrients which satisfies the following nonhomogeneous partial differential equation of integer order:

$$D_L \frac{\partial^2 C}{\partial x^2} - U\frac{\partial C}{\partial x} - \frac{\partial C}{\partial t} = \phi(x,t), \tag{2.1}$$

where U denotes the average fluid velocity considered over the flow area normal to the

tube, D_L is the coefficient of axial dispersion which describes the pattern of movement of erythrocytes with respect to a point in the system and $\phi(x,t)$ represents a twice continuously differentiable function which describes the nutrient transfer rate. It may be noted that the permeability of the walls of the capillaries (i.e., arteries) to the constituent is of significance. Because of this, the right hand side of Eq. (2.1) stays non-zero. We wish to study the time-fractional form of Eq. (2.1) which is

$$D_L \frac{\partial^2 C}{\partial x^2} - U\frac{\partial C}{\partial x} - \frac{\partial^\alpha C}{\partial t^\alpha} = \phi(x,t), \tag{2.2}$$

where $0 < \alpha \leq 1$. Here, we consider the Caputo fractional derivative (Podlubny [48], Caputo and Mainardi [5], Gorenflo and Mainardi [18]) of order α defined as in Eqs. (1.4)-(1.6).

Furthermore, the transfer rate $\phi(x,t)$, dependent on the nutrient concentration, satisfies the following partial differential equation:

$$D\frac{\partial^2 \phi}{\partial x^2} - K\phi(x,t) - \frac{\partial \phi}{\partial t} = 0, \tag{2.3}$$

where D and K are both positive constants describing the diffusivity of oxygen in the tissue in the nutrient and the transfer coefficient, respectively. It may be noted that, in the limit $\alpha \to 1$, Eq. (2.2) becomes Eq. (2.1). Now it is of utmost importance that we first obtain a solution $\phi(x,t)$ of Eq. (2.3) before turning our attention to Eq. (2.2) for solving $C(x,t)$.

The following initial and boundary conditions can be imposed:

$$\begin{cases} \phi(x,0) = \exp(-bx); & x \geq 0, K \geq a, \\ \phi(0,t) = \exp(-at); & t > 0, \\ \phi(x,t)|_{x\to\infty} = 0; & t > 0, \end{cases}$$

where $b^2 = \dfrac{K-a}{D}$ and a is a constant which needs to be conveniently chosen from a known value of $\phi(x,t)$. By applying separation of variables technique, Eq. (2.3) leads to the solution

$$\phi(x,t) = \exp\{-(at+bx)\}. \tag{2.4}$$

Furthermore, we consider the following initial and boundary conditions for solving Eq. (2.2):

$$\begin{cases} C(x,0) = 0; & x \geq 0, \\ C(0,t) = 1; & t > 0, \\ C(x,t)|_{x\to\infty} = 0; & t > 0. \end{cases} \tag{2.5}$$

The conditions (2.5) have already found sufficient importance in the works of Sharma et al. [56] and da Sousa et al. [7] with respect to obtaining the analytic solutions for their models and similar is the case for our generalised model too. The spatial variable x stands for the distance from the boundary of an artery. An increase in the concentration of nutrients in blood is observed as the boundary is approached (i.e., $x \to 0$) at which its maximum value is attained. This in turn gives rise to the boundary condition $C(0,t) = 1;\ \forall t > 0$. On the other hand, the concentration of nutrients reduces away from the boundary (i.e., for $x > 0$). In order to present a simplified model, the concentration is assumed to be zero at infinity giving rise to the other boundary condition $C(x,t) = 0$ as $t \to \infty$. Since the concentration is initially zero for every $x > 0$, the initial condition can be written as $C(x,0) = 0$. Relevance and understanding of these conditions will be clearer from the graphs that will be plotted in Section 2.3.

2.2 Analytical solution

It is a known fact that Laplace transform method is a very appropriate method to solve fractional differential equations. Therefore, we also employ the method of Laplace transform appropriately so that the nonhomogeneous time-fractional partial differential equation gets converted to a nonhomogeneous linear ordinary differential equation of integer order. This can be accomplished by taking Laplace transform with respect to t to both sides of Eq. (2.2) to get

$$D_L \frac{d^2}{dx^2}\bar{C}(x,s) - U\frac{d}{dx}\bar{C}(x,s) - s^{\alpha}\bar{C}(x,s) + s^{\alpha-1}C(x,0) = \frac{e^{-bx}}{s+a}, \tag{2.6}$$

where $\bar{C}(x,s) = \mathcal{L}\{C(x,t)\} = \int_0^{\infty} e^{-st}C(x,t)dt$ denotes the Laplace transform of $C(x,t)$ in the parameter s, $\mathrm{Re}(s) > 0$.

Incorporating the initial condition $C(x,0) = 0$, Eq. (2.6) becomes

$$D_L \frac{d^2}{dx^2}\bar{C}(x,s) - U\frac{d}{dx}\bar{C}(x,s) - s^{\alpha}\bar{C}(x,s) = \frac{\exp(-bx)}{s+a}. \tag{2.7}$$

Using the variation of parameters technique in Eq. (2.7), and then applying the boundary conditions, we obtain its solution $\bar{C}(x,s)$ as

$$\bar{C}(x,s) = \left(\frac{1}{s} + \frac{1}{(s+a)(s^{\alpha}-\beta)}\right)\exp\left\{\frac{x}{2}\left(\frac{U}{D_L} - \sqrt{\frac{U^2}{D_L^2} + \frac{4s^{\alpha}}{D_L}}\right)\right\} - \frac{\exp(-bx)}{(s+a)(s^{\alpha}-\beta)}, \tag{2.8}$$

where $\beta = D_L b^2 + Ub$.

In order to obtain the solution $C(x,t)$, inverse Laplace transform is applied to both sides of Eq. (2.8) to get

$$\begin{aligned} C(x,t) &= \mathcal{L}^{-1}\{\bar{C}(x,s)\} \\ &= \mathcal{L}^{-1}\left\{\frac{\exp\left\{\frac{x}{2}\left(\frac{U}{D_L}-\sqrt{\frac{U^2}{D_L^2}+\frac{4s^\alpha}{D_L}}\right)\right\}}{s}\right\} + \mathcal{L}^{-1}\left\{\frac{\exp\left\{\frac{x}{2}\left(\frac{U}{D_L}-\sqrt{\frac{U^2}{D_L^2}+\frac{4s^\alpha}{D_L}}\right)\right\}}{(s+a)(s^\alpha-\beta)}\right\} \\ &\quad - \mathcal{L}^{-1}\left\{\frac{\exp(-bx)}{(s+a)(s^\alpha-\beta)}\right\}, \end{aligned} \tag{2.9}$$

which can be rewritten in a compact form as

$$C(x,t) = \exp\left(\frac{xU}{2D_L}\right)\{C_1(x,t)+C_2(x,t)\} - \exp(-bx)C_3(x,t), \tag{2.10}$$

where

$$\begin{aligned} C_1(x,t) &= \mathcal{L}^{-1}\left\{\frac{\exp\left\{\frac{x}{2}\left(-\sqrt{\frac{U^2}{D_L^2}+\frac{4s^\alpha}{D_L}}\right)\right\}}{s}\right\}, \\ C_2(x,t) &= \mathcal{L}^{-1}\left\{\frac{\exp\left\{\frac{x}{2}\left(-\sqrt{\frac{U^2}{D_L^2}+\frac{4s^\alpha}{D_L}}\right)\right\}}{(s+a)(s^\alpha-\beta)}\right\}, \\ C_3(x,t) &= \lim_{x\to 0} C_2(x,t). \end{aligned}$$

Now each of the above inverses is calculated individually. For calculating $C_1(x,t)$, by expanding the exponential function and the binomial expression, we have

$$\begin{aligned} &\frac{\exp\left\{\frac{x}{2}\left(-\sqrt{\frac{U^2}{D_L^2}+\frac{4s^\alpha}{D_L}}\right)\right\}}{s} \\ &\quad = \sum_{k=0}^{\infty}\frac{\left(-\frac{x}{\sqrt{D_L}}\right)^k}{k!}\sum_{l=0}^{\infty}\frac{\left(\frac{k}{2}\right)\left(\frac{k}{2}-1\right)\ldots\left(\frac{k}{2}-l+1\right)}{l!}\left(\frac{U}{2\sqrt{D_L}}\right)^{2l} s^{-(1+\alpha l-\frac{\alpha k}{2})}, \end{aligned} \tag{2.11}$$

where $|\, s^{\alpha} \,| > U^2/4D_L$. Then, by taking inverse Laplace transform on Eq. (2.11), $C_1(x,t)$ is obtained as follows:

$$C_1(x,t) = \mathcal{L}^{-1}\left\{\frac{\exp\left\{\frac{x}{2}\left(-\sqrt{\frac{U^2}{D_L^2}+\frac{4s^{\alpha}}{D_L}}\right)\right\}}{s}\right\}$$

$$= \mathcal{L}^{-1}\left\{\sum_{k=0}^{\infty}\frac{\left(-\frac{x}{\sqrt{D_L}}\right)^k}{k!}\sum_{l=0}^{\infty}\frac{\left(\frac{k}{2}\right)\left(\frac{k}{2}-1\right)\ldots\left(\frac{k}{2}-l+1\right)}{l!}\left(\frac{U}{2\sqrt{D_L}}\right)^{2l} s^{-(1+\alpha l-\frac{\alpha k}{2})}\right\}$$

$$= \sum_{k=0}^{\infty}\frac{\left(-\frac{x}{\sqrt{D_L}}\right)^k}{k!}\sum_{l=0}^{\infty}\frac{\left(\frac{k}{2}\right)\left(\frac{k}{2}-1\right)\ldots\left(\frac{k}{2}-l+1\right)}{l!}\left(\frac{U}{2\sqrt{D_L}}\right)^{2l}\mathcal{L}^{-1}\left\{s^{-(1+\alpha l-\frac{\alpha k}{2})}\right\}. \quad (2.12)$$

Utilizing the standard result $\mathcal{L}^{-1}\left\{s^{-p_\alpha}\right\} = \dfrac{t^{p_\alpha-1}}{\Gamma(p_\alpha)}$, with $\mathrm{Re}(p_\alpha) > 0$, $p_\alpha = 1+\alpha l-\dfrac{\alpha k}{2}$, Eq. (2.12) can be rewritten as

$$C_1(x,t) = \sum_{k=0}^{\infty}\frac{\left(-\frac{x}{\sqrt{D_L}}\right)^k}{k!}\sum_{l=0}^{\infty}\frac{\left(\frac{k}{2}\right)\left(\frac{k}{2}-1\right)\ldots\left(\frac{k}{2}-l+1\right)\left(\frac{U}{2\sqrt{D_L}}\right)^{2l}}{l!}\frac{t^{(\alpha l-\frac{\alpha k}{2})}}{\Gamma(1+\alpha l-\frac{\alpha k}{2})}. \quad (2.13)$$

Proceeding in a similar manner, expanding the exponential and the binomial expression in $C_2(x,t)$, we get

$$\frac{\exp\left\{\frac{x}{2}\left(-\sqrt{\frac{U^2}{D_L^2}+\frac{4s^{\alpha}}{D_L}}\right)\right\}}{(s+a)(s^{\alpha}-\beta)}$$

$$= \sum_{k=0}^{\infty}\frac{\left(-\frac{x}{\sqrt{D_L}}\right)^k}{k!}\sum_{l=0}^{\infty}\frac{\left(\frac{k}{2}\right)\left(\frac{k}{2}-1\right)\ldots\left(\frac{k}{2}-l+1\right)}{l!}\left(\frac{U}{2\sqrt{D_L}}\right)^{2l}\frac{s^{-(\alpha l-\frac{\alpha k}{2})}}{(s+a)(s^{\alpha}-\beta)}. \quad (2.14)$$

Invoking inverse Laplace transform on Eq. (2.14), we get

$$\mathcal{L}^{-1}\left\{\frac{\exp\left\{\frac{x}{2}\left(-\sqrt{\frac{U^2}{A^2}+\frac{4s^{\alpha}}{D_L}}\right)\right\}}{(s+a)(s^{\alpha}-\beta)}\right\}$$

$$= \sum_{k=0}^{\infty}\frac{\left(-\frac{x}{\sqrt{D_L}}\right)^k}{k!}\sum_{l=0}^{\infty}\frac{\left(\frac{k}{2}\right)\left(\frac{k}{2}-1\right)\ldots\left(\frac{k}{2}-l+1\right)\left(\frac{U}{2\sqrt{D_L}}\right)^{2l}}{l!}\mathcal{L}^{-1}\left\{\frac{s^{-(\alpha l-\frac{\alpha k}{2})}}{(s+a)(s^{\alpha}-\beta)}\right\}.$$

Using the transformation formula followed by da Sousa et al. [7], we obtain

$$C_2(x,t) = t^{\alpha}\sum_{k=0}^{\infty}\frac{\left(-\frac{xt^{-\frac{\alpha}{2}}}{\sqrt{D_L}}\right)^k}{k!}\sum_{l=0}^{\infty}\frac{\Gamma(1+\frac{k}{2})\left(\frac{U^2t^{\alpha}}{4D_L}\right)^l}{l!\Gamma(1+\frac{k}{2}-l)}\sum_{m=0}^{\infty}(-at)^m\mathbb{E}_{\alpha,1+\alpha+\alpha l+m-\frac{\alpha k}{2}}(\beta t^{\alpha}), \tag{2.15}$$

where $\mathbb{E}_{\alpha,\beta}(.)$ represents the Mittag-Leffler function of two parameters. Next, obtaining the inverse Laplace transform of $C_3(x,t)$ is not a difficult task at all which can be obtained by considering $x \to 0$ in Eq. (2.15). Subsequently, this limit gives rise to only one term, that is, for $k = 0$ (which enforces l also to be zero), and we get

$$C_3(x,t) = t^{\alpha}\sum_{m=0}^{\infty}(-at)^m\mathbb{E}_{\alpha,1+\alpha+m}(\beta t^{\alpha}). \tag{2.16}$$

Thus, accumulating the results from Eqs. (2.13), (2.15) and (2.16), we obtain the solution of the full problem, i.e., a solution comprising the solutions of Eq. (2.2) and Eq. (2.5) as

$$\begin{aligned} C(x,t) = &\left(\sum_{k=0}^{\infty}\frac{\left(-\frac{x}{\sqrt{D_L}}\right)^k}{k!}\sum_{l=0}^{\infty}\frac{\left(\frac{k}{2}\right)\left(\frac{k}{2}-1\right)\ldots\left(\frac{k}{2}-l+1\right)}{l!}\left(\frac{U}{2\sqrt{D_L}}\right)^{2l}\frac{t^{(\alpha l-\frac{\alpha k}{2})}}{\Gamma(1+\alpha l-\frac{\alpha k}{2})}\right.\\ &\left.+t^{\alpha}\sum_{k=0}^{\infty}\frac{\left(-\frac{xt^{-\frac{\alpha}{2}}}{\sqrt{D_L}}\right)^k}{k!}\sum_{l=0}^{\infty}\frac{\Gamma(1+\frac{k}{2})\left(\frac{U^2t^{\alpha}}{4D_L}\right)^l}{l!\Gamma(1+\frac{k}{2}-l)}\sum_{m=0}^{\infty}(-at)^m\mathbb{E}_{\alpha,1+\alpha+\alpha l+m-\frac{\alpha k}{2}}(\beta t^{\alpha})\right)\\ &\times\exp\left(\frac{xU}{2D_L}\right)-\{\exp(-bx)\}t^{\alpha}\sum_{m=0}^{\infty}(-at)^m\mathbb{E}_{\alpha,1+\alpha+m}(\beta t^{\alpha}). \end{aligned} \tag{2.17}$$

2.3 Model verification

The fractional model considered in this work is a generalised model for describing the concentration of nutrients in blood cells that directly affects ESR. Consequently, this model must be able to recover the models of Sharma et al. [56] and da Sousa et al. [7] as particular cases. Now we are going to present two particular cases which will establish the agreement of our model to the above-mentioned models. From Eq. (2.2), it is evident that when the average blood velocity U is taken to be zero, the solution must match the solution presented by da Sousa et al. [7]. Further, when $\alpha \to 1$, then the present solution must match the solution presented by Sharma et al. [56].

When we put $U = 0$ in Eq. (2.17), it becomes

$$C(x,t) = \sum_{k=0}^{\infty} \frac{\left(-\frac{x}{\sqrt{D_L}}\right)^k}{k!} \frac{t^{-\frac{\alpha k}{2}}}{\Gamma(1-\frac{\alpha k}{2})} + t^{\alpha} \sum_{k=0}^{\infty} \frac{\left(-\frac{xt^{-\frac{\alpha}{2}}}{\sqrt{D_L}}\right)^k}{k!} \times \sum_{m=0}^{\infty} (-at)^m \mathbb{E}_{\alpha,1+\alpha+m-\frac{\alpha k}{2}}(\beta t^{\alpha}) - e^{-bx} t^{\alpha} \sum_{m=0}^{\infty} (-at)^m \mathbb{E}_{\alpha,1+\alpha+m}(\beta t^{\alpha}). \tag{2.18}$$

Now re-indexing Eq. (2.19) and introducing the Wright function, we get

$$\begin{aligned} C(x,t) &= \mathbb{W}\left(-\frac{\alpha}{2}, 1; -\frac{x}{\sqrt{D_L} t^{\frac{\alpha}{2}}}\right) + t^{\alpha} \sum_{m=0}^{\infty} \frac{\left(-\frac{xt^{-\frac{\alpha}{2}}}{\sqrt{D_L}}\right)^m}{m!} \sum_{k=0}^{\infty} (-at)^k \mathbb{E}_{\alpha,1+\alpha+k-\frac{\alpha m}{2}}(\beta t^{\alpha}) \\ &\quad - e^{-bx} t^{\alpha} \sum_{m=0}^{\infty} (-at)^m \mathbb{E}_{\alpha,1+\alpha+m}(\beta t^{\alpha}), \end{aligned} \tag{2.19}$$

where $\mathbb{W}(\alpha, \beta; .)$ is the two-parameter Wright function. Now it can be checked and easily noticed that solution (2.19) exactly matches the corresponding solution in da Sousa et al. [7].

Let us now analyse it in a graphical sense. For this purpose, there is a requirement to select values of some relevant parameters that appear in the solution given by Eq. (2.17). Based on information available from literature, the following values are considered: $D_L = 4.8 \times 10^{-4}$ (Schirmer et al. [53]); $D = 9.8 \times 10^{-5}$ (Grote et al. [20]); $K = 1.5 \times 10^{-4}$ (Aksnes et al. [2]) and $a = -0.005 \times 10^{-4}$ (Aksnes et al. [2]). Furthermore, the time is fixed at $t = 15$ and a certain interval for x is considered as $[0, 4]$, which can be extended if required. Furthermore, for the time being, we take the average blood velocity to be zero, i.e., $U = 0$. Later on, we will extend our discussion by considering the non-zero values of U. Further, the maximum number of iterations (N) is taken to be 70 (Sharma et al. [56], da Sousa et al. [7, 11]). This choice of $N = 70$ is established a little later.

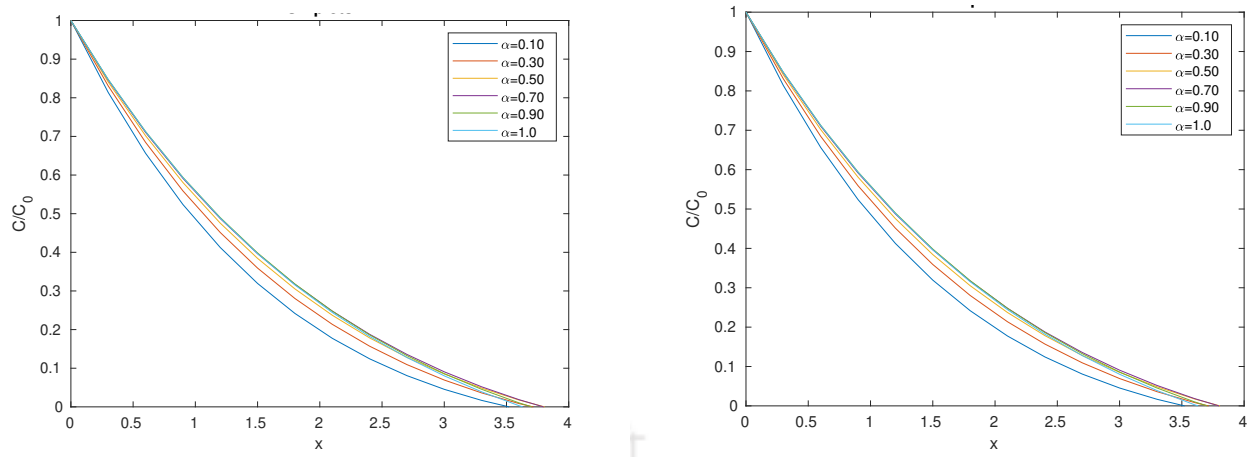

(a) (b)

Figure 2.1: Comparison of results for different values of α, with $U = 0$, $D_L = 4.8 \times 10^{-4}$, $D = 9.8 \times 10^{-5}$, $K = 1.5 \times 10^{-4}$, $a = -0.005 \times 10^{-4}$, $t = 15$ and $N = 70$: (a) *solution of da Sousa et al. [7],* (b) *present solution (2.17).*

Figure 2.1(a) corresponds to the analytical solution (2.19) while Fig. 2.1(b) corresponds to the present solution (2.17) while considering $U = 0$. It can be clearly observed that the plots of these two figures are identical. Therefore, graphical agreement between these two results is established.

Next, let us take the case into account when $\alpha \to 1$ but with non-zero U, in the solution (2.17). Here we discuss the cases graphically.

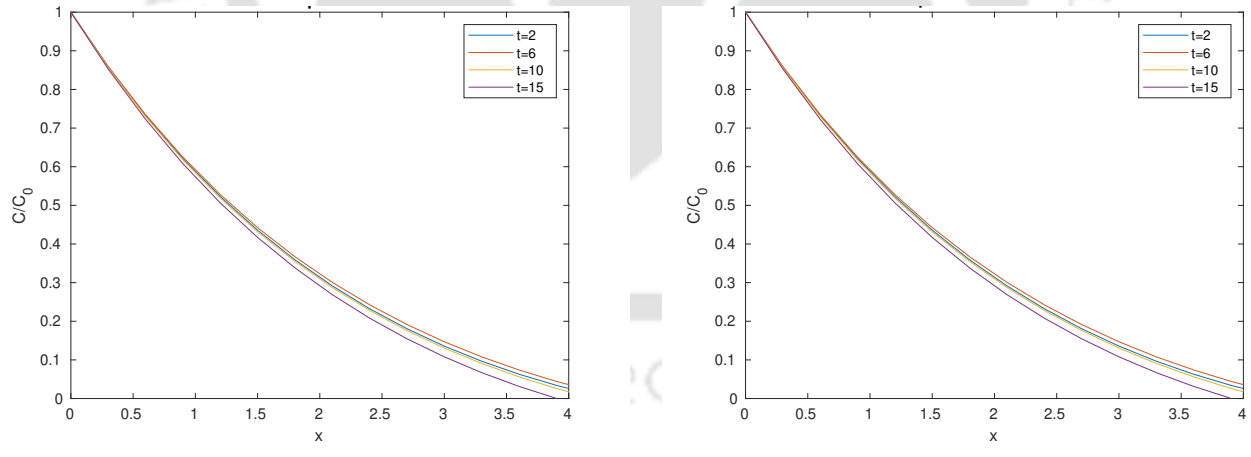

(a) (b)

Figure 2.2: Comparison of results for different t, with $U = 0.1$, $D_L = 4.8 \times 10^{-4}$, $D = 9.8 \times 10^{-5}$, $K = 1.5 \times 10^{-4}$, $a = -0.005 \times 10^{-4}$ and $N = 70$: (a) *solution of Sharma et al. [56],* (b) *present solution (2.17).*

Figure 2.2(a) represents the solution of Sharma et al. [56] at different time levels for a particular value of the average velocity U while Fig. 2.2(b) represents the present solution at these time levels and at the same value of U. Here, we consider the uniform blood

velocity $U = 0.1$, i.e., of order 10^{-1}. Considering another value of U, e.g., $U = 0.01$, i.e., when U is of order 10^{-2} and keeping all the parameters the same as before, the solutions are plotted for both models.

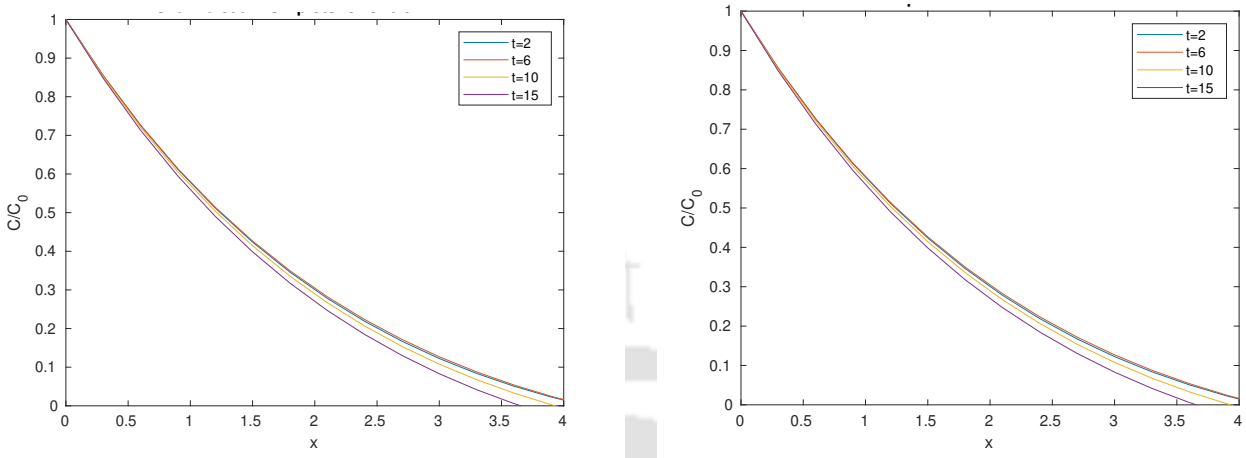

Figure 2.3: Comparison of solutions for different t, with $U = 0.01$, $D_L = 4.8 \times 10^{-4}$, $D = 9.8 \times 10^{-5}$, $K = 1.5 \times 10^{-4}$, $a = -0.005 \times 10^{-4}$ and $N = 70$: (a) *solution of Sharma et al. [56]*, (b) *present solution (2.17)*.

It is to be mentioned that, since U is the average velocity of blood, any arbitrary large value cannot be taken. It is also noticed that, when U is of the order 10^{-1} or 10^{-2} or smaller than these (i.e., of order 10^{-3}, 10^{-4},...), the solution of our model matches exactly (graphically) with that of Sharma et al. [56].

Finally, we conclude our discussion by having some insights on the choice of the appropriate iterations (N) used while conducting the graphical analysis throughout the work. Here, we present some plots for $U = 0$ and $U = 0.01$ with fixing the value of α so as to have resemblance with the earlier models of Sousa et al. [11] and Sharma et al. [56].

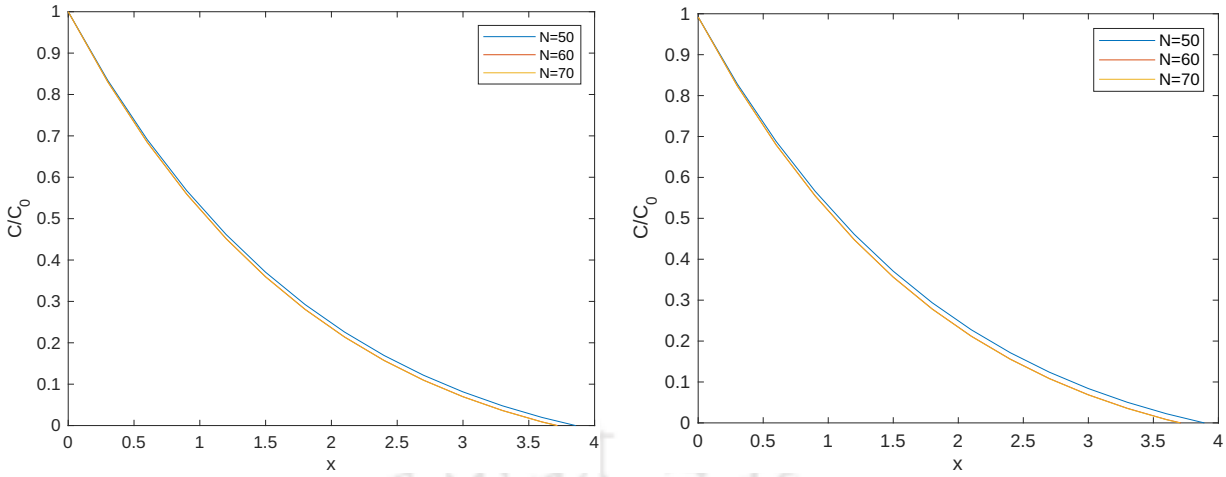

Figure 2.4: Plots for different N, with $D_L = 4.8 \times 10^{-4}$, $D = 9.8 \times 10^{-5}$, $K = 1.5 \times 10^{-4}$, $a = -0.005 \times 10^{-4}$, $\alpha = 0.3$ and $t = 15$: (a) for $U = 0$, (b) for $U = 0.01$.

Now, observing Fig. (2.4), it is clear that, for $N = 50,\ 60$, there exist some differences in the graphs plotted for C/C_0 against x for fixed values of some parameters. However, on the other hand, we find that the differences cease between $N = 60$ and $N = 70$. Although we show this here only for one instance for $\alpha = 0.3$, it can be shown that the pattern will be the same for other values of α too. Hence, we deem it appropriate to select $N = 70$ to be the best choice for the maximum number of iterations. Consequently, we go ahead with this value of maximum iteration for various plots related to our work. The same value of N is considered for the work in the next chapter too.

2.4 Results and discussion

The focus is now shifted to analyzing the graphs and data obtained from our work and examine their applicability by comparing them with the results in existing literature, e.g., Sharma et al. [56] and da Sousa et al. [7]. The endeavour is to consider the analytical solution (2.17) obtained for a number of values of parameters α and U. We also justify our choice for the most suitable value of α. As mentioned earlier on the choice of suitable values for U, i.e., in the range of 10^{-1} or smaller than that, we are going to present the data by comparing our experimental data with the above-mentioned existing works.

Table 2.1: Comparison of concentration $C(x,t)$ for $U = 0.1$, $\alpha = 1$, with $D_L = 4.8 \times 10^{-4}$, $D = 9.8 \times 10^{-5}$, $K = 1.5 \times 10^{-4}$, $a = -0.005 \times 10^{-4}$, $t = 15$ and $N = 70$.

x	Present work	Sharma et al. [56]	Difference
0	1	1.00000000005821	−5.821E-11
0.3	0.852784002578119	0.852784012153279	−9.575E-09
0.6	0.722677868994651	0.722677938232664	−6.923E-08
1.2	0.506378958976711	0.506378941106959	1.786E-08
1.8	0.33824762054428	0.338247656211024	−3.566E-08
2.4	0.208121641357138	0.208121757132176	−1.157E-07
3.0	0.107967878226191	0.107967846393876	3.183E-08
3.6	0.0314361465425463	0.0314349629261415	1.183E-06

Table 2.2: Comparison of concentration $C(x,t)$ for $U = 0.01$, $\alpha = 1$, with $D_L = 4.8 \times 10^{-4}$, $D = 9.8 \times 10^{-5}$, $K = 1.5 \times 10^{-4}$, $a = -0.005 \times 10^{-4}$, $t = 15$ and $N = 70$.

x	Present work	Sharma et al. [56]	Difference
0	1	0.999999999985448	1.455E-11
0.3	0.847708284476539	0.847708290268201	−5.791E-09
0.6	0.713301675918046	0.713301692914683	−1.699E-08
1.2	0.490373262378853	0.490373253269354	9.109E-09
1.8	0.317745267064311	0.317745225031104	4.203E-08
2.4	0.184770719628432	0.184770716026833	3.601E-09
3.0	0.083033792925562	0.0830334095953731	3.833E-07
3.6	0.00588234651149833	0.00588221217185492	1.343E-07

From Tables 2.1 and 2.2, it is not difficult to notice that, although the concentration differences are small, but at $x = 0$, the concentration must be exactly 1 (first boundary condition in (2.5)). But for both these cases of $U = 0.1$ and 0.01, the model of Sharma et al. [56] was unable to capture it which is a definite drawback. On the other hand, the present model recovers this condition appropriately. However, for smaller values of U, say $10^{-3}, 10^{-4}, \ldots$, the model in Sharma et al. [56] could exactly recover this condition which is accomplished by the present model too. Therefore, it can be concluded that, for these values of average velocity U, the present model performs better than that of Sharma et al. [56].

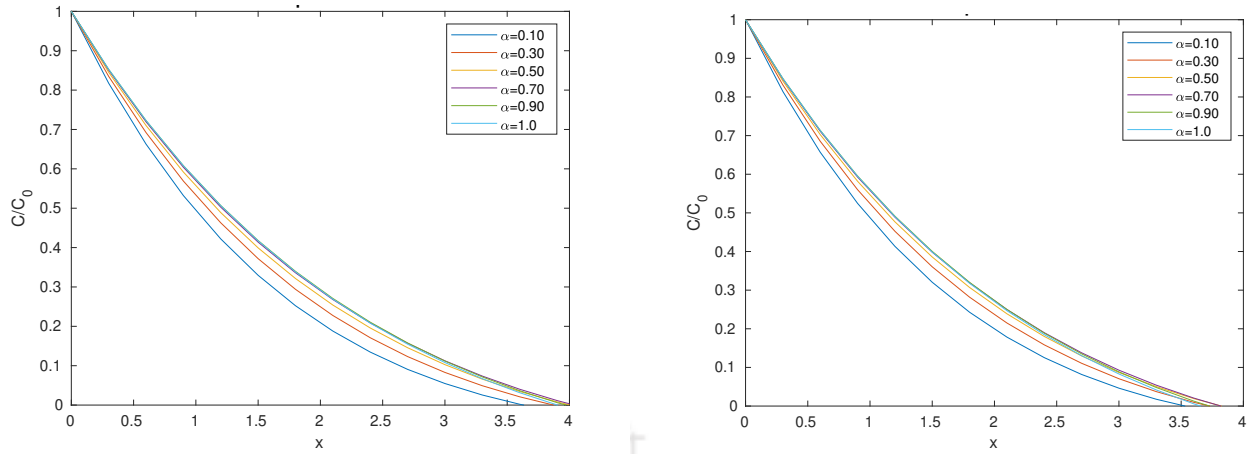

(a) (b)

Figure 2.5: Comparison of plots for different α and different U, with $D_L = 4.8 \times 10^{-4}$, $D = 9.8 \times 10^{-5}$, $K = 1.5 \times 10^{-4}$, $a = -0.005 \times 10^{-4}$, $t = 15$ and $N = 70$: (a) for $U = 0.1$, (b) for $U = 0.01$.

As seen from Table 2.1 and Table 2.2, the most appropriate values for U are $\leq 10^{-1}$. Now for these values of U, we are going to present the best choice for α.
The freedom given to the parameter α $(0 < \alpha \leq 1)$ makes it possible to provide a more accurate information with regard to the concentration of nutrients in the vicinity of the arterial extremity since the consideration of fractional derivative leads to the refinement of the solution. Observing Fig. 2.5(a) and Fig. 2.5(b), it is clear that, when we consider $\alpha = 0.10$ (further for $\alpha = 0.01$ too), the behaviour of the analytical solution remains the same near the artery $(x = 0)$ for a long time.

We consider the space variable $x \in [0, 4]$. The case when x lies in the range $[0, \infty)$ is also examined. However, it is noticed that, for $x \geq 3.8$, the level of C/C_0 remains below the x-axis and hence, it is sufficient to carry out the analysis only for the interval $[0, 4]$.

Although our analysis focuses on the analytical solutions restricted to six different values of the parameter α as $\alpha = 0.10, 0.30, 0.50, 0.70, 0.90, 1.0$, it is known that this parameter α is free and its other values could be considered too. We now justify our choice since, even if very smaller values of α are considered, e.g., $\alpha = 0.001$, the analysis would not be influenced - this fact can be easily established. We seek an appropriate value of α in such a way that the curve representing the analytical solution of Eq. (2.17) presents the best possible approximation to the curve obtained from real data (ESR test), as per the graphs presented in da Sousa et al. [11]. As we have already examined and chosen the appropriate values for the average blood velocity U, it is deemed appropriate to provide the appropriate value(s) of α corresponding to these values of U. To establish this fact, we are going to showcase some plots which will lead to the choice of the appropriate value(s) of α.

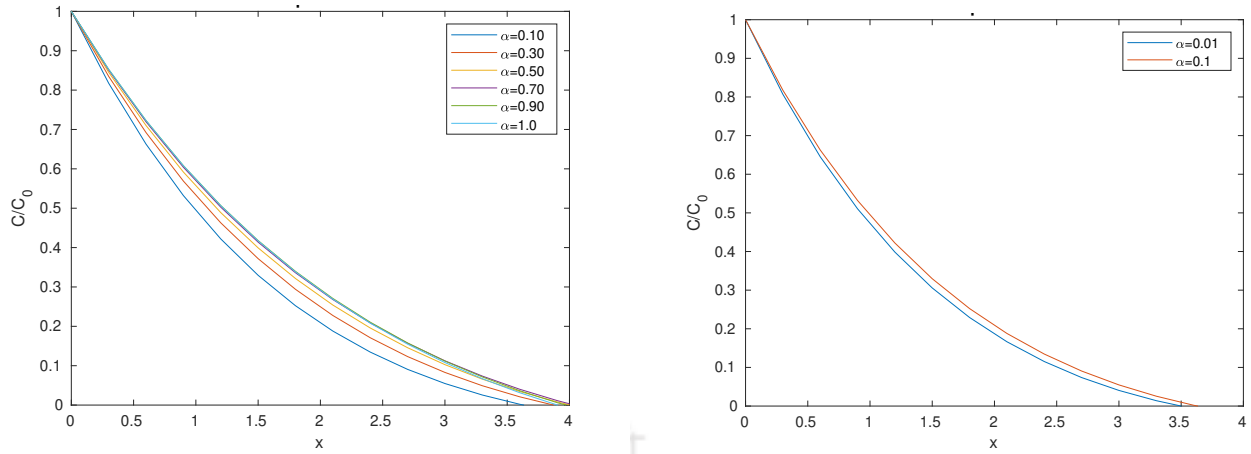

(a) (b)

Figure 2.6: Plots for different α, with $U = 0.1$, $D_L = 4.8 \times 10^{-4}$, $D = 9.8 \times 10^{-5}$, $K = 1.5 \times 10^{-4}$, $a = -0.005 \times 10^{-4}$, $t = 15$ and $N = 70$: (a) for $\alpha = 0.1, 0.3, 0.5, 0.7, 0.9, 1.0$, (b) for $\alpha = 0.01, 0.1$.

Apparently, we can obtain $\alpha = 0.1$ as a suitable choice for α by comparing our experimental results with the existing ones which is supported by Fig. 2.6(a). But we can actually achieve a better precision for α. Since Fig. 2.6(b) gives us the freedom to choose α to be 0.01, there occur some major differences in the concentration compared to the concentration due to $\alpha = 0.1$. For this case ($\alpha = 0.01$), the concentration curve is closer to the axes than that of the curve for $\alpha = 0.1$.

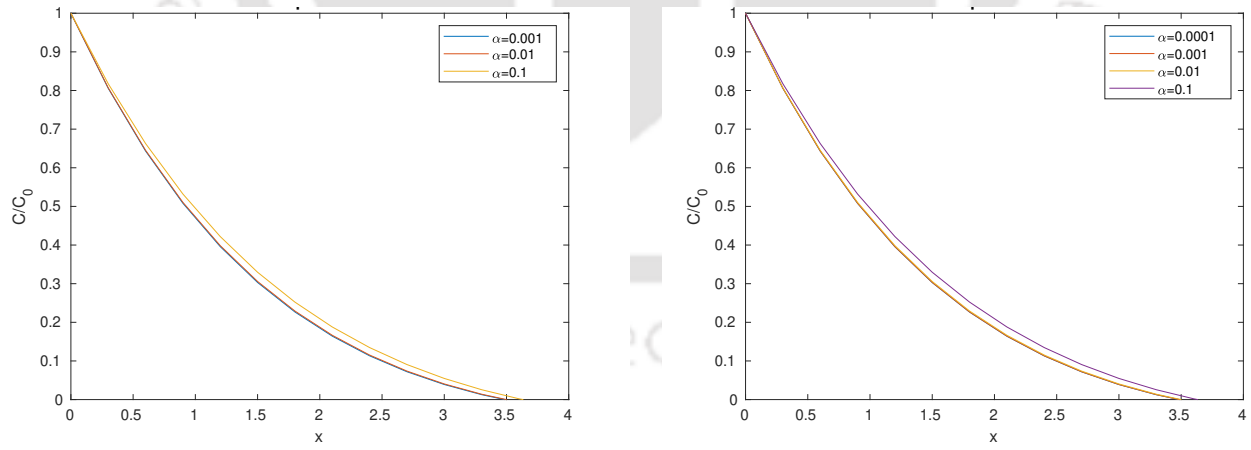

(a) (b)

Figure 2.7: Plots for different α, with $U = 0.1$, $D_L = 4.8 \times 10^{-4}$, $D = 9.8 \times 10^{-5}$, $K = 1.5 \times 10^{-4}$, $a = -0.005 \times 10^{-4}$, $t = 15$ and $N = 70$: (a) for $\alpha = 0.001, 0.01, 0.1$, (b) for $\alpha = 0.0001, 0.001, 0.01, 0.1$.

Figures 2.7(a) and 2.7(b) provide us a thought whether we should go below $\alpha = 0.01$ (e.g., $\alpha = 0.001$, 0.0001,...) since those curves overlap with that for $\alpha = 0.01$. Therefore,

we can prescribe $\alpha = 0.01$ to be the most appropriate choice of α for our model.

Now, we present a tabular comparison between the present model and that of da Sousa et al. [7]. For this case, we take all the relevant parameters to be the same, i.e., $U = 0$ and $\alpha = 0.01$.

Table 2.3: Comparison of concentration $C(x,t)$ for $U = 0$ and $\alpha = 0.01$, with $D_L = 4.8 \times 10^{-4}$, $D = 9.8 \times 10^{-5}$, $K = 1.5 \times 10^{-4}$, $a = -0.005 \times 10^{-4}$, $t = 15$ and $N = 70$.

x	Present work	da Sousa et al. [7]	Difference
0	1	1	0
0.3	0.803373371515465	0.803373371515465	0
0.6	0.639359753499042	0.639359753499042	0
1.2	0.389978992057281	0.389978992057281	0
1.8	0.220114176004586	0.220114176004587	−9.992E-16
2.4	0.106664481130936	0.106664481130937	−9.992E-16
3.0	0.0328905121671856	0.0328905121671856	0

Hence, by comparing the data from Table 2.3, it can be concluded that the present model relatively captures more accurate values of the concentration of ESR. All above mentioned essential computations and plottings are being carried out with the help of MATLAB R2021b.

2.5 Concluding remarks

As remarked by da Sousa et al. [11] that, for non-zero values of the blood velocity U, better results might exist, we have proceeded with that goal and successfully obtained it. This quantity U, however, appears in the model of Sharma et al. [56] governed by an integer-order partial differential equation. After analyzing all the results by taking U to be both zero and non-zero, we have presented some interesting results which can be termed better than the existing ones since these capture more attributes. For example, we can say that da Sousa et al. [7] previously obtained reasonable results for $\alpha = 0.1$ (fractional order of the differential equation) in their work, and we now have gone one step further since we have considered even a lower-order derivative with $\alpha = 0.01$. This gives a better approximation to the clinical data used in da Sousa et al. [11]. Therefore, we can infer that the incorporation of the non-zero average blood velocity has given us the freedom to go beyond the previous values of α. In a nutshell, we can claim that the present model is more appropriate in two senses: consideration of non-zero average blood velocity which is a more realistic scenario, and the generalization of the order of the time-fractional derivative to real order. Furthermore, appropriate values of the uniform average blood velocity and the order of the fractional derivative have been proposed which are expected to be helpful for future research in this direction.

3

Incorporation of concentration gradient of blood nutrients in ESR fractional model with non-zero uniform average blood velocity

A new insight is presented into the solution of the erythrocyte sedimentation rate (ESR) model, based on fractional derivative with respect to time, with non-zero uniform velocity of blood by incorporating the concentration gradient of the blood nutrients. An analytical solution is acquired for the modified ESR fractional model in addition to presenting some new interesting results. The best possible suitable range for the concentration gradient is found for the model whose use will be helpful in approximating the clinical data from laboratory tests in a profound and accurate manner, and also in diagnosing the ESR more accurately. Further, an appropriate range is proposed for the fractional order of the time derivative to construct the feasible model. In addition, it is also shown what value of the fractional order gives a closer resemblance to the clinical data. Validation and verification of the obtained results against earlier results demonstrate the effectiveness of the proposed model.

3.1 Modified ESR fractional model with concentration gradient

In this section, we present an efficient and modified mathematical model for the ESR test which was initially formulated by Sharma et al. [56] and then extended in the previous chapter by introducing the non-zero average blood velocity to achieve the best possible result till now. We further develop the ESR fractional model by incorporating the concentration gradient of the blood nutrients and utilizing appropriate tools to solve the formulated problem. This modified fractional model will be used to investigate the ESR test for understanding the behaviour of the concentration of nutrients in blood cells which directly influences ESR in a significant manner. The Caputo time-fractional derivative

is to be employed for finding an efficient and feasible solution corresponding to a more practical scenario.

Following Sharma et al. [56], we assume $C(x,t)$ to be the concentration of the nutrients in blood which is governed by the following non-homogeneous partial differential equation (which is the same as Eq. (2.1)):

$$D_L\frac{\partial^2 C}{\partial x^2} - U\frac{\partial C}{\partial x} - \frac{\partial C}{\partial t} = \phi(x,t), \tag{3.1}$$

where U is the average velocity of blood with the consideration of the blood flow to be uniform, D_L denotes the axial dispersion coefficient which implicates the behaviour of red blood cells with reference to a certain point in blood, and $\phi(x,t)$, a C^2-function, denotes the rate of nutrient transfer in blood. It is necessary to consider the permeability of the capillary walls (i.e., the wall of the arteries) as it influences the constituent. As a result, the right-hand side of Eq. (3.1) becomes non-homogeneous. We intend to study this equation with the incorporation of the time-fractional Caputo derivative in Eq. (3.1) (which is the same as Eq. (2.2)):

$$D_L\frac{\partial^2 C}{\partial x^2} - U\frac{\partial C}{\partial x} - \frac{\partial^\alpha C}{\partial t^\alpha} = \phi(x,t), \tag{3.2}$$

with $\alpha \in (0,1]$.

Moreover, $\phi(x,t)$, the function for rate of transfer of nutrients, varies according to the concentration of the nutrients of blood and is governed by the equation (which is the same as Eq. (2.3))

$$D\frac{\partial^2 \phi}{\partial x^2} - K\phi(x,t) - \frac{\partial \phi}{\partial t} = 0. \tag{3.3}$$

It is quite clear that, as $\alpha \to 1$, Eq. (3.2) takes the initial form, that is, Eq. (3.1).

Now, it is essential to obtain the expression for $\phi(x,t)$ explicitly by solving Eq. (3.3) before going for an expression for $C(x,t)$ for Eq. (3.2). Furthermore, we make use of the following initial and boundary conditions [56] with respect to Eq. (3.3):

$$\begin{cases} \phi(x,0) = \exp(-bx); & x \geq 0, K \geq a, \\ \phi(0,t) = \exp(-at); & t > 0, \\ \phi(x,t)|_{x\to\infty} = 0; & t > 0. \end{cases} \tag{3.4}$$

Rendering the method of separation of variables, we obtain the solution to Eq. (3.3) corresponding to the initial and boundary conditions in Eq. (3.4) as

$$\phi(x,t) = \exp\{-(at+bx)\}. \tag{3.5}$$

In addition, the following initial and boundary conditions are taken into account to solve Eq. (3.2):

$$\begin{cases} C(x,0) = C_0, & x \geq 0, \\ \frac{\partial C}{\partial x}(0,t) = C_1, & t > 0, \\ C(x,t)|_{x\to\infty} = C_2, & t > 0, \end{cases} \tag{3.6}$$

with C_0, C_1 and C_2 all as constants. Later on, while solving the fractional-order equation (3.2) by incorporating the prescribed initial and boundary conditions given by Eq. (3.6), it can be seen that the constants C_0 and C_2 take the same value, i.e., $C_0 = C_2$, and we subsequently take $C_0 = C_2 = 0$ by maintaining the physical significance of these constants. Further, the concentration gradient at the upper boundary is taken to be non-zero pertaining to the physical interpretation; otherwise, for zero concentration gradient, the flow of nutrients ceases to occur. The initial condition is considered to be constant here, and the most important aspect is the concentration gradient, i.e., the second expression of Eq. (3.6). It can be observed that this initial condition is not going to affect the flux or concentration gradient term, as the flux is associated at the upper boundary only and in the course of discussion, we establish that negative concentration gradient (having the usual interpretation) is going to play a pivotal role in the clinical data approximation.

The prescribed initial and boundary conditions for Eq. (3.2) were of paramount importance in Sharma et al. [56] and da Sousa et al. [7] for acquiring analytical solutions to the governing equations for the models. In the present model, almost the same initial and boundary conditions are considered with the addition of the concentration gradient condition at the starting boundary. In the course of the discussion to follow, it will be seen that the incorporation of this aforementioned concentration gradient helps not only in reaching an efficient solution but also in achieving the best possible solution.

The space variable x represents the distance of an artery from the boundary wall. The constant value of the concentration gradient at the starting boundary generally interprets the flow of blood from the higher concentration zone to the lower concentration zone. This fact is implicated by the negative value of the concentration gradient. This will be clearer when we plot the solutions for the variation of the concentration gradient. To make the model simpler, we consider the concentration to be zero at the other end which leads to the condition for the boundary at infinity to be $C(x,t) = 0$ as $x \to \infty$, which is a realistic one since the concentration gets reduced as it is absorbed by the cells at this end. We write the initial condition as $C(x,0) = 0$ since there is no concentration initially for every $x > 0$. Better understanding and a clearer insight will follow when we plot the solutions and analyze them in Section 3.3.

3.2 Analytical solution

By employing Laplace transform with respect to t to both sides of Eq. (3.2) (with the aid of Eq. (1.15)), we obtain

$$D_L\frac{d^2\bar{C}}{dx^2}(x,s)+s^{\alpha-1}C(x,0)-U\frac{d\bar{C}}{dx}(x,s)-s^{\alpha}\bar{C}(x,s)=\frac{\exp(-bx)}{s+a}. \tag{3.7}$$

Upon utilizing the initial condition $C(x,0)=0$, Eq. (3.7) leads to

$$D_L\frac{d^2\bar{C}}{dx^2}(x,s)-U\frac{d\bar{C}}{dx}(x,s)-s^{\alpha}\bar{C}(x,s)=\frac{\exp(-bx)}{s+a}. \tag{3.8}$$

At first, using the method of variation of parameters in Eq. (3.8), and then incorporating the boundary conditions, the solution $\bar{C}(x,s)$ of Eq. (3.7) is obtained as

$$\bar{C}(x,s)=\left(\frac{2D_L}{U-\sqrt{U^2+4D_Ls^{\alpha}}}\right)\left(\frac{C_1}{s}-\frac{b}{(s+a)(s^{\alpha}-\beta)}\right)\exp\left\{\frac{x}{2}\left(\frac{U}{D_L}-\sqrt{\frac{U^2}{D_L^2}+\frac{4s^{\alpha}}{D_L}}\right)\right\}+\frac{\exp(-bx)}{(s+a)(s^{\alpha}-\beta)}, \tag{3.9}$$

where $\beta=D_Lb^2+Ub$.

For obtaining the solution in the time variable, i.e., $C(x,t)$, inverse Laplace transform is applied to both sides of Eq. (3.9) to get

$$\begin{aligned}C(x,t)&=\mathcal{L}^{-1}\{\bar{C}(x,s)\}\\&=C_1\mathcal{L}^{-1}\left\{\frac{(2D_L)\exp\left\{\frac{x}{2}\left(\frac{U}{A}-\sqrt{\frac{U^2}{D_L^2}+\frac{4s^{\alpha}}{D_L}}\right)\right\}}{s(U-\sqrt{U^2+4D_Ls^{\alpha}})}\right\}\\&\quad-b\mathcal{L}^{-1}\left\{\frac{(2D_L)\exp\left\{\frac{x}{2}\left(\frac{U}{D_L}-\sqrt{\frac{U^2}{D_L^2}+\frac{4s^{\alpha}}{D_L}}\right)\right\}}{(s+a)(s^{\alpha}-\beta)(U-\sqrt{U^2+4D_Ls^{\alpha}})}\right\}+\mathcal{L}^{-1}\left\{\frac{\exp(-bx)}{(s+a)(s^{\alpha}-\beta)}\right\},\end{aligned} \tag{3.10}$$

which can be rewritten in the following manner:

$$C(x,t)=\exp\left(\frac{xU}{2D_L}\right)\{d_1(x,t)-d_2(x,t)\}+\exp(-bx)d_3(x,t), \tag{3.11}$$

with

$$d_1(x,t) = \mathcal{L}^{-1}\left\{\frac{(2D_L)\exp\left\{\frac{x}{2}\left(-\sqrt{\frac{U^2}{D_L^2}+\frac{4s^\alpha}{D_L}}\right)\right\}}{s(U-\sqrt{U^2+4D_Ls^\alpha})}\right\},$$

$$d_2(x,t) = b\mathcal{L}^{-1}\left\{\frac{(2D_L)\exp\left\{\frac{x}{2}\left(-\sqrt{\frac{U^2}{D_L^2}+\frac{4s^\alpha}{D_L}}\right)\right\}}{(s+a)(s^\alpha-\beta)((U-\sqrt{U^2+4D_Ls^\alpha}))}\right\},$$

$$d_3(x,t) = \mathcal{L}^{-1}\left\{\frac{\exp(-bx)}{(s+a)(s^\alpha-\beta)}\right\}.$$

Consequently, the above inverses are calculated one by one. For the calculation of $d_1(x,t)$, we expand the exponential function and then the binomial expression to get

$$\begin{aligned}
&\frac{(2D_L)\exp\left\{\frac{x}{2}\left(-\sqrt{\frac{U^2}{D_L^2}+\frac{4s^\alpha}{D_L}}\right)\right\}}{s(U-\sqrt{U^2+4D_Ls^\alpha})} \\
&= -\left(\frac{U}{2}+\sqrt{D_L}\sqrt{\frac{U^2}{4D_L}+s^\alpha}\right)\frac{\exp\left\{\frac{x}{2}\left(-\sqrt{\frac{U^2}{D_L^2}+\frac{4s^\alpha}{D_L}}\right)\right\}}{s^{\alpha+1}} \\
&= -\frac{U}{2}\left[\sum_{k=0}^{\infty}\frac{\left(-\frac{x}{\sqrt{D_L}}\right)^k}{k!}\sum_{l=0}^{\infty}\frac{\left(\frac{k}{2}\right)\left(\frac{k}{2}-1\right)\ldots\left(\frac{k}{2}-l+1\right)}{l!}\left(\frac{U}{2\sqrt{D_L}}\right)^{2l}s^{-(1+\alpha l+\alpha-\frac{\alpha k}{2})}\right] \\
&- \left[\sqrt{D_L}\sum_{k=0}^{\infty}\frac{\left(-\frac{x}{\sqrt{D_L}}\right)^k}{k!}\sum_{l=0}^{\infty}\frac{\left(\frac{k+1}{2}\right)\left(\frac{k+1}{2}-1\right)\ldots\left(\frac{k+1}{2}-l+1\right)}{l!}\left(\frac{U}{2\sqrt{D_L}}\right)^{2l}s^{-(1+\alpha l+\frac{\alpha}{2}-\frac{\alpha k}{2})}\right],
\end{aligned} \tag{3.12}$$

where $\mid s^\alpha \mid > U^2/4D_L$. Applying inverse Laplace transform to Eq. (3.12), $d_1(x,t)$ has the

following form:

$$d_1(x,t) = C_1\mathcal{L}^{-1}\left\{\frac{(2D_L)\exp\left\{\frac{x}{2}\left(-\sqrt{\frac{U^2}{D_L^2}+\frac{4s^\alpha}{D_L}}\right)\right\}}{s(U-\sqrt{U^2+4D_Ls^\alpha})}\right\}$$

$$= -\frac{C_1U}{2}\left[\sum_{k=0}^{\infty}\frac{\left(-\frac{x}{\sqrt{D_L}}\right)^k}{k!}\sum_{l=0}^{\infty}\frac{\left(\frac{k}{2}\right)\left(\frac{k}{2}-1\right)...\left(\frac{k}{2}-l+1\right)}{l!}\left(\frac{U}{2\sqrt{D_L}}\right)^{2l}\times\right.$$

$$\mathcal{L}^{-1}\left\{s^{-(1+\alpha l+\alpha-\frac{\alpha k}{2})}\right\} \quad \left.+\sqrt{D_L}\sum_{k=0}^{\infty}\frac{\left(-\frac{x}{\sqrt{D_L}}\right)^k}{k!}\sum_{l=0}^{\infty}\frac{\left(\frac{k+1}{2}\right)\left(\frac{k+1}{2}-1\right)...\left(\frac{k+1}{2}-l+1\right)}{l!}\times\right.$$

$$\left.\left(\frac{U}{2\sqrt{D_L}}\right)^{2l}\times\mathcal{L}^{-1}\left\{s^{-(1+\alpha l+\frac{\alpha}{2}-\frac{\alpha k}{2})}\right\}\right]. \tag{3.13}$$

Upon using the well-known result $\mathcal{L}^{-1}\left\{s^{-p_\alpha}\right\} = \frac{t^{p_\alpha-1}}{\Gamma(p_\alpha)}$, with $\mathrm{Re}(p_\alpha) > 0$, $p_\alpha = 1+\alpha l+\alpha-\frac{\alpha k}{2}$ and $p_\alpha = 1+\alpha l+\frac{\alpha}{2}-\frac{\alpha k}{2}$, we get $d_1(x,t)$ as

$$d_1(x,t)$$

$$= -\frac{C_1U}{2}\left[\sum_{k=0}^{\infty}\frac{\left(-\frac{x}{\sqrt{D_L}}\right)^k}{k!}\sum_{l=0}^{\infty}\frac{\left(\frac{k}{2}\right)\left(\frac{k}{2}-1\right)...\left(\frac{k}{2}-l+1\right)\left(\frac{U}{2\sqrt{D_L}}\right)^{2l}}{l!}\frac{t^{(\alpha+\alpha l-\frac{\alpha k}{2})}}{\Gamma(1+\alpha+\alpha l-\frac{\alpha k}{2})}\right.$$

$$\left.+\sqrt{D_L}\sum_{k=0}^{\infty}\frac{\left(-\frac{x}{\sqrt{D_L}}\right)^k}{k!}\sum_{l=0}^{\infty}\frac{\left(\frac{k+1}{2}\right)\left(\frac{k+1}{2}-1\right)...\left(\frac{k+1}{2}-l+1\right)\left(\frac{U}{2\sqrt{D_L}}\right)^{2l}}{l!}\times\frac{t^{(\frac{\alpha}{2}+\alpha l-\frac{\alpha k}{2})}}{\Gamma(1+\frac{\alpha}{2}+\alpha l-\frac{\alpha k}{2})}\right]. \tag{3.14}$$

Following the aforementioned procedure also for $d_2(x,t)$, we get

$$\begin{aligned}
&\frac{(2D_L)\exp\left\{\frac{x}{2}\left(-\sqrt{\frac{U^2}{D_L^2}+\frac{4s^\alpha}{D_L}}\right)\right\}}{(s+a)(s^\alpha-\beta)((U-\sqrt{U^2+4D_Ls^\alpha}))}\\
&= -\left(\frac{U}{2}+\sqrt{D_L}\sqrt{\frac{U^2}{4D_L}+s^\alpha}\right)\frac{\exp\left\{\frac{x}{2}\left(-\sqrt{\frac{U^2}{D_L^2}+\frac{4s^\alpha}{D_L}}\right)\right\}}{s^\alpha(s+a)(s^\alpha-\beta)}\\
&= -\frac{U}{2}\left[\sum_{k=0}^{\infty}\frac{\left(-\frac{x}{\sqrt{D_L}}\right)^k}{k!}\sum_{l=0}^{\infty}\frac{\left(\frac{k}{2}\right)\left(\frac{k}{2}-1\right)...\left(\frac{k}{2}-l+1\right)}{l!}\left(\frac{U}{2\sqrt{D_L}}\right)^{2l}\frac{s^{-(\alpha l+\alpha-\frac{\alpha k}{2})}}{(s+a)(s^\alpha-\beta)}\right]\\
&- \left[\sqrt{D_L}\sum_{k=0}^{\infty}\frac{\left(-\frac{x}{\sqrt{D_L}}\right)^k}{k!}\sum_{l=0}^{\infty}\frac{\left(\frac{k+1}{2}\right)\left(\frac{k+1}{2}-1\right)...\left(\frac{k+1}{2}-l+1\right)}{l!}\left(\frac{U}{2\sqrt{D_L}}\right)^{2l}\frac{s^{-(\alpha l+\frac{\alpha}{2}-\frac{\alpha k}{2})}}{(s+a)(s^\alpha-\beta)}\right].
\end{aligned} \tag{3.15}$$

Then, adopting the transformation technique used in da Sousa et al. [7], $d_2(x,t)$ has the following form:

$$\begin{aligned}
&d_2(x,t)\\
&= -b\left[t^{2\alpha}\sum_{k=0}^{\infty}\frac{\left(-\frac{xt^{-\frac{\alpha}{2}}}{\sqrt{D_L}}\right)^k}{k!}\sum_{l=0}^{\infty}\frac{\Gamma(1+\frac{k}{2})\left(\frac{U^2t^\alpha}{4D_L}\right)^l}{l!\Gamma(1+\frac{k}{2}-l)}\sum_{m=0}^{\infty}(-at)^m\mathbb{E}_{\alpha,1+\alpha+\alpha l+m-\frac{\alpha(k-2)}{2}}(\beta t^\alpha)\right.\\
&\left.+\,t^{\frac{3\alpha}{2}}\sum_{k=0}^{\infty}\frac{\left(-\frac{xt^{-\frac{\alpha}{2}}}{\sqrt{D_L}}\right)^k}{k!}\times\sum_{l=0}^{\infty}\frac{\Gamma(1+\frac{k+1}{2})\left(\frac{U^2t^\alpha}{4D_L}\right)^l}{l!\Gamma(1+\frac{k+1}{2}-l)}\sum_{m=0}^{\infty}(-at)^m\mathbb{E}_{\alpha,1+\alpha+\alpha l+m-\frac{\alpha(k-1)}{2}}(\beta t^\alpha)\right],
\end{aligned} \tag{3.16}$$

where $\mathbb{E}_{\alpha,\beta}(.)$ stands for the two-parameter Mittag-Leffler function.

Finding the inverse Laplace transform of $d_3(x,t)$ is a straightforward task and it can be obtained by putting $x\to 0$ in Eq. (3.15), and then simplifying to get

$$d_3(x,t)=t^\alpha\sum_{m=0}^{\infty}(-at)^m\mathbb{E}_{\alpha,1+\alpha+m}(\beta t^\alpha). \tag{3.17}$$

Collecting the results from Eqs. (3.14), (3.16) and (3.17), the solution to the problem

corresponding to Eqs. (3.2) and (3.6) can be obtained as

$$
\begin{aligned}
&C(x,t)\\
&= -\frac{C_1 U}{2}\left[\sum_{k=0}^{\infty}\frac{\left(-\frac{x}{\sqrt{D_L}}\right)^k}{k!}\sum_{l=0}^{\infty}\frac{\left(\frac{k}{2}\right)\left(\frac{k}{2}-1\right)\ldots\left(\frac{k}{2}-l+1\right)\left(\frac{U}{2\sqrt{D_L}}\right)^{2l}}{l!}\frac{t^{(\alpha+\alpha l-\frac{\alpha k}{2})}}{\Gamma(1+\alpha+\alpha l-\frac{\alpha k}{2})}\right.\\
&\left.+\sqrt{D_L}\sum_{k=0}^{\infty}\frac{\left(-\frac{x}{\sqrt{D_L}}\right)^k}{k!}\sum_{l=0}^{\infty}\frac{\left(\frac{k+1}{2}\right)\left(\frac{k+1}{2}-1\right)\ldots\left(\frac{k+1}{2}-l+1\right)\left(\frac{U}{2\sqrt{D_L}}\right)^{2l}}{l!}\frac{t^{(\frac{\alpha}{2}+\alpha l-\frac{\alpha k}{2})}}{\Gamma(1+\frac{\alpha}{2}+\alpha l-\frac{\alpha k}{2})}\right]\\
&+b\left[t^{2\alpha}\sum_{k=0}^{\infty}\frac{\left(-\frac{xt^{-\frac{\alpha}{2}}}{\sqrt{D_L}}\right)^k}{k!}\sum_{l=0}^{\infty}\frac{\Gamma(1+\frac{k}{2})\left(\frac{U^2t^{\alpha}}{4D_L}\right)^l}{l!\Gamma(1+\frac{k}{2}-l)}\sum_{m=0}^{\infty}(-at)^m\mathbb{E}_{\alpha,1+\alpha+\alpha l+m-\frac{\alpha(k-2)}{2}}(\beta t^{\alpha})\right.\\
&\left.+t^{\frac{3\alpha}{2}}\sum_{k=0}^{\infty}\frac{\left(-\frac{xt^{-\frac{\alpha}{2}}}{\sqrt{D_L}}\right)^k}{k!}\sum_{l=0}^{\infty}\frac{\Gamma(1+\frac{k+1}{2})\left(\frac{U^2t^{\alpha}}{4D_L}\right)^l}{l!\Gamma(1+\frac{k+1}{2}-l)}\sum_{m=0}^{\infty}(-at)^m\mathbb{E}_{\alpha,1+\alpha+\alpha l+m-\frac{\alpha(k-1)}{2}}(\beta t^{\alpha})\right]\\
&-t^{\alpha}\sum_{m=0}^{\infty}(-at)^m\mathbb{E}_{\alpha,1+\alpha+m}(\beta t^{\alpha}).
\end{aligned}
\tag{3.18}
$$

3.3 Validation

In this section, we validate our model against the available clinical data from a laboratory test performed by da Sousa et al. [11]. Earlier, da Sousa et al. [8] performed a laboratory test in order to obtain clinical data to validate their fractional ESR model. They undertook an experiment with blood samples taken from 8 individuals with an equal number of samples from males and females. Later on, they (da Sousa et al. [11]) again performed another set of experiments having only healthy males and females discarding any familiar pathology that could affect ESR. They considered 28 individuals in place of 8 to get more experimental clinical data, which allowed them to perform a robust validation. However, in these models, the non-zero uniform blood velocity and the concentration gradient of the blood nutrients were not taken into account. Taking these into consideration now, we intend to validate our model which accounts for the aforementioned parameters against the available data existing in literature (da Sousa et al. [8, 11]).

Before going into further discussion, let us shed some light on the procedure, that is, how we validate our solution against the clinical data. We mainly focus on achieving the goal of matching the clinical data more accurately with the analytical solution from our model, which considers non-zero uniform blood velocity as well as the concentration gradient of the blood nutrients. As per our best knowledge, no other mathematical model has ever included those above-mentioned parameters. Therefore, we plot our solution against the available clinical data taken from laboratory test (da Sousa et al. [8, 11]) and

exhibit how close our solution is to this data. A successful implementation eventually helps in validating our proposed model.

To validate our model against the above-mentioned clinical data, we need to plot our solution given by Eq. (3.18). For this purpose, we are required to select values for the relevant parameters appearing in the solution. Now relying on the information available in literature [8, 11], we consider the following values: $D_L = 4.8 \times 10^{-4}$ (Schirmer et al. [53]); $D = 9.8 \times 10^{-5}$ (Grote et al. [20]); $K = 1.5 \times 10^{-4}$ (Aksnes et al. [2]) and $a = -0.005 \times 10^{-4}$ (Aksnes et al. [2]). Furthermore, we fix the time at $t = 15$ and take a suitable interval for x as $[0, 4]$, which can be extended if required. Furthermore, the most suitable average blood velocity, as given in Chapter 2, is taken to be of order 10^{-3}, i.e., $U = 10^{-3}$. For the time being, the concentration gradient is considered to be negative; further discussion on this will be made available in the following section. Moreover, we take the maximum number for iterations as $N = 70$, as already addressed in Chapter 2 in which a brief discussion, along with necessary illustration, was provided.

For plotting the graphs with the help of MATLAB R2021b, a normalization of the obtained data is done by dividing every value found in the test by the maximum sedimentation rate so as to have a comparison with the graphs drawn by using the analytical solution obtained from the modified ESR fractional model. In the aforementioned graphs, the horizontal x-axis stands for the normalized distance of the pipette measured in mm, whereas the vertical y-axis represents the normalized sedimentary amount.

Now, we present some plots that ensure the closeness of our solution to the clinical data mentioned earlier. First, we present our solution against the data presented by da Sousa et al. [8] in which they experimented with 8 individuals.

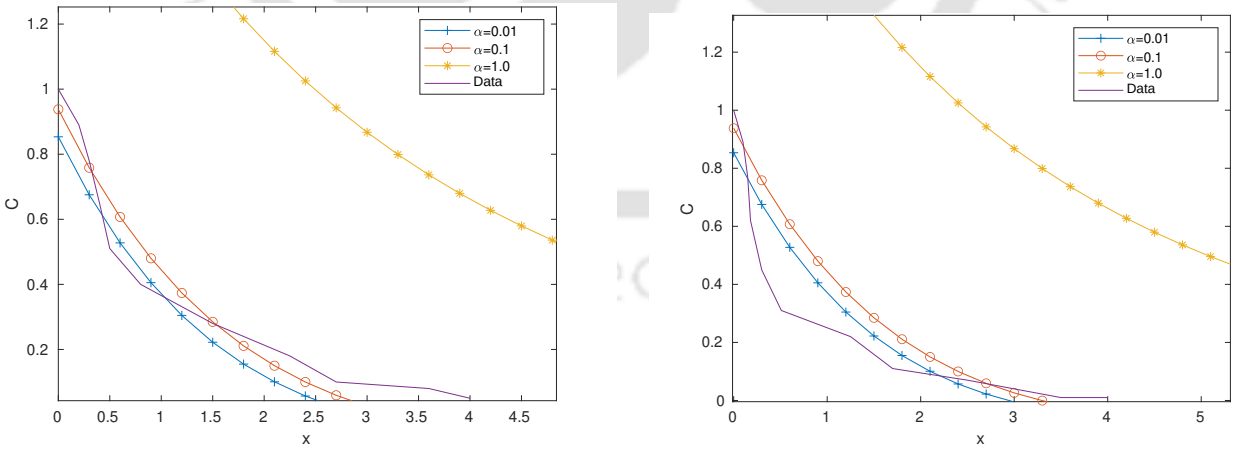

(a) (b)

Figure 3.1: Concentration C for various fractional-order α, with $U = 0.001$, $C_1 = -0.65$, $D_L = 4.8 \times 10^{-4}$, $D = 9.8 \times 10^{-5}$, $K = 1.5 \times 10^{-4}$, $a = -0.005 \times 10^{-4}$, $t = 15$ and $N = 70$: (a) for *male,* (b) for *female.*

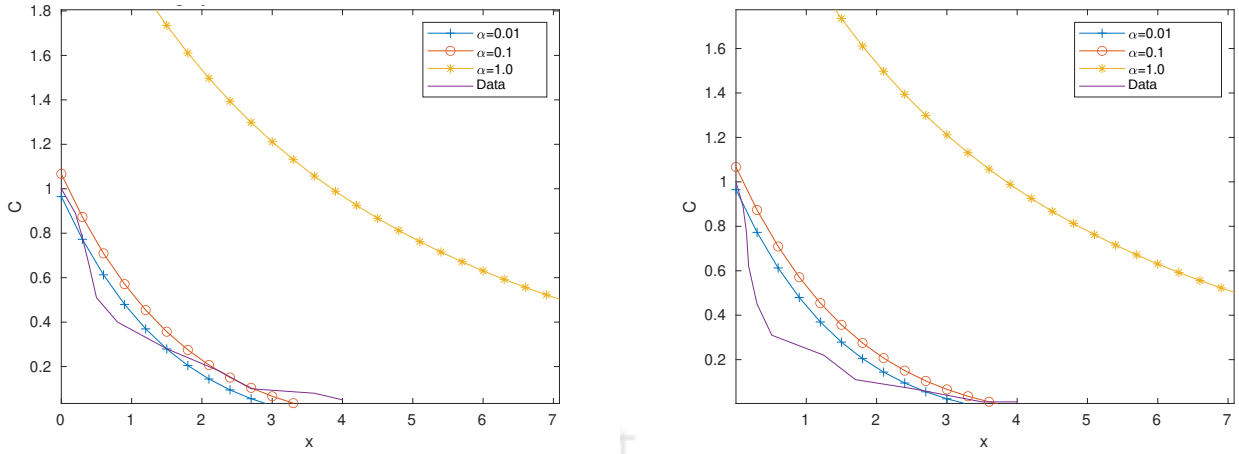

(a) (b)

Figure 3.2: Concentration C for various fractional-order α, with $U = 0.001$, $C_1 = -0.70$, $D_L = 4.8 \times 10^{-4}$, $D = 9.8 \times 10^{-5}$, $K = 1.5 \times 10^{-4}$, $a = -0.005 \times 10^{-4}$, $t = 15$ and $N = 70$: (a) for *male,* (b) for *female.*

From Figs. 3.1 and 3.2, it can be easily depicted that, for both male and female individuals, the fractional order $\alpha = 0.01$ shows a close match with the clinical data for $U = 0.001$, $C_1 = -0.65$ or $C_1 = -0.70$, which certainly leads to the validation of our model.

Next, we test our solution against the model of da Soussa et al. [11] which was based on the experiment with 28 individuals.

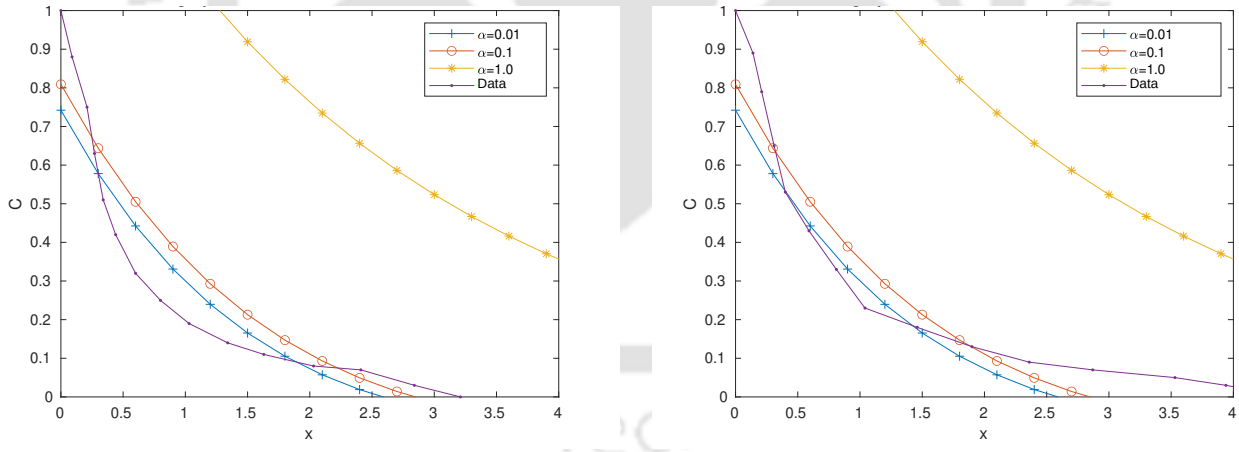

(a) (b)

Figure 3.3: Concentration C for various fractional-order α, with $U = 0.001$, $C_1 = -0.60$, $D_L = 4.8 \times 10^{-4}$, $D = 9.8 \times 10^{-5}$, $K = 1.5 \times 10^{-4}$, $a = -0.005 \times 10^{-4}$, $t = 15$ and $N = 70$: (a) for *male,* (b) for *female.*

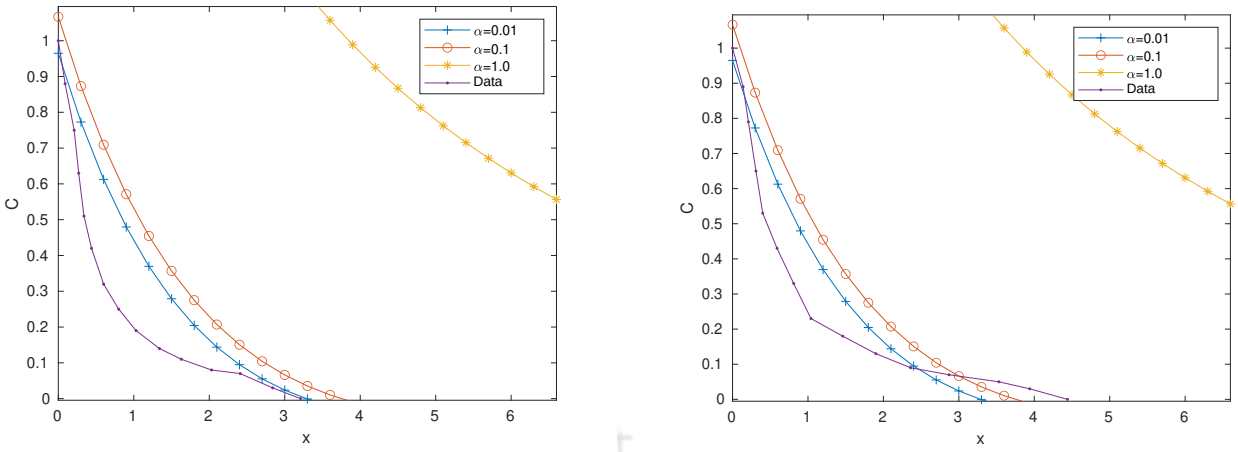

(a) (b)

Figure 3.4: Concentration C for various α, with $U = 0.001$, $C_1 = -0.70$, $D_L = 4.8 \times 10^{-4}$, $D = 9.8 \times 10^{-5}$, $K = 1.5 \times 10^{-4}$, $a = -0.005 \times 10^{-4}$, $t = 15$ and $N = 70$: (a) for *male,* (b) for *female.*

From Figs. 3.3 and 6.11, it is not difficult to infer that, for $U = 0.001$, $C_1 = -0.60$ or $C_1 = -0.70$, the value $\alpha = 0.01$ best suits the clinical data for both male and female samples, which was earlier established in Chapter 2 and this definitely helps in validating our model against the clinical data.

Having validated our model against two established models (da Sousa et al. [8, 11]), it can be inferred that the proposed model is suitable for studying various issues related to the ESR test.

3.4 Results and discussion

Here, the focus is on elaborating the graphs and data acquired by our model and comparing them with the clinical data already available in literature (da Sousa et al. [11]). In the course of the discussion in this section, it will be possible to comment on a suitable range of the concentration gradient for which our graph best matches with the clinical data. Apart from the consideration of the non-zero velocity of blood and fractional order of the governing differential equation, the introduction of the extra parameter in the form of the concentration gradient helps in reaching as close as possible to the clinical data by an analytical solution till date. The incorporation of the concentration gradient has not only enabled us to have a better approximation to the clinical data but also made our model more realistic in nature. This is because the negative values of the concentration gradient capture the realistic blood flow in the arteries. Furthermore, this observation becomes clearer by analyzing Fig. 3.5.

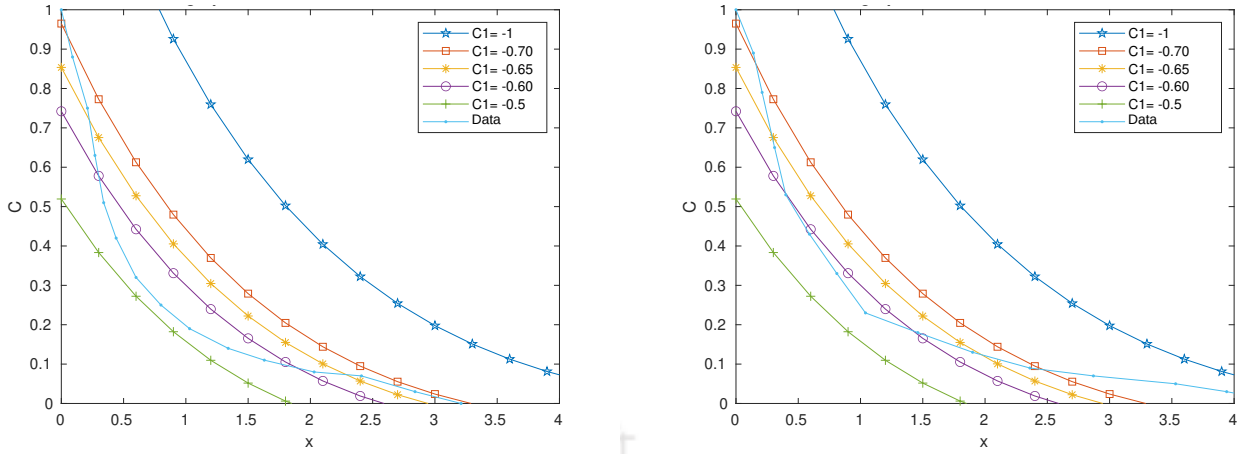

(a) (b)

Figure 3.5: Concentration C for various C_1, with $U = 0.001$, $\alpha = 0.01$, $D_L = 4.8 \times 10^{-4}$, $D = 9.8 \times 10^{-5}$, $K = 1.5 \times 10^{-4}$, $a = -0.005 \times 10^{-4}$, $t = 15$ and $N = 70$: (a) for *male,* (b) for *female.*

Figure 3.5 demonstrates the matching with clinical data for both female and male samples, which can be considered a significant finding. It is deemed appropriate to present a range for the concentration gradient for which it becomes possible to get the closest match with the clinical data by the analytical solution of Eq. (3.17).

An efficient range for blood velocity was already considered in Chapter 2. Hence, in order to strengthen our case, we consider another numerical experiment in which the value $U = 0.01$ is considered.

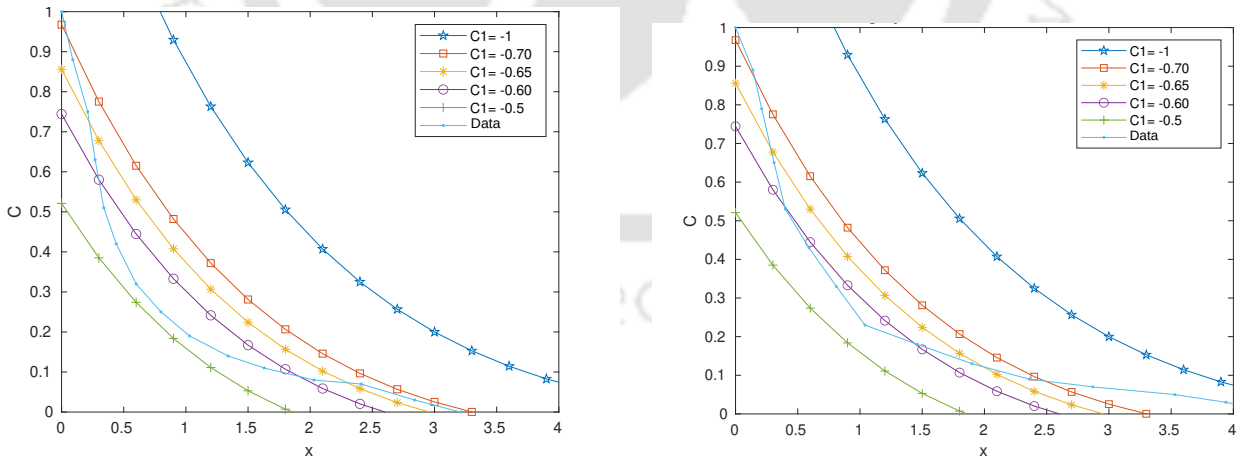

(a) (b)

Figure 3.6: Concentration C for various C_1, with $U = 0.01$, $\alpha = 0.01$, $D_L = 4.8 \times 10^{-4}$, $D = 9.8 \times 10^{-5}$, $K = 1.5 \times 10^{-4}$, $a = -0.005 \times 10^{-4}$, $t = 15$ and $N = 70$: (a) for *male,* (b) for *female.*

By observing Figs. 3.5 and 3.6, it is reasonable to conclude that, for the analytical solution

of Eq. (3.18), if we pick C_1 in the interval $[-.70, -.60]$, then we can approximate our result to the clinical data more accurately.

One more aspect to be noted in this regard, as mentioned in Section 3.1, is the effect of the negative concentration gradient and the boundary conditions which will be clear when the analytical solution is plotted. From Figs. 3.5 and 3.6, it can easily be observed that, when we approach the boundary ($x = 0$), the concentration of the nutrients increases. On the other hand, when we move to the end of the artery ($x \neq 0$), the concentration decreases. A decrease in solute concentration implies that the transport near the artery is greater than its extremity. Therefore, in this situation, the nutrient supply occurs, transported by diffusion through carrier protein present in the plasma membrane, from the higher concentration regions to the lower concentration regions. This means that the boundary conditions are perfectly captured by the graphs of the analytical solution. The transport of the nutrients from higher concentration region to lower concentration region results in the negative concentration gradient which appropriately justifies its role in real-life scenarios.

We present a few more graphs to show how our solution, obtained from the ESR fractional model, is better-suited than the existing ones in Sharma et al. [56], da Sousa [11] and the one in Chapter 2. Since the model in Chapter 2 earlier presented a better solution than the existing ones in Sharma et al. [56] and da Sousa et al. [11] we compare our result with this latest one obtained in Chapter 2.

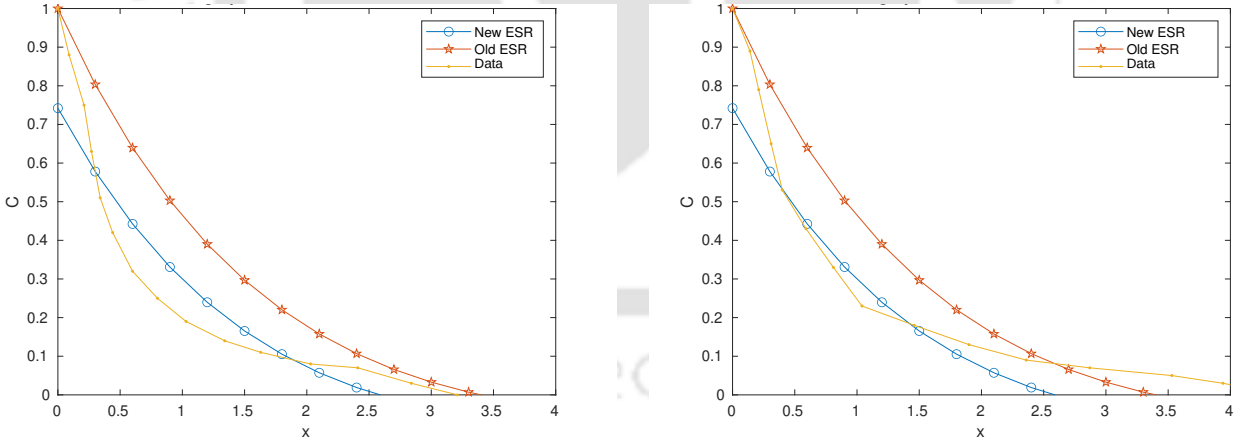

(a) (b)

Figure 3.7: Concentration C for various $C_1 = -0.60$, with $U = 0.01$, $\alpha = 0.01$, $D_L = 4.8 \times 10^{-4}$, $D = 9.8 \times 10^{-5}$, $K = 1.5 \times 10^{-4}$, $a = -0.005 \times 10^{-4}$, $t = 15$ and $N = 70$: (a) for *male,* (b) for *female.*

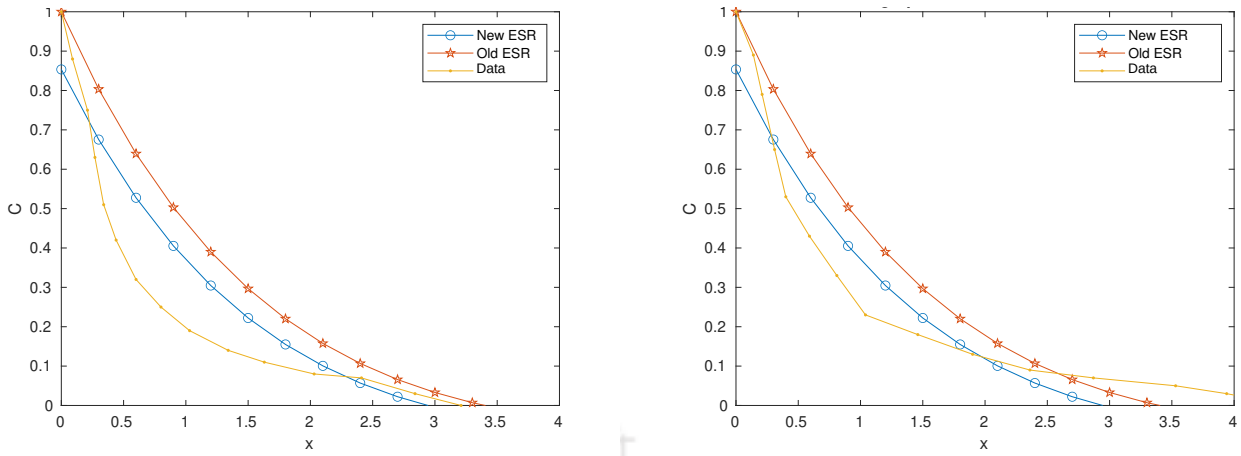

(a) (b)

Figure 3.8: Concentration C for various $C_1 = -0.65$, with $U = 0.01$, $\alpha = 0.01$, $D_L = 4.8 \times 10^{-4}$, $D = 9.8 \times 10^{-5}$, $K = 1.5 \times 10^{-4}$, $a = -0.005 \times 10^{-4}$, $t = 15$ and $N = 70$: (a) for *male,* (b) for *female.*

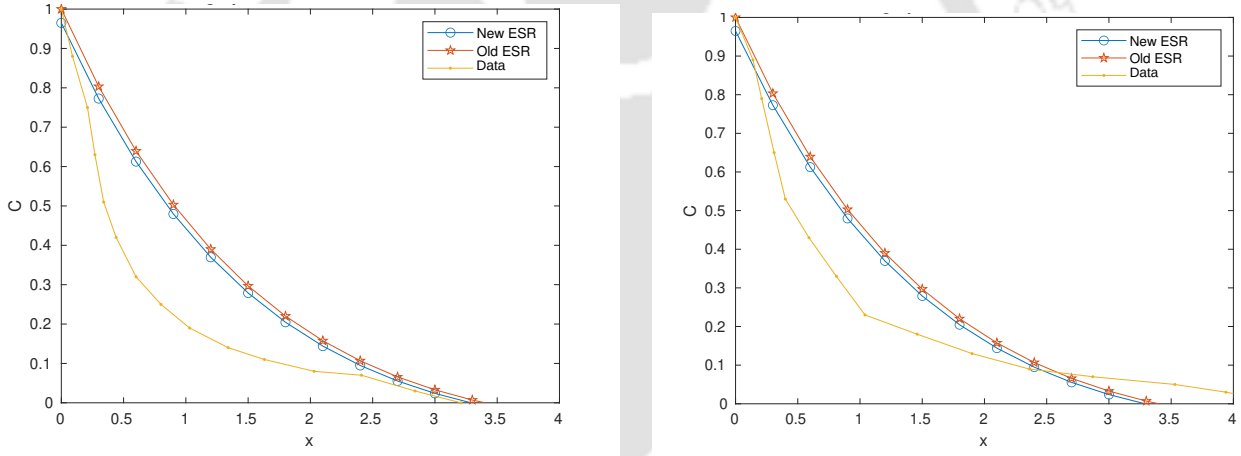

(a) (b)

Figure 3.9: Concentration C for various $C_1 = -0.70$, with $U = 0.01$, $\alpha = 0.01$, $D_L = 4.8 \times 10^{-4}$, $D = 9.8 \times 10^{-5}$, $K = 1.5 \times 10^{-4}$, $a = -0.005 \times 10^{-4}$, $t = 15$ and $N = 70$: (a) for *male,* (b) for *female.*

From Figs. 3.7–3.9, it can be easily concluded that, for the most suitable uniform velocity of blood and fractional order of the governing differential equation, the best possible range for the concentration gradient is $[-0.70, -0.60]$ for both male and female individuals to reach closer to the clinical data. This fulfills our desired goal, which, to the best of our knowledge, has not been achieved till now.

Another interesting aspect of our experiment is to be mentioned in this regard. The concentration gradient not only prescribes the best possible range to approximate the clinical data taken from the laboratory (da Sousa et al. [11]) but also provides the freedom to approximate a wide class of clinical data by selecting its value appropriately. This claim

will be clearer by analyzing the graphs in Fig. 3.10.

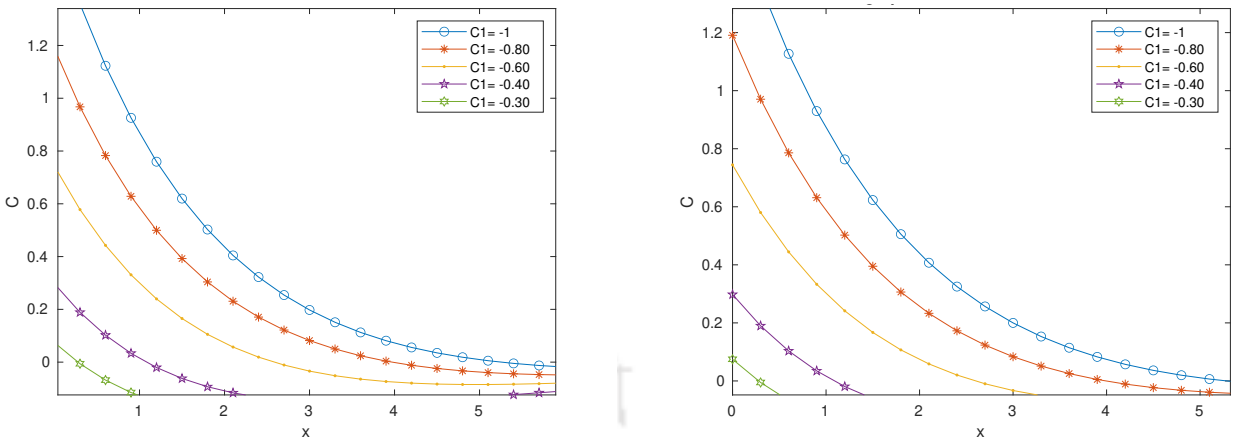

(a) (b)

Figure 3.10: Concentration C for various C_1 with $\alpha = 0.01$, $D_L = 4.8 \times 10^{-4}$, $D = 9.8 \times 10^{-5}$, $K = 1.5 \times 10^{-4}$, $a = -0.005 \times 10^{-4}$, $t = 15$ and $N = 70$: (a) for *U=0.001*, (b) for *U=0.01*.

Looking at Fig. 3.10, it is quite clear that, by selecting an appropriate value for concentration gradient, it is possible to come closer to the axes and also to go away from the axes. The most usual trend for the clinical data from the laboratory, available in literature (da Sousa et al. [8, 11]), is to lie between the graphs displayed in Fig. 3.10. Hence, it is deemed appropriate to claim that we have found the range for the most suitable concentration gradient, which works for negative values, i.e., $C_1 < 0$, to approximate a wide range of clinical data, which, to the best of our knowledge is quite new in the research of ESR test through an analytical solution.
The representation of our experimental data in Table 3.1 exhibits the effectiveness of the solution gained so far.

Table 3.1: Analogy of nutrient concentration with $U = 0.001$, $\alpha = 0.01$, $D_L = 4.8 \times 10^{-4}$, $D = 9.8 \times 10^{-5}$, $K = 1.5 \times 10^{-4}$, $a = -0.005 \times 10^{-4}$, $t = 15$ and $N = 70$.

x	Present work	Earlier work (Chapter 2)	Difference
0	0.96	1	−0.04
0.3	0.77	0.80	−0.03
0.6	0.61	0.64	−0.03
1.2	0.37	0.39	−0.02
1.8	0.20	0.22	−0.02
2.4	0.09	0.11	−0.02
3.0	0.02	0.03	−0.01

From Table 3.1, it can be inferred that the present data obtained by using the analytical solution from the present model is more accurate than the data presented by the earlier model in Chapter 2 as the negative signs exhibited in the difference column infer the closeness of the obtained results to the clinical data than the earlier model.

3.5 Concluding remarks

After an appropriate introduction to the ESR time-fractional model, which includes non-zero blood velocity along with the concentration gradient of the blood nutrient, we have presented an analytical solution to the governing equation as well as a rigorous graphical analysis that follows the validation of the solution with clinical data. With the inclusion of the concentration gradient, this solution not only provides the freedom in choosing an appropriate range of the non-zero uniform velocity of blood and the order of the fractional governing equation, but it also leads to a fruitful range for the concentration gradient to get the best possible approximation to the clinical data. Henceforth, it is quite justified to claim that we have succeeded in addressing the remark made in Chapter 2 that, by taking some other parameters into consideration, better results might be obtained. Taking these parameters (concentration gradient, non-zero average blood velocity and fractional order of the governing equation) into account, we have reached the clinical data as close as possible, whereas the existing models in da Sousa et al. [8, 11] and the one in Chapter 2 were not efficient enough after a certain stage. In other words, we have provided a new insight into the ESR fractional model with the incorporation of the concentration gradient of blood nutrients, which may assume an important role in obtaining more interesting results in future research in this direction.

A notable finding is that, with the incorporation of concentration gradient of nutrients, the present model appears to be more realistic than the earlier ones. It not only presents better-suited results but also has a nearly matching resemblance with the ESR test. Also, the freedom given to the fractional order α $(0 < \alpha \leq 1)$ is of a great advantage. By choosing it appropriately (for our model, it is found to be $\alpha = 0.01$), we can reach the laboratory data to a great extent. It also helps us analyze the concentration of nutrients in certain intervals and regions, which also makes this model closer to reality.

4

Mass transport in brain cells: integer-order and fractional-order modelling

This chapter elucidates the process of mass transport to brain tissues in a mathematical framework by considering the concepts of porosity and tortuosity in terms of both integer-order and fractional-order models. Henceforth, the analytical solutions to the mass transport model are also obtained to find the response functions by means of which the transport process becomes quite explicit. For better insight into the transport process, graphical analysis is also taken into account. The newly-developed fractional version not only presents better-suited analytical solutions to the model, but additionally the graphs also show the matching of the solutions for both integer-order and fractional models. Based on the approximation for four sets of experimental data made by the analytical solution through the means of graphical and numerical results, the fractional model also leads to the selection of the best possible values for the fractional order. We also establish the credibility of the fractional-order model in approximating a wide class of experimental data taken from the laboratory.

4.1 Mass transport model (integer-order)

Following Jain et al. [29] and Huang et al. [31], it is quite clear that mass transport in brain tissues is similar to the mass transport in porous media. As mass transport in porous media is affected by a large number of processes and porous media properties, mass transport in the brain is also affected by the properties of the media like porosity, tortuosity, etc. To investigate this process via mathematical modelling, the transport equations are modified for porous brain tissues, based on Nicholson and Phillips [44, 45], as

$$\frac{\partial C}{\partial t} = \frac{D}{\lambda^2}\nabla^2 C + \frac{S}{e} - f(C) - U.\nabla C, \tag{4.1}$$

where C is the concentration of mass (blood nutrients), D denotes the apparent diffusivity, λ is the tortuosity, S represents mass source density, e is the porosity of the porous medium, U denotes the blood velocity and $f(C)$ represents the cellular uptake. Jain et al. [29] also considered the same type of equations as Eq. (4.1) in two different layers with the uptake term $f(C) = KC$ and $U = 0$ to study the process of mass transport analytically, K being the reaction coefficient.

4.1.1 Mathematical formulation

The present model is based on the concept of mass transport in a porous medium with the aid of diffusion-reaction equations in biological tissues, to be precise, in brain tissues. Here, we use the same governing equations used in Jain et al. [29] to obtain the correct analytical solutions of these governing equations, which were carried out earlier, but contained some major wrong mathematical calculations. The diffusion-reaction equation for the concentration in both layers are

$$\frac{\partial C_i}{\partial t} = \frac{D_i}{\lambda_i^2}\frac{\partial^2 C_i}{\partial x^2} - KC_i(x,t) + \frac{S_i}{e_i}, \tag{4.2}$$

where $C_i(x,t)$ is the concentration of mass (blood nutrients) transport in the i-th layer; K is the co-efficient of chemical reaction; D_i represents the coefficient of diffusion, λ_i the tortuosity, S_i the mass source density and e_i the porosity of the i-th layer, for $i = 1, 2$.

Here, we consider the interface lying between the two layers to be located at $x = a$. In addition, we assume that the two layers are in perfect contact at $x = a$ where the concentrations are the same. Furthermore, the associated initial and boundary conditions for Eq. (4.2) are the following:

$$\begin{cases} C_1(x,t) = C_0(x); & 0 \le x \le 0, t = 0, \\ C_2(x,t) = C_0(x); & 0 \le x < \infty, t = 0, \\ C_1(0,t) = d_0; & t > 0, \\ \left.\frac{\partial C_1}{\partial x}\right|_{x\to\infty} = 0; & t > 0, \\ \left.\frac{\partial C_2}{\partial x}\right|_{x\to\infty} = 0; & t > 0. \end{cases} \tag{4.3}$$

Now, we also impose the following matching condition across the interface:

$$C_1(x,t) = C_2(x,t); \quad x = a, \ t > 0. \tag{4.4}$$

For the time being, we assume that $C_0(x) = C_0$, i.e., C_0 is a constant and d_0 is also a constant.

4.1.2 Analytical solution

We seek the analytical solutions for the governing equations in (4.2) subject to the initial and boundary conditions given by Eqs. (4.3) and (4.4). Now, employing the Laplace transform concerning the time variable t to both sides of Eq. (4.2) we get

$$\frac{d^2}{dx^2}\bar{C}_1(x,s)-\frac{K\lambda_1^2}{D_1}\bar{C}_1(x,s)-\frac{\lambda_1^2}{D_1}[s\bar{C}_1(x,s)-C_1(x,0)]=-\frac{S_1\lambda_1^2}{e_1D_1}\frac{1}{s}, \tag{4.5}$$

and

$$\frac{d^2}{dx^2}\bar{C}_2(x,s)-\frac{K\lambda_2^2}{D_2}\bar{C}_2(x,s)-\frac{\lambda_2^2}{D_2}[s\bar{C}_2(x,s)-C_2(x,0)]=-\frac{S_2\lambda_2^2}{e_2D_2}\frac{1}{s}, \tag{4.6}$$

where $\bar{C}_1(x,s)$ and $\bar{C}_2(x,s)$, respectively, represent the Laplace transforms of $C_1(x,t)$ and $C_2(x,t)$ with $\mathrm{Re}(s)>0$.

Utilizing the initial conditions $C_1(x,0)=C_0$ and $C_2(x,0)=C_0$, the above equations (4.5)-(4.6) can be cast in the following forms:

$$\frac{d^2}{dx^2}\bar{C}_1(x,s)-p_1^2\bar{C}_1(x,s)=q_1, \tag{4.7}$$

and

$$\frac{d^2}{dx^2}\bar{C}_2(x,s)-p_2^2\bar{C}_1(x,s)=q_2, \tag{4.8}$$

where $p_1^2=\frac{\lambda_1^2}{D_1}[K+s]$, $p_2^2=\frac{\lambda_2^2}{D_2}[K+s]$, $q_1=-\frac{\lambda_1^2}{D_1}\left[C_0+\frac{S_1}{e_1s}\right]$, $q_2=-\frac{\lambda_2^2}{D_2}\left[C_0+\frac{S_2}{e_2s}\right]$.

Now, using the variation of parameters technique in Eqs. (4.7) and (4.8), we obtain the corresponding general solutions as

$$\bar{C}_1(x,s)=\beta_1e^{p_1x}+\beta_2e^{-p_1x}-\frac{q_1}{p_1^2}, \tag{4.9}$$

and

$$\bar{C}_2(x,s)=\beta_3e^{p_2x}+\beta_4e^{-p_2x}-\frac{q_2}{p_2^2}, \tag{4.10}$$

where β_1, β_2, β_3 and β_4 are arbitrary constants, to be determined subject to the boundary and matching conditions given by Eqs. (4.3) and (4.4).

The transformed boundary and matching conditions in the Laplace transform domain are the following:

$$\begin{cases}\frac{d}{dx}\bar{C}_1(x,s)\Big|_{x\to\infty}=0; & s>0,\\ \frac{d}{dx}\bar{C}_2(x,s)\Big|_{x\to\infty}=0; & s>0,\\ \bar{C}_1(0,s)=\frac{d_0}{s}; & s>0,\\ \bar{C}_1(x,s)=\bar{C}_2(x,s); & x=a, s>0.\end{cases} \tag{4.11}$$

Incorporating the above-mentioned conditions (4.11) in solutions (4.9) and (4.10), we

obtain the particular solutions for the system of equations in (4.2) as

$$\begin{aligned}
&\bar{C}_1(x,s)\\
&=\left(d_0-\frac{S_1}{e_1K}\right)\frac{\exp\left\{-\left(\frac{\lambda_1 x}{\sqrt{D_1}}\right)\sqrt{K+s}\right\}}{s}+\left(\frac{S_1}{e_1K}-C_0\right)\frac{\exp\left\{-\left(\frac{\lambda_1 x}{\sqrt{D_1}}\right)\sqrt{(K+s)}\right\}}{(K+s)}\\
&+\left(C_0-\frac{S_1}{e_1K}\right)\frac{1}{(K+s)}+\frac{\left(\frac{S_1}{e_1K}\right)}{s},
\end{aligned}\tag{4.12}$$

and

$$\begin{aligned}
&\bar{C}_2(x,s)\\
&=\left[\left(d_0-\frac{S_1}{e_1K}\right)\frac{\exp\left\{-\left(\frac{\lambda_2(x-a)}{\sqrt{D_2}}+\frac{\lambda_1 a}{\sqrt{D_1}}\right)\sqrt{K+s}\right\}}{s}+\left(\frac{S_1}{e_1K}-C_0\right)\times\right.\\
&\left.\frac{\exp\left\{-\left(\frac{\lambda_2(x-a)}{\sqrt{D_2}}+\frac{\lambda_1 a}{\sqrt{D_1}}\right)\sqrt{K+s}\right\}}{(K+s)}\right]+\left[\left(C_0-\frac{S_2}{e_2K}\right)\frac{1}{(K+s)}+\frac{\left(\frac{S_2}{e_2K}\right)}{s}\right]\\
&+\left[\left(\frac{S_1}{e_1K}-\frac{S_2}{e_2K}\right)\left(\frac{\exp\left\{-\left(\frac{\lambda_2(x-a)}{\sqrt{D_2}}\right)\sqrt{K+s}\right\}}{s}-\frac{\exp\left\{-\left(\frac{\lambda_2(x-a)}{\sqrt{D_2}}\right)\sqrt{K+s}\right\}}{(K+s)}\right)\right].
\end{aligned}\tag{4.13}$$

To restore the solutions to the time domain, we employ the inverse Laplace transform on both sides of Eqs. (4.12) and (4.13) to obtain

$$\begin{aligned}
&C_1(x,t)=\mathcal{L}^{-1}\{\bar{C}_1(x,s)\}\\
&=\left(d_0-\frac{S_1}{e_1K}\right)\mathcal{L}^{-1}\left\{\frac{\exp\left\{-\left(\frac{\lambda_1 x}{\sqrt{D_1}}\right)\sqrt{K+s}\right\}}{s}\right\}+\left(\frac{S_1}{e_1K}-C_0\right)\times\\
&\mathcal{L}^{-1}\left\{\frac{\exp\left\{-\left(\frac{\lambda_1 x}{\sqrt{D_1}}\right)\sqrt{(K+s)}\right\}}{(K+s)}\right\}+\left(C_0-\frac{S_1}{e_1K}\right)\mathcal{L}^{-1}\left\{\frac{1}{(K+s)}\right\}+\mathcal{L}^{-1}\left\{\frac{\left(\frac{S_1}{e_1K}\right)}{s}\right\},
\end{aligned}\tag{4.14}$$

and

$$C_2(x,t) = \mathcal{L}^{-1}\{\bar{C}_2(x,s)\}$$
$$= \left[\left(d_0 - \frac{S_1}{e_1K}\right) L^{-1}\left\{\frac{\exp\left\{-\left(\frac{\lambda_2(x-a)}{\sqrt{D_2}} + \frac{\lambda_1 a}{\sqrt{D_1}}\right)\sqrt{K+s}\right\}}{s}\right\} + \left(\frac{S_1}{e_1K} - C_0\right) \times$$
$$L^{-1}\left\{\frac{\exp\left\{-\left(\frac{\lambda_2(x-a)}{\sqrt{D_2}} + \frac{\lambda_1 a}{\sqrt{D_1}}\right)\sqrt{K+s}\right\}}{(K+s)}\right\}\right] + \left(C_0 - \frac{S_2}{e_2K}\right) L^{-1}\left\{\frac{1}{(K+s)}\right\} + L^{-1}\left\{\frac{\left(\frac{S_2}{e_2K}\right)}{s}\right\}$$
$$+ \left[\left(\frac{S_1}{e_1K} - \frac{S_2}{e_2K}\right) L^{-1}\left\{\left(\frac{\exp\left\{-\left(\frac{\lambda_2(x-a)}{\sqrt{D_2}}\right)\sqrt{K+s}\right\}}{s} - \frac{\exp\left\{-\left(\frac{\lambda_2(x-a)}{\sqrt{D_2}}\right)\sqrt{K+s}\right\}}{(K+s)}\right)\right\}\right]. \tag{4.15}$$

Now, following the procedures similar to those used in Abramowitz and Stegun [1], and Chapter 2, inverse Laplace transform for Eqs. (4.14) and (4.15) can be written as

$$C_1(x,t) \tag{4.16}$$
$$= \frac{1}{2}\left(d_0 - \frac{S_1}{e_1K}\right)\left[\exp\left\{-\left(\frac{\lambda_1 x\sqrt{K}}{\sqrt{D_1}}\right)\right\}\operatorname{erfc}\left(-\sqrt{Kt} + \frac{\lambda_1 x}{2\sqrt{D_1 t}}\right) +\right.$$
$$\left.\exp\left\{\left(\frac{\lambda_1 x\sqrt{K}}{\sqrt{D_1}}\right)\right\}\operatorname{erfc}\left(\sqrt{Kt} + \frac{\lambda_1 x}{2\sqrt{D_1 t}}\right)\right] + \left(\frac{S_1}{e_1K} - C_0\right) \times \exp(-Kt) \times \operatorname{erfc}\left(\frac{\lambda_1 x}{2\sqrt{D_1 t}}\right)$$
$$+ \left(C_0 - \frac{S_1}{e_1K}\right) \times \exp(-Kt) + \left(\frac{S_1}{e_1K}\right), \tag{4.17}$$

and

$$C_2(x,t)$$
$$= \frac{1}{2}\left(d_0 - \frac{S_1}{e_1K}\right)\left[\exp\left\{-\left(\frac{\lambda_2(x-a)}{\sqrt{D_2}} + \frac{\lambda_1 a}{\sqrt{D_1}}\right)\sqrt{K}\right\}\operatorname{erfc}\left(-\sqrt{Kt} + \frac{\left(\frac{\lambda_2(x-a)}{\sqrt{D_2}} + \frac{\lambda_1 a}{\sqrt{D_1}}\right)}{2\sqrt{t}}\right)\right.$$
$$\left.+\exp\left\{\left(\frac{\lambda_2(x-a)}{\sqrt{D_2}} + \frac{\lambda_1 a}{\sqrt{D_1}}\right)\sqrt{K}\right\}\operatorname{erfc}\left(\sqrt{Kt} + \frac{\left(\frac{\lambda_2(x-a)}{\sqrt{D_2}} + \frac{\lambda_1 a}{\sqrt{D_1}}\right)}{2\sqrt{t}}\right)\right] + \left(\frac{S_1}{e_1K} - C_0\right) \times$$
$$\exp(-Kt) \times \operatorname{erfc}\left(\frac{\left(\frac{\lambda_2(x-a)}{\sqrt{D_2}} + \frac{\lambda_1 a}{\sqrt{D_1}}\right)}{2\sqrt{t}}\right) + \left[\left(C_0 - \frac{S_2}{e_2K}\right) \times e^{-Kt} + \left(\frac{S_2}{e_2K}\right)\right]$$
$$+ \left(\frac{S_1}{e_1K} - \frac{S_2}{e_2K}\right)\left[\frac{1}{2}\left\{\exp\left(-\left(\frac{\lambda_2(x-a)}{\sqrt{D_2}}\right)\sqrt{K}\right)\operatorname{erfc}\left(-\sqrt{Kt} + \frac{\left(\frac{\lambda_2(x-a)}{\sqrt{D_2}}\right)}{2\sqrt{t}}\right)\right.\right.$$
$$\left.\left.+ \exp\left(\left(\frac{\lambda_2(x-a)}{\sqrt{D_2}}\right)\sqrt{K}\right)\operatorname{erfc}\left(\sqrt{Kt} + \frac{\left(\frac{\lambda_2(x-a)}{\sqrt{D_2}}\right)}{2\sqrt{t}}\right)\right\} - \exp(-Kt)\operatorname{erfc}\left(\frac{\left(\frac{\lambda_2(x-a)}{\sqrt{D_2}}\right)}{2\sqrt{t}}\right)\right], \tag{4.18}$$

where erfc(.) is the complementary error function.

Let us now execute a graphical analysis. To do so, we choose some values for the parameters used in Eqs. (4.16) and (4.18). Here, we use the following values: the diffusivity of the first layer, i.e., of the blood in capillary $D_1 = 3 \times 10^{-9}$ (Gholampour et al. [17]); the diffusivity of the second layer, i.e., of the brain tissue $D_2 = 0.7 \times 10^{-9}$ (Gholampour et al. [17]); the radius of capillary $a = 85$; the tortuosity of blood $\lambda_1 = 0.25$; the tortuosity of brain tissue $\lambda_2 = 1.6$; the mass source density of the first layer $S_1 = 1055 \times 10^{-3}$; the mass source density of the second layer $S_2 = 998.2 \times 10^{-3}$; the porosity of blood $e_1 = 0.57$; the porosity of brain tissue $e_2 = 0.3$; the chemical reaction coefficient $K = 1.76 \times 10^{-5}$. We also take the time as $t = 50$ along with two sets of initial and boundary conditions. First, we consider $C_0 = 0$ and $d_0 = 0$.

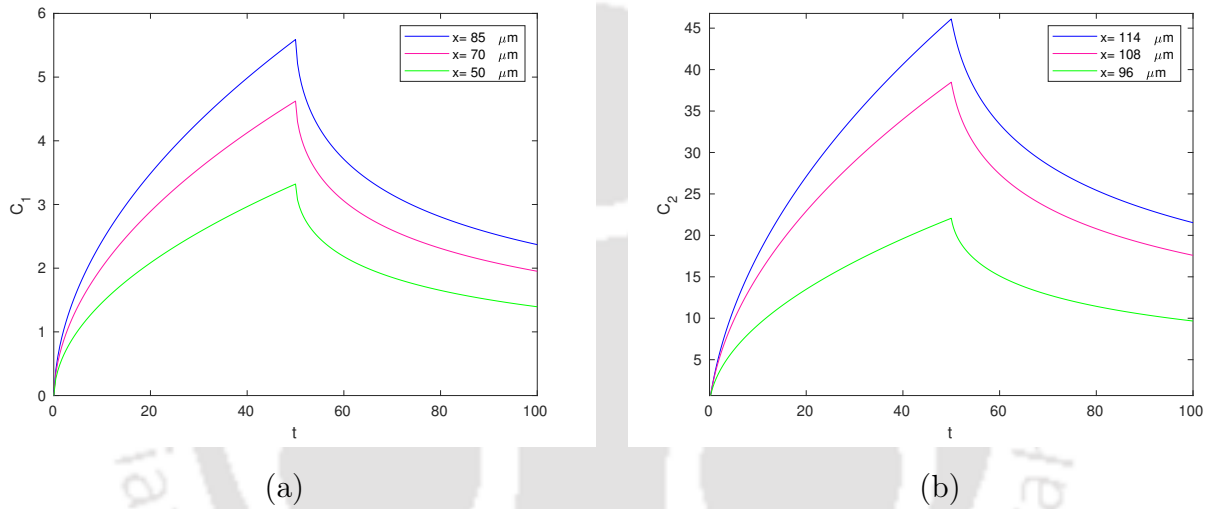

(a) (b)

Figure 4.1: Comparison of concentration of mass transport in both layers for different x, with $D_1 = 3 \times 10^{-9}$, $D_2 = 0.7 \times 10^{-9}$, $a = 85$, $\lambda_1 = 0.25$, $\lambda_2 = 1.6$, $S_1 = 1055 \times 10^{-3}$, $S_2 = 998.2 \times 10^{-3}$, $e_1 = 0.57$, $e_2 = 0.3$ and $K = 1.76 \times 10^{-5}$ (with appropriate units): (a) *in the first layer*, (b) *in the second layer*.

Next, we present the plots corresponding to the nonhomogeneous initial and boundary conditions, i.e., $C_0 = 1$ and $d_0 = 1$.

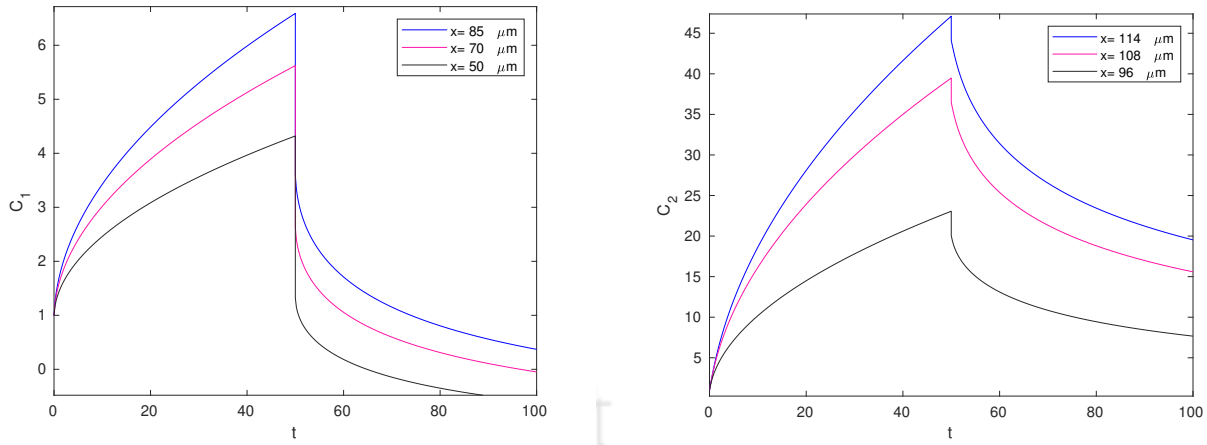

(a) (b)

Figure 4.2: Comparison of concentration of mass transport in both layers for different x, with $D_1 = 3 \times 10^{-9}$, $D_2 = 0.7 \times 10^{-9}$, $a = 85$, $\lambda_1 = 0.25$, $\lambda_2 = 1.6$, $S_1 = 1055 \times 10^{-3}$, $S_2 = 998.2 \times 10^{-3}$, $e_1 = 0.57$, $e_2 = 0.3$ and $K = 1.76 \times 10^{-5}$ (with appropriate units): (a) *in the first layer*, (b) *in the second layer.*

In Figs. 4.1 and 4.2, the horizontal axis indicates time t and the vertical axis represents the concentration of nutrients in the blood to be transported into the brain tissue. Looking at these figures, it can be observed that they also follow the same trend as that of the ones in [44, 45], which means the concentrations have an upward trend up to $t = 50$ (the terminal time for the activated source) and then decrease when the source is deactivated and replaced with a sink with the same magnitude but opposite sign.

4.1.3 Data fitting

In this subsection, we mainly focus on approximating the experimental data (along with the locations x too) taken from the work by Nicholson and Phillips [44] by the model solution. Here, we try to fit our integer-order model solution with the experimental data for various locations of the brain tissues. Therefore, we present a few plots depicting the data approximation made by the integer-order model solution.

First, we present the plots for the locations $x = 114$ and $x = 85$ taking the experimental data into consideration.

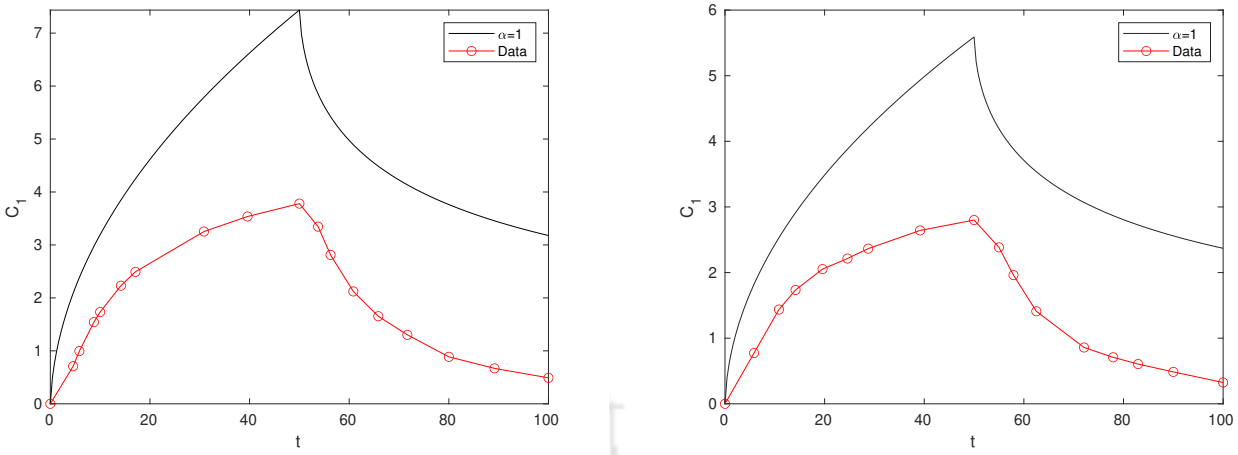

(a) (b)

Figure 4.3: Comparison of concentration of mass transport in the first layer for different x, with $D_1 = 3 \times 10^{-9}$, $D_2 = 0.7 \times 10^{-9}$, $a = 85$, $\lambda_1 = 0.25$, $\lambda_2 = 1.6$, $S_1 = 1055 \times 10^{-3}$, $S_2 = 998.2 \times 10^{-3}$, $e_1 = 0.57$, $e_2 = 0.3$ and $K = 1.76 \times 10^{-5}$ (with appropriate units) along with the experimental data [44]: (a) $x = 114$, (b) $x = 85$.

Next, we showcase the plots for the locations $x = 108\mu m$ and $x = 96\mu m$ along with the experimental data.

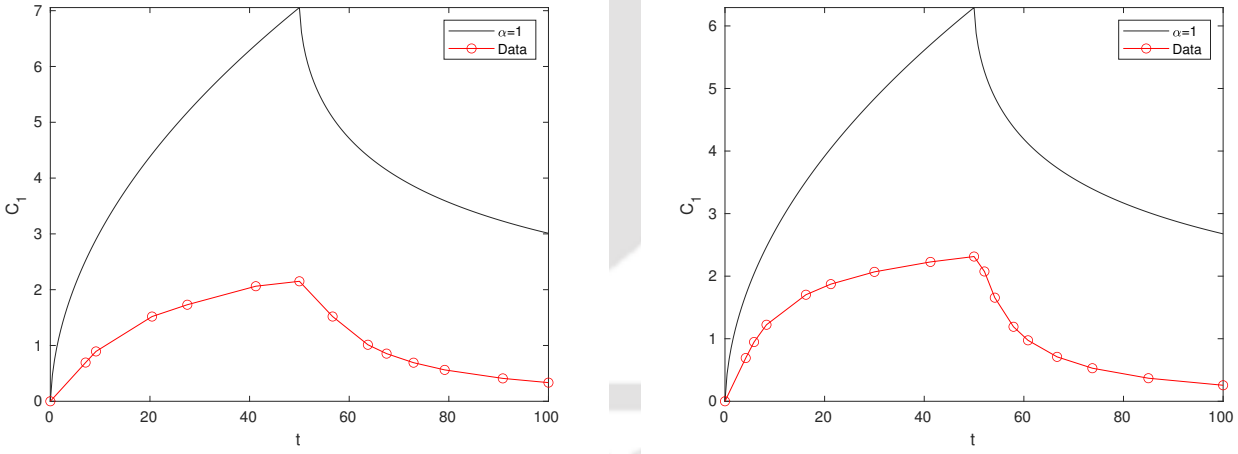

(a) (b)

Figure 4.4: Comparison of concentration of mass transport in the first layer for different x, with $D_1 = 3 \times 10^{-9}$, $D_2 = 0.7 \times 10^{-9}$, $a = 85$, $\lambda_1 = 0.25$, $\lambda_2 = 1.6$, $S_1 = 1055 \times 10^{-3}$, $S_2 = 998.2 \times 10^{-3}$, $e_1 = 0.57$, $e_2 = 0.3$ and $K = 1.76 \times 10^{-5}$ (with appropriate units) along with the experimental data [44]: (a) $x = 108$, (b) $x = 96$.

Looking at Figs. 4.3 and 4.4, it can be observed that the plots corresponding to the integer-order model solution follow the same pattern as followed by the experimental data, which we claimed earlier in Section 4.1.2. Therefore, our claim is justified, but for Figs. 4.3 and 4.4 both, the experimental data is far from the integer-order solution plots. As we have experimented with all the other parameters and the best results are presented here, so this graphical disparity makes us rethink about the modelling. Some interesting instances where the integer-order model solutions stayed far away from the experimental data were presented in Chapters 2 and 3; the fractional version of those models were established to be efficient enough that the experimental data were well-approximated. Being motivated by these works, we intend to apply the same methodology to investigate whether we can approximate the experimental data well enough or not for our present model. Hence, we present a fractional version of the mass transport model in the following section.

4.2 Fractional mass transport model

4.2.1 Mathematical formulation

In this section, we exhibit a fractional version of the linear partial differential equations governing the mass transport in brain tissues (Jain et al. [29]). Our present model can be considered as a generalization of the work of Jain et al. [29] as it can recover the original model, which we shall present in the course of our discussion.

The mass concentrations (blood nutrients) are assumed to satisfy the following non-homogeneous time-fractional partial differential equations:

$$\frac{\partial^{\alpha} C_i}{\partial t^{\alpha}} = \frac{D_i}{\lambda_i^2}\frac{\partial^2 C_i}{\partial x^2} - KC_i(x,t) + \frac{S_i}{e_i}, \tag{4.19}$$

where $0 < \alpha \leq 1$, $i = 1,\ 2$ and all the other variables and parameters carry the same meaning as mentioned earlier. Here, we use the fractional derivative of order α in the Caputo sense, defined in Eqs. (1.4)-(1.6).

Here also, we impose the same initial and boundary conditions as before, i.e., Eq. (4.3). Now, we also impose the following matching conditions like earlier, that is, Eq. (4.4). We again assume $C_0(x) = C_0$, i.e., C_0 is a constant.

4.2.2 Analytical solution

Applying Laplace transform with respect to time variable t to both sides of Eq. (4.19), we have

$$\frac{d^2}{dx^2}\bar{C}_1(x,s) - \frac{K\lambda_1^2}{D_1}\bar{C}_1(x,s) - \frac{\lambda_1^2}{D_1}[s^\alpha \bar{C}_1(x,s) - s^{\alpha-1}C_1(x,0)] = -\frac{S_1\lambda_1^2}{e_1 D_1}\frac{1}{s}, \tag{4.20}$$

and

$$\frac{d^2}{dx^2}\bar{C}_2(x,s) - \frac{K\lambda_2^2}{D_2}\bar{C}_2(x,s) - \frac{\lambda_2^2}{D_2}[s^\alpha \bar{C}_2(x,s) - s^{\alpha-1}C_2(x,0)] = -\frac{S_2\lambda_2^2}{e_2 D_2}\frac{1}{s}, \tag{4.21}$$

where $\bar{C}_1(x,s)$ and $\bar{C}_1(x,s)$ are the Laplace transforms of $C_1(x,t)$ and $C_2(x,t)$, respectively, with $\mathrm{Re}(s) > 0$.

Utilizing the initial conditions $C_1(x,0) = C_0$ and $C_2(x,0) = C_0$, the above equations (4.20)-(4.21) can be put in the following forms:

$$\frac{d^2}{dx^2}\bar{C}_1(x,s) - p_1^2\bar{C}_1(x,s) = q_1, \tag{4.22}$$

and

$$\frac{d^2}{dx^2}\bar{C}_2(x,s) - p_2^2\bar{C}_1(x,s) = q_2, \tag{4.23}$$

where $p_1^2 = \frac{\lambda_1^2}{D_1}[R + s^\alpha]$, $p_2^2 = \frac{\lambda_2^2}{D_2}[K + s^\alpha]$, $q_1 = -\frac{\lambda_1^2}{D_1}\left[s^{\alpha-1}C_0 + \frac{S_1}{e_1 s}\right]$, $q_2 = -\frac{\lambda_2^2}{D_2}\left[s^{\alpha-1}C_0 + \frac{S_2}{e_2 s}\right]$.

Now, proceeding as before, using the variation of parameters technique in Eqs. (4.22) and (4.23), we obtain the corresponding general solutions as

$$\bar{C}_1(x,s) = \beta_1 e^{p_1 x} + \beta_2 e^{-p_1 x} - \frac{q_1}{p_1^2}, \tag{4.24}$$

and

$$\bar{C}_2(x,s) = \beta_3 e^{p_2 x} + \beta_4 e^{-p_2 x} - \frac{q_2}{p_2^2}, \tag{4.25}$$

where $\beta_1, \beta_2, \beta_3$ and β_4 are arbitrary constants, to be determined subject to the boundary and matching conditions given by Eqs. (4.24)-(4.25).

The transformed boundary and matching conditions in the Laplace domain are the same as Eq. (4.11).

Incorporating the above-mentioned conditions (4.11) in solutions (4.24) and (4.25), we

obtain the particular solutions for the system of equations (4.22)-(4.23) as

$$\begin{aligned}
&\bar{C}_1(x,s)\\
&= (d_0 - C_0)\frac{\exp\left\{-\left(\frac{\lambda_1 x}{\sqrt{D_1}}\right)\sqrt{K+s^\alpha}\right\}}{s} + \left(C_0 K - \frac{S_1}{e_1}\right)\frac{\exp\left\{-\left(\frac{\lambda_1 x}{\sqrt{D_1}}\right)\sqrt{(K+s^\alpha)}\right\}}{s(K+s^\alpha)}\\
&+ \left(C_0 - \frac{S_1}{e_1 K}\right)\frac{s^{\alpha-1}}{(K+s^\alpha)} + \frac{\left(\frac{S_1}{e_1 K}\right)}{s},
\end{aligned} \tag{4.26}$$

and

$$\begin{aligned}
&\bar{C}_2(x,s)\\
&= \left[(d_0 - C_0)\frac{\exp\left\{-\left(\frac{\lambda_2(x-a)}{\sqrt{D_2}} + \frac{\lambda_1 a}{\sqrt{D_1}}\right)\sqrt{K+s^\alpha}\right\}}{s} + \left(C_0 K - \frac{S_1}{e_1}\right)\times\right.\\
&\left.\frac{\exp\left\{-\left(\frac{\lambda_2(x-a)}{\sqrt{D_2}} + \frac{\lambda_1 a}{\sqrt{D_1}}\right)\sqrt{K+s^\alpha}\right\}}{s(K+s^\alpha)}\right] + \left[\left(C_0 - \frac{S_2}{e_2 K}\right)\frac{s^{\alpha-1}}{(K+s^\alpha)} + \frac{\left(\frac{S_2}{e_2 K}\right)}{s}\right]\\
&+ \left[\left(\frac{S_1}{e_1} - \frac{S_2}{e_2}\right)\left(\frac{\exp\left\{-\left(\frac{\lambda_2(x-a)}{\sqrt{d_2}}\right)\sqrt{K+s^\alpha}\right\}}{s(K+s^\alpha)}\right)\right].
\end{aligned} \tag{4.27}$$

In order to restore the solutions to the time domain, we employ the inverse Laplace transform to both sides of Eqs. (4.26) and (4.27) to obtain

$$\begin{aligned}
&C_1(x,t)\\
&= \mathcal{L}^{-1}\{\bar{C}_1(x,s)\}\\
&= (d_0 - C_0)\mathcal{L}^{-1}\left\{\frac{\exp\left\{-\left(\frac{\lambda_1 x}{\sqrt{D_1}}\right)\sqrt{K+s^\alpha}\right\}}{s}\right\} + \left(C_0 K - \frac{S_1}{e_1}\right)\times\\
&\mathcal{L}^{-1}\left\{\frac{\exp\left\{-\left(\frac{\lambda_1 x}{\sqrt{D_1}}\right)\sqrt{(K+s^\alpha)}\right\}}{s(K+s^\alpha)}\right\} + \left(C_0 - \frac{S_1}{e_1 K}\right)\mathcal{L}^{-1}\left\{\frac{s^{\alpha-1}}{(K+s^\alpha)}\right\} + \mathcal{L}^{-1}\left\{\frac{\left(\frac{S_1}{e_1 K}\right)}{s}\right\},
\end{aligned} \tag{4.28}$$

and

$$
\begin{aligned}
&C_2(x,t)\\
&=\mathcal{L}^{-1}\{\bar{C_2}(x,s)\}\\
&=\left[(d_0-C_0)\,\mathcal{L}^{-1}\left\{\frac{\exp\left\{-\left(\frac{\lambda_2(x-a)}{\sqrt{D_2}}+\frac{\lambda_1 a}{\sqrt{D_1}}\right)\sqrt{K+s^\alpha}\right\}}{s}\right\}+\left(C_0K-\frac{S_1}{e_1}\right)\times\right.\\
&\left.\mathcal{L}^{-1}\left\{\frac{\exp\left\{-\left(\frac{\lambda_2(x-a)}{\sqrt{D_2}}+\frac{\lambda_1 a}{\sqrt{D_1}}\right)\sqrt{K+s^\alpha}\right\}}{s(K+s^\alpha)}\right\}\right]+\left[\left(C_0-\frac{S_2}{e_2K}\right)\mathcal{L}^{-1}\left\{\frac{s^{\alpha-1}}{(K+s^\alpha)}\right\}\right.\\
&\left.+\mathcal{L}^{-1}\left\{\frac{\left(\frac{S_2}{e_2K}\right)}{s}\right\}\right]+\left[\left(\frac{S_1}{e_1}-\frac{S_2}{e_2}\right)\mathcal{L}^{-1}\left\{\left(\frac{\exp\left\{-\left(\frac{\lambda_2(x-a)}{\sqrt{D_2}}\right)\sqrt{K+s^\alpha}\right\}}{s(K+s^\alpha)}\right)\right\}\right].
\end{aligned}
\tag{4.29}
$$

Now, following the inverse Laplace transform technique used in the earlier chapters, inverse Laplace transform applied to Eqs. (4.28) and (4.29) gives

$$
\begin{aligned}
&C_1(x,t)\\
&=(d_0-C_0)\sum_{k=0}^{\infty}\frac{\left(-\frac{\lambda_1 x}{\sqrt{D_1}}\right)^k}{k!}\sum_{l=0}^{\infty}\frac{(k)^l\Gamma(1+\frac{k}{2})}{l!\Gamma(1+\frac{k}{2}-l)}\times\frac{t^{\alpha l-\frac{\alpha k}{2}}}{\Gamma(1+\alpha l-\frac{\alpha k}{2})}+\left(C_0K-\frac{S_1}{e_1}\right)\times t^\alpha\times\\
&\sum_{k=0}^{\infty}\frac{\left(-\frac{\lambda_1 x}{\sqrt{D_1}}t^{-\frac{\alpha}{2}}\right)^k}{k!}\sum_{l=0}^{\infty}\frac{(kt^\alpha)^l\Gamma(1+\frac{k}{2})}{l!\Gamma(1+\frac{k}{2}-l)}\mathbb{E}_{\alpha,1+\alpha+\alpha l-\frac{\alpha k}{2}}(-Kt^\alpha)+\left(C_0-\frac{S_1}{e_1K}\right)\mathbb{E}_\alpha(-Kt^\alpha)\\
&+\left(\frac{S_1}{e_1K}\right),
\end{aligned}
\tag{4.30}
$$

and

$$
\begin{aligned}
&C_2(x,t)\\
&=(d_0-C_0)\sum_{k=0}^{\infty}\frac{\left(-\left(\frac{\lambda_2(x-a)}{\sqrt{D_2}}+\frac{\lambda_1 a}{\sqrt{D_1}}\right)\right)^k}{k!}\sum_{l=0}^{\infty}\frac{(k)^l\Gamma(1+\frac{k}{2})}{l!\Gamma(1+\frac{k}{2}-l)}\times\frac{t^{\alpha l-\frac{\alpha k}{2}}}{\Gamma(1+\alpha l-\frac{\alpha k}{2})}\\
&+\left(C_0K-\frac{S_1}{e_1}\right)\times t^\alpha\times\sum_{k=0}^{\infty}\frac{\left(-\left(\frac{\lambda_2(x-a)}{\sqrt{D_2}}+\frac{\lambda_1 a}{\sqrt{D_1}}\right)t^{-\frac{\alpha}{2}}\right)^k}{k!}\sum_{l=0}^{\infty}\frac{(kt^\alpha)^l\Gamma(1+\frac{k}{2})}{l!\Gamma(1+\frac{k}{2}-l)}\times\\
&\mathbb{E}_{\alpha,1+\alpha+\alpha l-\frac{\alpha k}{2}}(-Kt^\alpha)+\left(C_0-\frac{S_2}{e_2K}\right)\mathbb{E}_\alpha(-Kt^\alpha)+\left(\frac{S_2}{e_2K}\right)\\
&+\left(\frac{S_1}{e_1}-\frac{S_2}{e_2}\right)\times t^\alpha\times\sum_{k=0}^{\infty}\frac{\left(-\left(\frac{\lambda_2(x-a)}{\sqrt{D_2}}\right)t^{-\frac{\alpha}{2}}\right)^k}{k!}\sum_{l=0}^{\infty}\frac{(kt^\alpha)^l\Gamma(1+\frac{k}{2})}{l!\Gamma(1+\frac{k}{2}-l)}\times\\
&\mathbb{E}_{\alpha,1+\alpha+\alpha l-\frac{\alpha k}{2}}(-Kt^\alpha),
\end{aligned}
\tag{4.31}
$$

where $\mathbb{E}_{\alpha,\beta}(.)$ and $\mathbb{E}_\alpha(.)$ are the Mittag-Leffler function of two parameters and one pa-

rameter, respectively.

4.3 Model verification

As proposed, this fractional mass transport model is the generalized version of the one proposed by Jain et al. [29], describing the mass transport in brain tissues. As a consequence, our proposed model must have the capability to recover the earlier model of Jain et al. [29] for some particular values of the parameters, as it is previously established in Section 4.2 that, as $\alpha \to 1$, our proposed model retrieves the original model. This is what we are going to establish in this section. In this model, we generalize the fractional order of the derivative; henceforth, if we take $\alpha \to 1$, then this model should exhibit exactly the same solution as that of the corrected version of integer-order model [29].

Here, we showcase the verification of our proposed model by graphical means. To do so, we plot the solutions (4.30) and (4.31) with $\alpha \to 1$. Further, while plotting, we use the same values for the parameters used in the solutions as used in Section 4.1 along with the homogeneous initial and boundary conditions, i.e., $C_0 = 0$ and $d_0 = 0$.

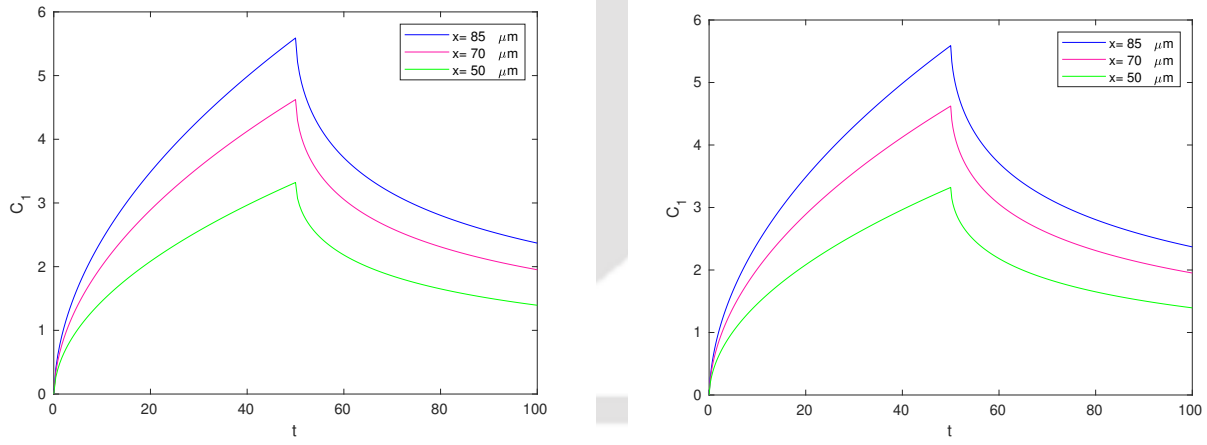

(a) (b)

Figure 4.5: Comparison of concentration of mass transport in the first layer for different x, with $D_1 = 3 \times 10^{-9}$, $D_2 = 0.7 \times 10^{-9}$, $a = 85$, $\lambda_1 = 0.25$, $\lambda_2 = 1.6$, $S_1 = 1055 \times 10^{-3}$, $S_2 = 998.2 \times 10^{-3}$, $e_1 = 0.57$, $e_2 = 0.3$ and $K = 1.76 \times 10^{-5}$ (with appropriate units): (a) *integer-order model*, (b) *fractional-order model (with $\alpha = 1$)*.

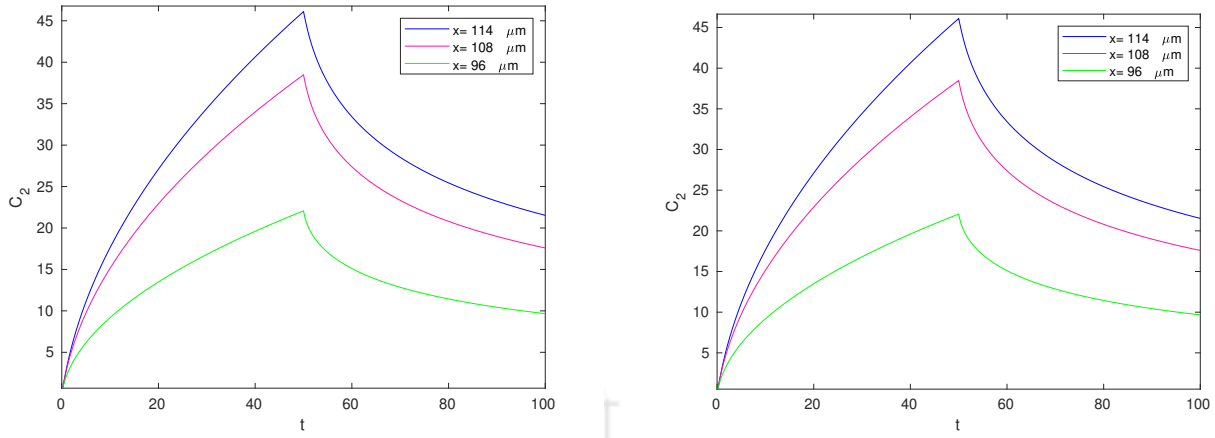

(a) (b)

Figure 4.6: Comparison of concentration of mass transport in the second layer for different x, with $D_1 = 3 \times 10^{-9}$, $D_2 = 0.7 \times 10^{-9}$, $a = 85$, $\lambda_1 = 0.25$, $\lambda_2 = 1.6$, $S_1 = 1055 \times 10^{-3}$, $S_2 = 998.2 \times 10^{-3}$, $e_1 = 0.57$, $e_2 = 0.3$ and $K = 1.76 \times 10^{-5}$ (with appropriate units): (a) *integer-order model*, (b) *fractional-order model (with* $\alpha = 1$*)*.

Figures 4.5(a) and 4.6(a) correspond to the plots for the integer-order model at different locations in both layers, whereas Figs. 4.5(b) and 4.6(b) are the plots corresponding to the fractional-order model at those same locations for both layers. Now, looking at these figures, it can be easily observed that Figs. 4.5(a) and 4.5(b) are exactly identical. Further, Figs. 4.6(a) and 4.6(b) exhibit graphical agreement. Hence, we successfully establish not only the agreement for both the models but also the solutions, under a particular case $\alpha \to 1$.

Next, we consider another set of initial and boundary conditions to strengthen our claim. For this case, we proceed for the nonhomogeneous ones, viz., $C_0 = 1$ and $d_0 = 1$.

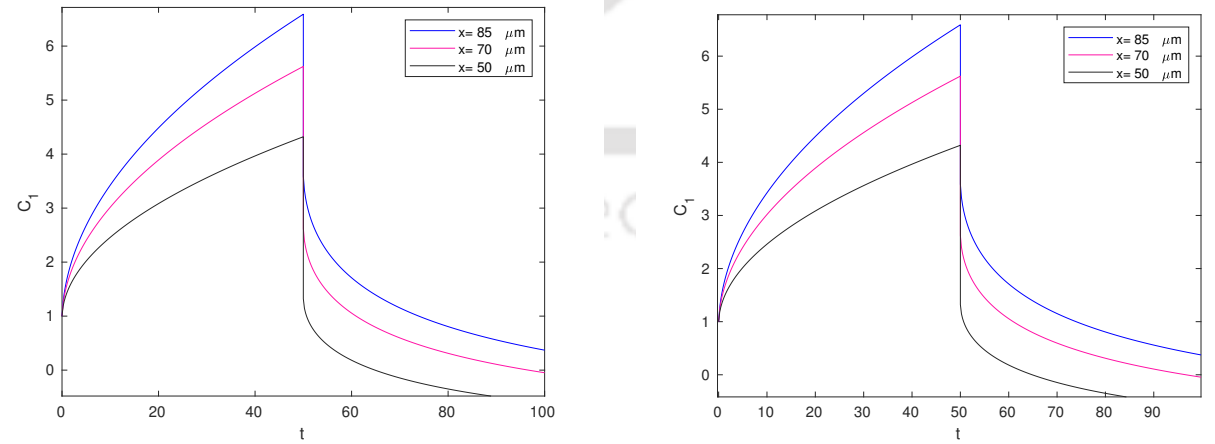

(a) (b)

Figure 4.7: Comparison of concentration of mass transport in the first layer for different x, with $D_1 = 3 \times 10^{-9}$, $D_2 = 0.7 \times 10^{-9}$, $a = 85$, $\lambda_1 = 0.25$, $\lambda_2 = 1.6$, $S_1 = 1055 \times 10^{-3}$, $S_2 = 998.2 \times 10^{-3}$, $e_1 = 0.57$, $e_2 = 0.3$ and $K = 1.76 \times 10^{-5}$ (with appropriate units): (a) *integer-order model*, (b) *fractional-order model (with* $\alpha = 1$*)*.

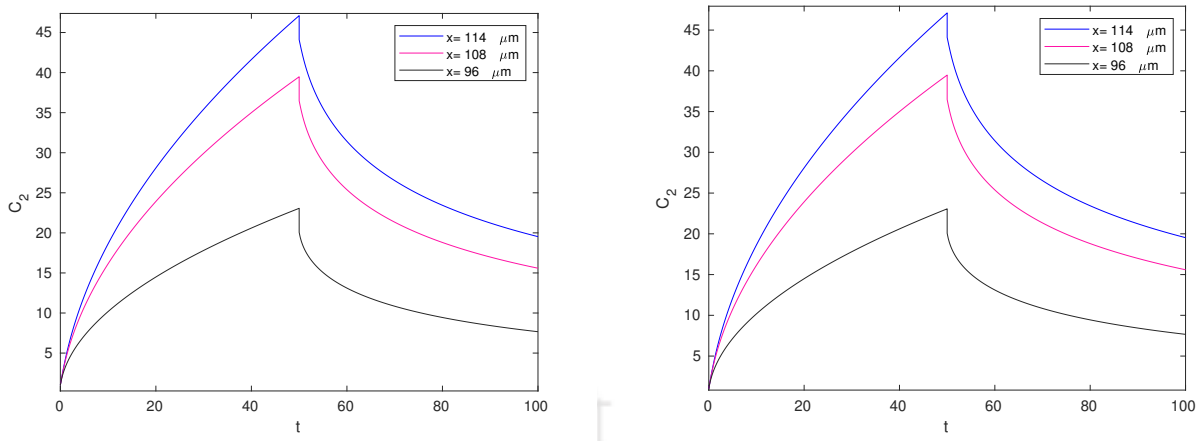

Figure 4.8: Comparison of concentration of mass transport in the second layer for different x, with $D_1 = 3 \times 10^{-9}$, $D_2 = 0.7 \times 10^{-9}$, $a = 85$, $\lambda_1 = 0.25$, $\lambda_2 = 1.6$, $S_1 = 1055 \times 10^{-3}$, $S_2 = 998.2 \times 10^{-3}$, $e_1 = 0.57$, $e_2 = 0.3$ and $K = 1.76 \times 10^{-5}$ (with appropriate units): (a) *integer-order model*, (b) *fractional-order model (with* $\alpha = 1$*)*.

Figures 4.7(a) and 4.8(a) correspond to the plots for the integer-order model at different locations in both layers, whereas Figs. 4.7(b) and 4.8(b) correspond to the plots for the fractional-order model at those same locations for both layers. Here also, it can be observed that Figs. 4.7 and 4.8 agree with each other for the particular case $\alpha \to 1$. Hence, we deem it appropriate to claim that the verification of both the models is successfully achieved by means of graphical agreement.

4.4 Results and discussion

In this section, we elucidate the obtained graphs and data by using the solution of the fractional-order model in the form of results and discuss their applicability by comparing them with the existing literature (Nicholson and Phillips [44]). Further, we show how the proposed fractional-order model outperforms the integer-order one. Here, we intend to consider various values for the fractional order of the derivative and examine how this new parameter impacts the analytical solution in terms of approximating the real-life data. Furthermore, we present the best probable value for the fractional order of the derivative used in the proposed model for the best approximation.

Before proceeding further, let us explain the procedure we render to elucidate the obtained graphs and data. We utilize the experimental data obtained by Nicholson and Phillips [44], where they experimented with SD rats $(200 - 400\text{g})$ or laboratory rats and performed the ion transport in the cerebellum of the rats. Here, we make our model analogous to that of Nicholson and Phillips. Hence, we examine whether our model too

catches these experimental data closely or not.

Here, we present four sets of experimental data and test whether our proposed model solution is capable to capture them closely or not. To begin with, we experiment with two sets of experimental data, presented through Fig. 4.9.

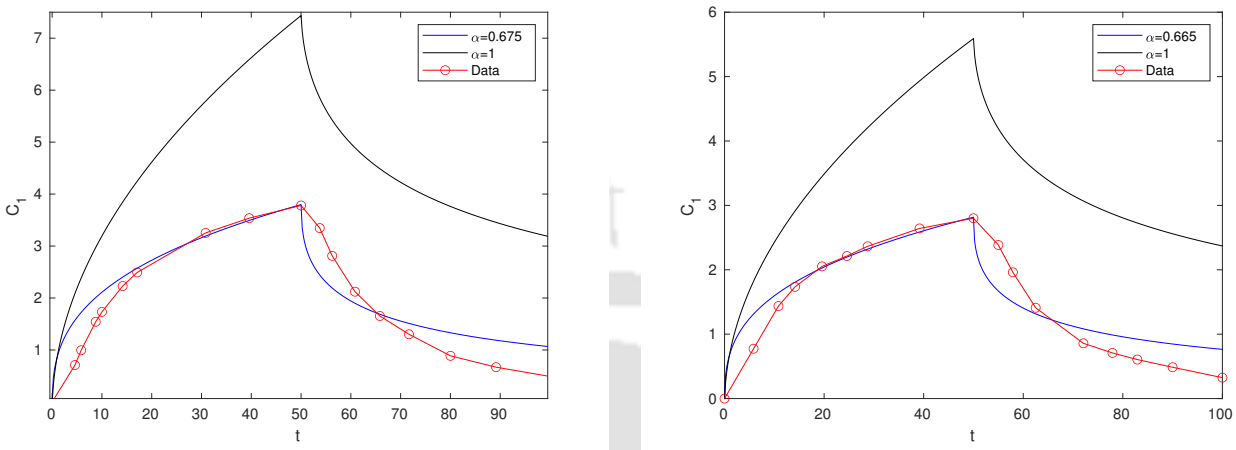

(a) (b)

Figure 4.9: Concentration curves along with experimental data for different values x and α, with $D_1 = 3 \times 10^{-9}$, $D_2 = 0.7 \times 10^{-9}$, $a = 85$, $\lambda_1 = 0.25$, $\lambda_2 = 1.6$, $S_1 = 1055 \times 10^{-3}$, $S_2 = 998.2 \times 10^{-3}$, $e_1 = 0.57$, $e_2 = 0.3$ and $K = 1.76 \times 10^{-5}$ (with appropriate units): (a) $x = 114$, (b) $x = 85$.

Figures 4.9(a) and 4.9(b) correspond to the plot for the mass transport at the location $x = 114\mu m$ and $x = 85\mu m$, respectively, along with the experimental data from [44] with different values of α (note that the values of x are part of this data). Now, observing these two figures, it is quite clear that, although the integer-order model stays far from the experimental data, the fractional-order model closely approximates the experimental data. As suggested by the graphical agreement, it is now evident that, for the fractional order of the derivative, $\alpha = 0.675$ and $\alpha = 0.665$ are the best probable values to closely capture the experimental data shown in Figs. 4.9(a) and 4.9(b), respectively.

Tables 4.1 and 4.2 certainly help in having a clear vision for the data approximation of the experimental data made by our proposed fractional-order model.

Table 4.1: Analogy of concentration C_1 at $x = 114\mu m$, with different α, $D_1 = 3 \times 10^{-9}$, $D_2 = 0.7 \times 10^{-9}$, $a = 85$, $\lambda_1 = 0.25$, $\lambda_2 = 1.6$, $S_1 = 1055 \times 10^{-3}$, $S_2 = 998.2 \times 10^{-3}$, $e_1 = 0.57$, $e_2 = 0.3$ and $K = 1.76 \times 10^{-5}$.

t	For $\alpha = 1$	For $\alpha = 0.675$	Experimental data
14.1667	3.8459	2.402	2.2303
17.0833	4.2465	2.5734	2.492
30.8333	5.7871	3.1914	3.25276
39.5833	6.5889	3.4925	3.53687
50	7.4349	3.7981	3.78053
60.8333	4.892	1.8992	2.1217
65.8333	4.4871	1.6878	1.65378

Table 4.2: Analogy of concentration C_1 at $x = 85\mu m$, with different α, $D_1 = 3 \times 10^{-9}$, $D_2 = 0.7 \times 10^{-9}$, $a = 85$, $\lambda_1 = 0.25$, $\lambda_2 = 1.6$, $S_1 = 1055 \times 10^{-3}$, $S_2 = 998.2 \times 10^{-3}$, $e_1 = 0.57$, $e_2 = 0.3$ and $K = 1.76 \times 10^{-5}$.

t	For $\alpha = 1$	For $\alpha = 0.665$	Experimental data
14.1667	2.9129	1.8073	1.73467
19.5833	3.4483	2.0274	2.0527
24.5833	3.8796	2.1968	2.21366
28.75	4.2065	2.3211	2.3647
39.1667	4.9321	2.5866	2.64192
50	5.59	2.8165	2.80041
62.5	3.5373	1.3152	1.40996

By observing Tables 4.1 and 4.2, it can be followed that, for both locations $x = 114\mu m$ and $x = 85\mu m$, while the integer-order model stays far from the experimental data, our proposed fractional-order model approximates the experimental data to a great extent, which certainly shows the effectiveness of the fractional-order model and unifies our findings.

For a robust understanding, we present two more sets of experimental data and examine the credibility of our fractional-order model.

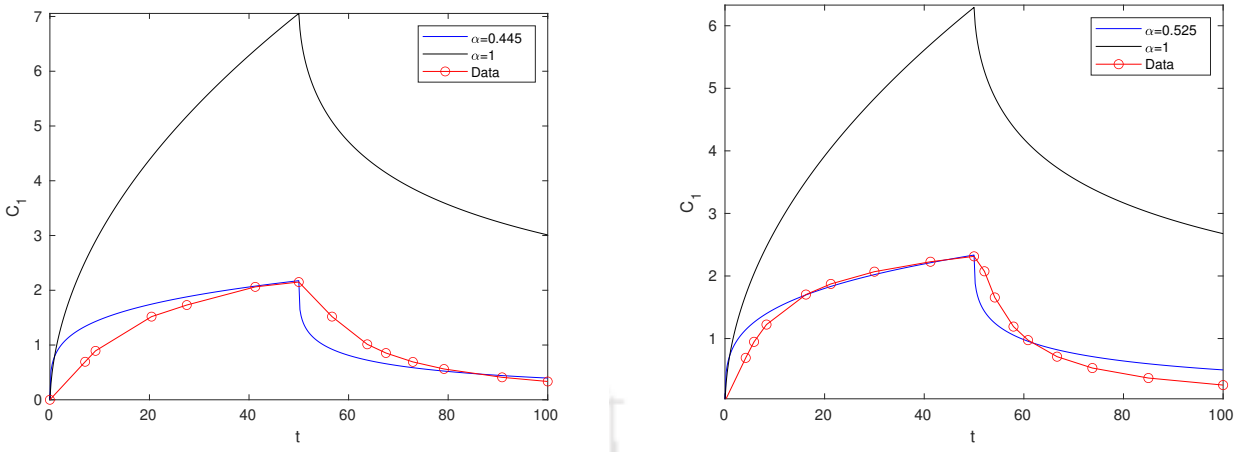

(a) (b)

Figure 4.10: Concentration curves along with experimental data for different values x and α, with $D_1 = 3 \times 10^{-9}$, $D_2 = 0.7 \times 10^{-9}$, $a = 85$, $\lambda_1 = 0.25$, $\lambda_2 = 1.6$, $S_1 = 1055 \times 10^{-3}$, $S_2 = 998.2 \times 10^{-3}$, $e_1 = 0.57$, $e_2 = 0.3$ and $K = 1.76 \times 10^{-5}$ (with appropriate units): (a) $x = 108$, (b) $x = 96$.

Figures 4.10(a) and 4.10(b) are the plots corresponding to the mass transport at the locations $x = 108\mu m$ and $x = 96\mu m$, respectively, along with the experimental data from [44] with different values of α (note that the values of x are part of this data). Looking at these figures, it is affirmative that, while the integer-order model fails to capture the experimental data, the fractional-order model approximates the experimental data in a far better way. Now, the graphical analysis suggests the best probable value for the fractional order of the derivative as $\alpha = 0.445$ and $\alpha = 0.525$ for a close agreement with the experimental data presented in Figs. 4.10(a) and 4.10(b).

Tables 4.3 and 4.4 give a clear elucidation of Figs. 4.10(a) and 4.10(b) in approximating the experimental data by our proposed fractional-order model.

One can now easily follow how Tables 4.3 and 4.4 perfectly capture the fractional-order model approximating the experimental data in a more accurate manner than the corresponding integer-order ones. Hence, the accuracy availed by our proposed fractional-order model which earlier was intangible by the integer-order one, certainly unifies our proposed model in the research of bio-mathematics modelling and approximating laboratory data by an analytical solution.

It needs to be mentioned that Nicholson and Phillips [44] worked only with the solution given by $C_1(x,t)$, and that is why we also show the graphical agreement by our first solution $C_1(x,t)$ only. The other solution $C_2(x,t)$ can also be used to approximate the experimental data once some data are made available in the literature. Still both the

Table 4.3: Analogy of concentration C_1 at $x = 108\mu m$, with different α, $D_1 = 3 \times 10^{-9}$, $D_2 = 0.7 \times 10^{-9}$, $a = 85$, $\lambda_1 = 0.25$, $\lambda_2 = 1.6$, $S_1 = 1055 \times 10^{-3}$, $S_2 = 998.2 \times 10^{-3}$, $e_1 = 0.57$, $e_2 = 0.3$ and $K = 1.76 \times 10^{-5}$.

t	For $\alpha = 1$	For $\alpha = 0.445$	Experimental data
20.4167	4.4311	1.7464	1.51856
27.5	5.1771	1.8795	1.73037
41.25	6.389	2.0756	2.06209
50	7.0558	2.1751	2.15029
72.9167	3.8577	0.5862	0.691603
79.1667	3.5954	0.5241	0.562517
90.8333	3.2285	0.4423	0.410275

Table 4.4: Analogy of concentration C_1 at $x = 96\mu m$ with different α, $D_1 = 3 \times 10^{-9}$, $D_2 = 0.7 \times 10^{-9}$, $a = 85$, $\lambda_1 = 0.25$, $\lambda_2 = 1.6$, $S_1 = 1055 \times 10^{-3}$, $S_2 = 998.2 \times 10^{-3}$, $e_1 = 0.57$, $e_2 = 0.3$ and $K = 1.76 \times 10^{-5}$.

t	For $\alpha = 1$	For $\alpha = 0.525$	Experimental data
8.3333	2.469	1.3991	1.22329
16.25	3.5146	1.6973	1.70311
21.25	4.0435	1.8327	1.87282
30	4.8365	2.0215	2.06872
41.25	5.7007	2.2119	2.22761
50	6.2934	2.3349	2.31382
66.6667	3.7317	0.8212	0.710168
73.75	3.3951	0.7115	0.528499

solutions can be used to approximate a wide class of experimental data. This claim will be clear by looking at Fig. 4.11.

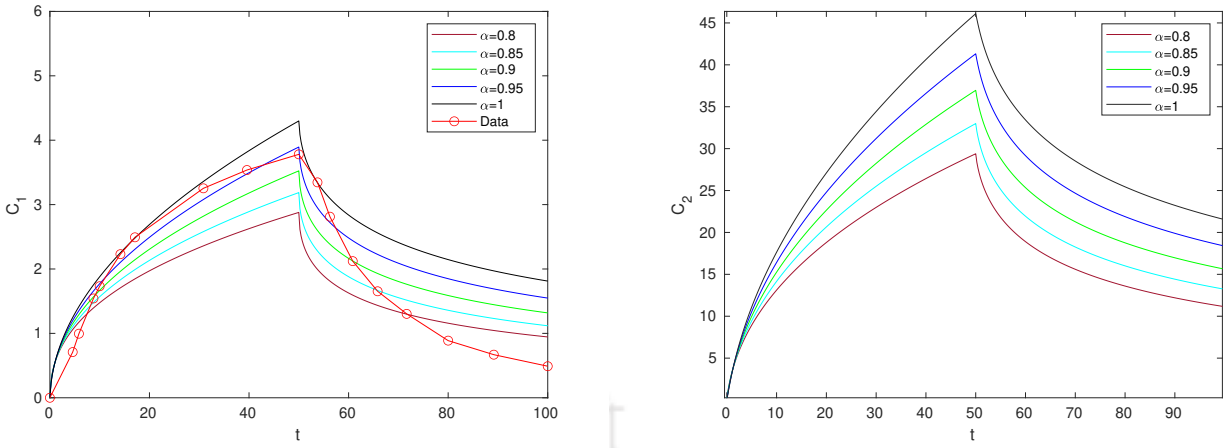

(a) (b)

Figure 4.11: Comparison of concentration of mass transport in both layers for different x, with $D_1 = 3 \times 10^{-9}$, $D_2 = 0.7 \times 10^{-9}$, $a = 85$, $\lambda_1 = 0.25$, $\lambda_2 = 1.6$, $S_1 = 1055 \times 10^{-3}$, $S_2 = 998.2 \times 10^{-3}$, $e_1 = 0.57$, $e_2 = 0.3$ and $K = 1.76 \times 10^{-5}$ (with appropriate units): (a) *in the first layer*, (b) *in the second layer*.

It can be clearly observed from Fig. 4.11(a) that the data lies between the graphs presented for different values for the fractional order α of the derivative. This enables us to deal with a large class of experimental data from the laboratory. Being motivated by the previous case, for Fig. 4.11(b) too, we are hopeful that it also possesses the ability to capture a wide class of experimental data. With the freedom given to the arbitrary order of the derivative, we try our best to utilize it in approximating the experimental data available in literature [44] and come up with some new attributes in capturing the physical data in a more profound manner.

4.5 Conclusion

As the integer-order model for mass transport to brain tissues presented by Jain et al. [29] was found to be incorrect due to some significant wrong calculations, we have revisited the model and found new analytical solutions for the integer-order model. The graphical analysis showed the transportation of nutrients in blood capillaries in brain tissues. Thus, we have successfully presented the mathematical framework of the transport model (which is based on the model in [29]) along with analytical solutions followed by a rigorous graphical analysis, fulfilling the prediction made by Ray et al. [51] that the mathematical modeling of the transport process might prove to be a powerful tool in investigating the transport process in its entirety. We have also established our claim and exhibited what made us to revisit the model and proceed with a fractional one. While executing the graphical analysis and the numerical implementations, we have observed that the

porosity and tortuosity played a crucial role in the diffusion procedure which has the usual implications, as the cell geometry (illustrated in terms of porosity and tortuosity) affects the diffusion process in a great extent. Looking at the analytical expressions too, it can be found that porosity (e_1, e_2) and tortuosity (λ_1, λ_2), appearing in the denominator of the expressions only and inside the exponential and complementary error functions, respectively, affect the solutions to a great extent. Further, the data from [44] presented in the work showed the same in this regard; so, our work also maintains the same analogy. Thereafter, we have presented a fractional version of the transport model to satisfy our query whether the analytical solution could be found or not, since the fractional derivative is known to capture some attributes that the integer-order ones cannot. In this direction, we successfully found the analytical solutions for the present model, and for a very particular case, when $\alpha \to 1$, we have shown that the solutions from the modified integer-order model (based on [29]) and the present fractional-order one match by means of graphical agreements. We have not only presented the analytical solutions to both models but also have recommended the choice of the best possible value for the fractional order in approximating four sets of experimental data available in [44]. Later on, we showed that not only a handful of data could be approximated but also a wide class of data from laboratory could be approximated by using the fractional-order model.

On the other hand, a number of limitations remain, which, in the future, can be tackled by taking into account more realistic conditions resulting in a more robust mathematical model. When the concern is about the brain, then it obviously is a sensitive issue, especially when it comes to brain surgery. Therefore, our focus was to study a model which could nearly capture the process of transport in such a way that when there are some abnormalities (apart from the serious illnesses like some fatal head injuries) in the human brain, our model can suggest a way out for treatment. We can now hope that the explicit solutions of our model will be handy for serving this purpose. It may seem a bit ambitious, but it is prudent to expect that such a model has the ability to provide sufficient information for treatment without touching the affected parts of the brain. Furthermore, it is believed that the present work is appropriate enough to encourage researchers in this field to study the complicated mass transport process through analytical solutions which will very likely lead to some important application sooner than later.

5

Fractional model for blood flow in a stenosed artery under MHD effect through a porous medium

This chapter presents a fractional model as a substitute to the integer-order model, describing the magnetohydrodynamics (MHD) effect of blood flow in a stenosed artery. We obtain an analytical solution for the fractional governing equation and also present an expression for the wall-shear stress. After the successful verification of our model with established models, we carry out a two-step validation with the experimental data existing in literature. Then, we analyze the obtained plots using the analytic expression. We exhibit how fractional model is helpful for controlling the blood flow through a stenosed artery. This study also indicates that magnetic field intensity significantly controls the flow velocity and wall-shear stress to a great extent. We also show that the external magnetic field, along with the fractional order of the governing equation, plays a pivotal role in the solution of the problem involving the treatment of stenosis. Finally, we conduct some experimental data approximation by the solution to establish the credibility of the proposed fractional order model.

5.1 Mathematical formulation

We consider a cosine-shaped stenosis in the artery with the consideration of the artery to be symmetric along the axis of blood flow. The following relation represents the mathematical formula, depicting the geometry of the stenosis (Singh et al. [59]):

$$\frac{R}{R_0} = 1 - \frac{\epsilon}{2R_0}\left(1 + \cos\frac{\pi z}{L_0}\right),$$

where the z-axis is the direction of the blood flow, L the length of the artery, R_0 and R the radii of the artery and of the stenotic region of the artery, respectively. Here, ϵ and L_0 are the maximum height of the stenotic region and the length of the stenotic region, respectively. Figure 5.1 presents the schematic for the stenosis in an artery.

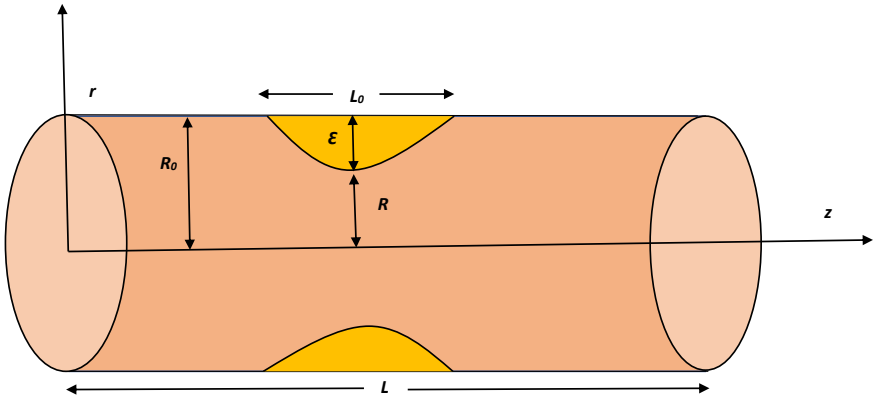

Figure 5.1: Schematic diagram of cosine-shaped stenosis in an artery.

We consider the blood to be incompressible and Newtonian. Further, we consider the blood flow to be axially symmetric (appealing to the realistic arterial flow situation) without taking any body forces into account (following Singh et al. [59]). Now, the continuity and the momentum equations in the cylindrical coordinates (r, θ, z) are the following:

$$\frac{\partial w}{\partial z} = 0, \tag{5.1}$$

$$\frac{\partial p}{\partial r} = 0, \tag{5.2}$$

$$\frac{1}{r}\frac{\partial p}{\partial \theta} = 0, \tag{5.3}$$

$$\rho \frac{\partial^{\alpha} w}{\partial t^{\alpha}} = -\frac{\partial p}{\partial z} + \mu \left(\frac{\partial^2 w}{\partial r^2} + \frac{1}{r}\frac{\partial w}{\partial r} \right) - \left(\nu B_0^2 - \frac{\mu}{e} \right) w, \tag{5.4}$$

where $0 \leq r \leq R$, $-\pi \leq \theta \leq \pi$, $z \geq 0$, $t \geq 0$, $0 < \alpha \leq 1$, w is the axial velocity of blood, p the fluid pressure, ρ the fluid density, e the porous parameter, ν the coefficient of conductivity, B_0 the applied transverse magnetic field intensity and μ is the viscosity of the fluid. For the time-fractional derivative in Eq. (5.4), we adopt Caputo fractional derivative of order $\alpha \in (0, 1]$, which is defined in Eqs. (1.4)−(1.6).

Further, the prescribed boundary conditions are the following:

$$\frac{\partial w}{\partial r} = 0; \quad \text{at } r = 0, \tag{5.5}$$

$$w = 0; \quad \text{at } r = R, \tag{5.6}$$

where we consider the blood velocity at the wall of the stenosis in the artery $(r = R)$ to be zero, which actually replicates the well-known no-slip condition at the wall of the stenosis. At present, we do not consider any velocity gradient for the blood flow in the artery.

5.2 Analytical solution

It is quite evident from Eq. (5.1) that w is independent of z. Also from Eqs. (5.2) and (5.3), it is clear that p is independent of both r and θ. We consider the following with both the quantities being time harmonic:

$$w(r,t) = \bar{w}(r)e^{\mathrm{i}\sigma t}, \text{ and } \quad \frac{\partial p}{\partial z} = -Pe^{\mathrm{i}\sigma t},$$

where $\mathrm{i} = \sqrt{-1}$, σ denotes the frequency of pulse and P is the constant pressure in the artery.

Using the above-mentioned expressions in Eq. (5.4), we obtain

$$\frac{d^2\bar{w}}{dr^2} + \frac{1}{r}\frac{d\bar{w}}{dr} - \left(\frac{\nu B_0^2}{\mu} - \frac{1}{e} + \frac{\rho(\mathrm{i}\sigma)^\alpha}{\mu}\right)\bar{w} = -\frac{P}{\mu}. \tag{5.7}$$

Using the method of undetermined coefficients, we can obtain the explicit analytic solution in a closed form as

$$\bar{w}(r) = \frac{P}{\mu\alpha_1^2}\left[\frac{J_0(\alpha_1 r)}{J_0(\alpha_1 R)} - 1\right], \tag{5.8}$$

where $\alpha_1^2 = \left(\frac{1}{e} - \frac{\nu B_0^2}{\mu} - \frac{\rho(\mathrm{i}\sigma)^\alpha}{\mu}\right)$ and J_0 is the Bessel function of first kind of order zero with complex argument.

Therefore, the closed-form solution $w(r,t)$ can be written as

$$w(r,t) = \frac{P}{\mu\alpha_1^2}\left[\frac{J_0(\alpha_1 r)}{J_0(\alpha_1 R)} - 1\right]e^{\mathrm{i}\sigma t}. \tag{5.9}$$

Furthermore, we calculate the expression for the wall-shear stress exerted by the blood to the stenosis. This quantity also plays a crucial role, like the blood velocity, in finding a probable solution for the treatment of a stenosed artery. Hence, to have a better understanding, we require the explicit expression for the same, and a rigorous analysis will be carried out in the course of discussion.

Following Singh et al. [59], we have the expression for the wall-shear stress at the stenosis wall as

$$\tau_s = -\left(\mu\frac{\partial w}{\partial r}\right)_{r=R}. \tag{5.10}$$

Now, rendering the expression for the blood velocity $w(r,t)$ from Eq. (5.9), the final expression for the wall-shear stress at the stenosis wall is found as

$$\tau_s = \frac{P}{\alpha_1} \times \frac{J_1(\alpha_1 R)}{J_0(\alpha_1 R)} \times e^{\mathrm{i}\sigma t}, \tag{5.11}$$

where J_1 is the Bessel function of first kind of order one with complex argument.

5.3 Model verification

In our work, the governing equation appears as a time-fractional one with order α ($0 < \alpha \leq 1$) which is the generalization of the existing integer-order model of Singh et al. [59]. Hence, under the particular case $\alpha \to 1$, our fractional model must retrieve the original integer-order model of Singh et al. [59] and so is true for the solution (5.8).

As $\alpha \to 1$, the solution (5.8) becomes

$$w(r,t) = \frac{P}{\mu\alpha_2^2}\left[\frac{J_0(\alpha_2 r)}{J_0(\alpha_2 R)} - 1\right] e^{i\sigma t}, \tag{5.12}$$

where $\alpha_2^2 = \left(\frac{1}{e} - \frac{\nu B_0^2}{\mu} - \frac{\rho(i\sigma)}{\mu}\right)$.

Looking at the solution (5.12), it is quite clear that this solution exactly matches that of the integer-order one by Singh et al. [59].

To have a better insight, we present the graphical agreement for the solutions of the integer-order and fractional-order ones. To do so, we choose some suitable values for the parameters used in the solutions Eq. (5.9) and (5.12). Here, we use the non-dimensional values for the magnetic number $M = \nu B_0^2 R_0^2 = 1.5$, radius of the artery $R = 2.0$, maximum height of the stenosis $\epsilon = 1$, magnetic intensity $\nu = 0.05$, porous medium parameter $e = 0.8$, viscosity $\mu = 0.06$, density of blood $\rho = 0.08$, the constant pressure $P = 0.4$ and frequency $\sigma = \pi/2$. We render the values of the used parameters for the graphical illustrations from Singh et al. [59].

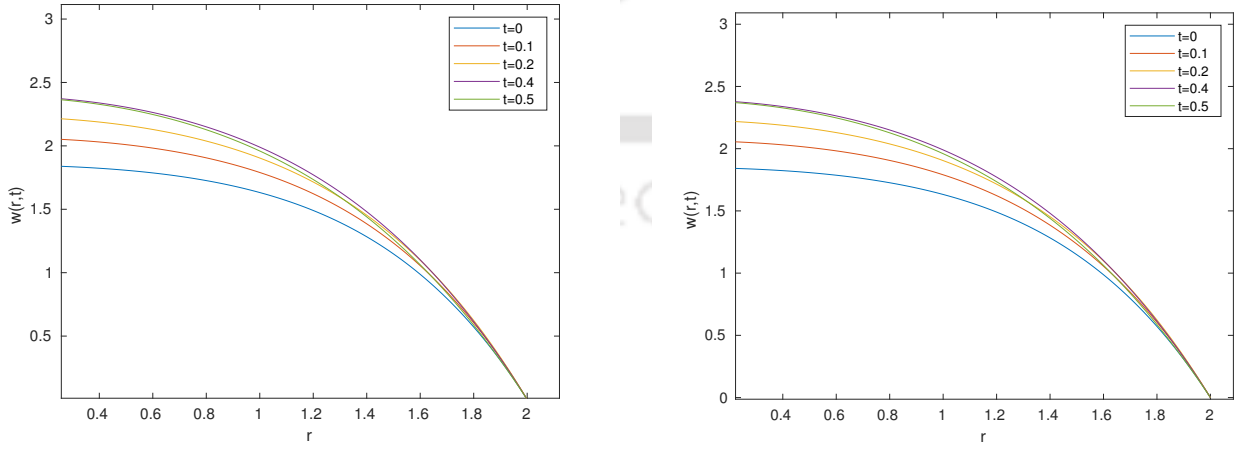

(a) (b)

Figure 5.2: Stenosed-artery blood flow for different time t, with $\alpha = 1$, $R = 2.0$, $\epsilon = 1$, $\nu = 0.05$, $e = 0.8$, $\mu = 0.06$, $\rho = 0.08$, $P = 0.4$, $\sigma = \pi/2$ and $M = 1$: (a) *integer-order model*, (b) *fractional-order model*.

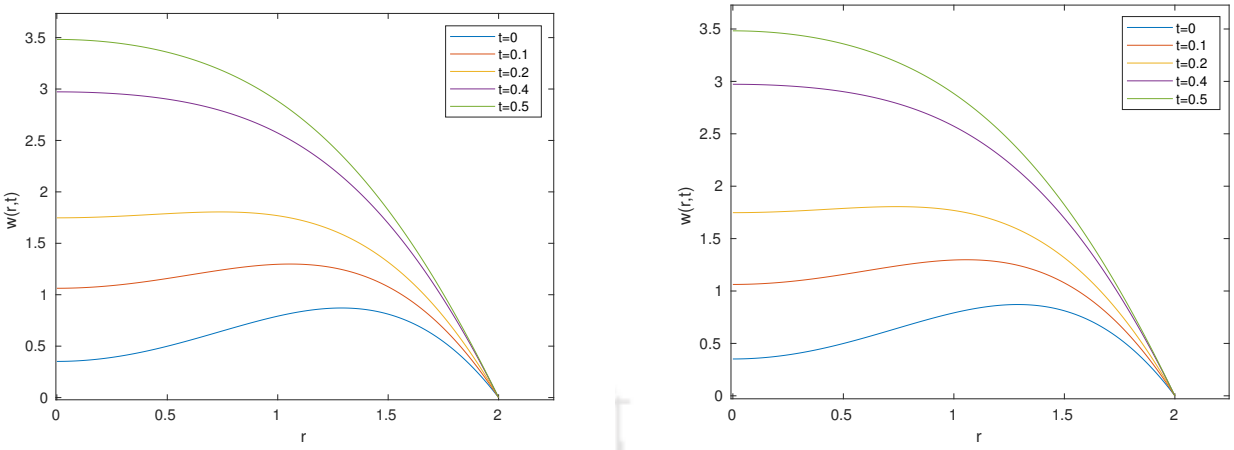

(a) (b)

Figure 5.3: Stenosed-artery blood flow for different time t, with $\alpha = 1$, $R = 2.0$, $\epsilon = 1$, $\nu = 0.05$, $e = 0.8$, $\mu = 0.06$, $\rho = 0.08$, $P = 0.4$, $\sigma = \pi/2$ and $M = 0.1$: (a) *integer-order model*, (b) *fractional-order model*.

Figures 5.2(a) and 5.3(a) correspond to the analytical solution of the integer-order model by Singh et al. [59] while Figs. 5.2(b) and 5.3(b) correspond to the present fractional-order model, for two different magnetic numbers (first $M = 1$ and then $M = 0.1$). Giving a thorough glance at these plots, it can be easily checked that they match exactly, which enables us to verify our model graphically.

Hereafter, we present a few more plots to have the nuance of the magnetic number in this study. Later on, we try to elucidate the role of this magnetic number in details as the discussion progresses. For the time being, we use the plots for verification purpose only.

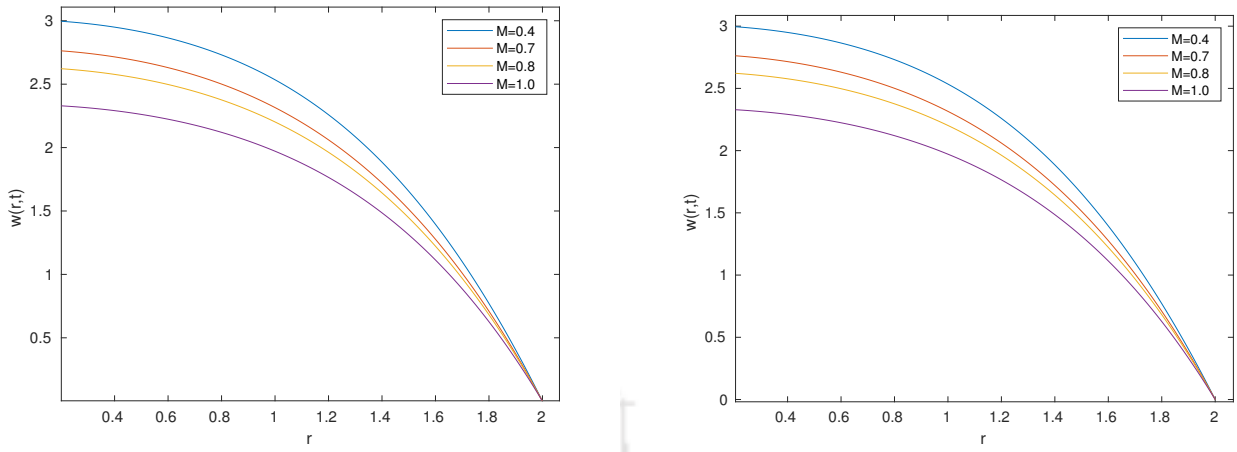

(a) (b)

Figure 5.4: Stenosed-artery blood flow for different M, with $\alpha = 1$, $R = 2.0$, $\epsilon = 1$, $\nu = 0.05$, $e = 0.8$, $\mu = 0.06$, $\rho = 0.08$, $P = 0.4$, $\sigma = \pi/2$ and $t = 0.3$: (a) *integer-order model*, (b) *fractional-order model*.

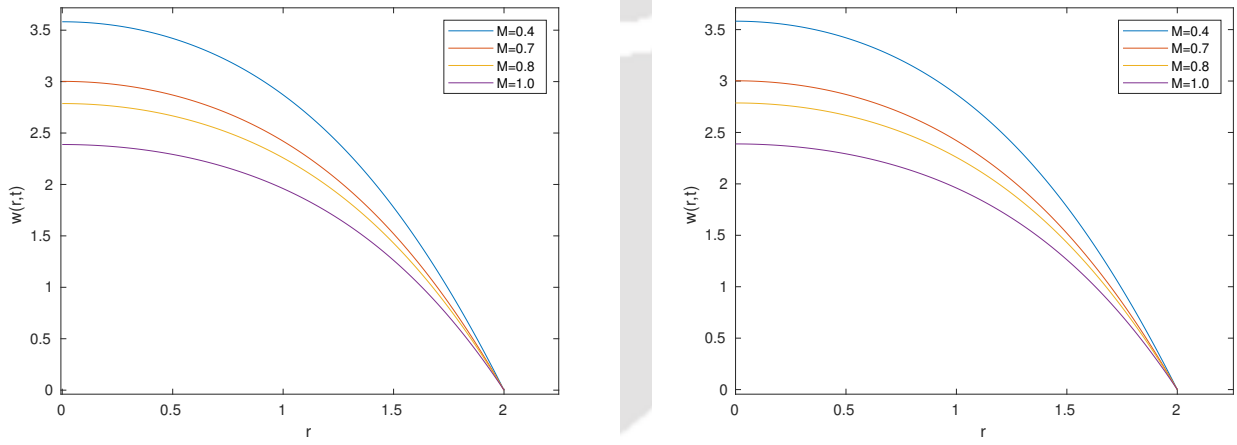

(a) (b)

Figure 5.5: Stenosed-artery blood flow for different magnetic number M with $\alpha = 1$ and time $t = 0.5$: (a) *integer-order model*, (b) *fractional-order model*.

Looking at Figs. 5.4 and 5.5, it can be noticed that, for different magnetic numbers, both the integer-order model and fractional-order model agree exactly. Although we present two particular instances for time (i.e., $t = 0.3$ and $t = 0.5$), the plots from both the models will have the exact matching even if we consider any other time.

5.4 Validation

In this section, we carry out a two-step validation of our model against the experimental data, existing in literature. First, we compare our model solution with the experimental

data fetched from the model of Shah et al. [54], where the authors studied the effects of the magnetic field and the fractional order of the governing differential equation on the blood flow in a cylindrical domain without any stenosis. To make our model analogous to their model, we choose $\epsilon = 0$, which shares the key responsibility for the stenosis in our model. Later on, we showcase how our solution closely matches the experimental data presented by Singh et al. [59], where they considered the stenosis in their model.

Before going for further discussion, let us elaborate the method, by means of which we conduct the validation. Here, we primarily aim to achieve the exact matching or a close matching with existing experimental data in literature by the model solution. Therefore, we plot our solution against the available data taken from existing literature and exhibit how closely our solution matches this data. A successful implementation eventually helps in validating our proposed model.

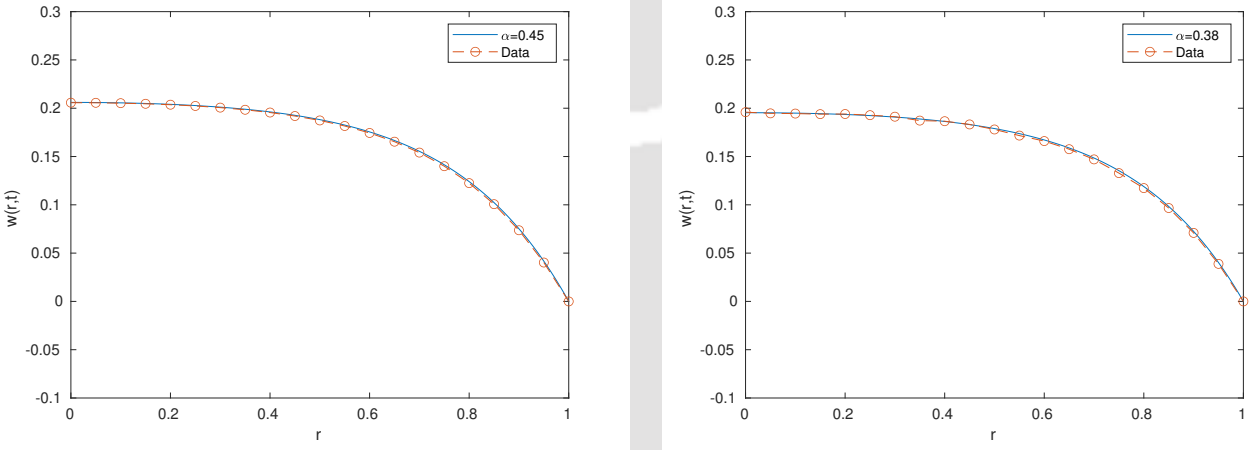

(a) (b)

Figure 5.6: Stenosed-artery blood flow for different α, with $R = 2.0$, $\epsilon = 0$, $\nu = 0.05$, $e = 0.8$, $\mu = 0.06$, $\rho = 0.08$, $P = 0.4$, $\sigma = \pi/4$, $t = 1$ and $M = 1$: (a) *comparison with data (having fractional-order* 0.8 *[54])*, (b) *comparison with data (having fractional-order* 0.6 *[54]).*

Figure 5.6 corresponds to $\sigma = \frac{\pi}{4}$, $R = 1$, $t = 1$, $\epsilon = 0$, $M = 1$ and all the other parameters are as they are. Figure 5.6(a) corresponds to the fractional order 0.8 of the derivative in the model of Shah et al. [54] and Fig. 5.6(b) corresponds to the fractional order 0.6. Now, observing both figures, it can be followed that our model closely agrees with the data fetched from their model. Since, they did not consider any magnetic number in their model, that is why we get some different values for the fractional order of the derivative in our model while matching with their data.

Now, we consider another set of data taken from Singh et al. [59], where the stenosis is present, to validate our model. The plots in Fig. 5.7 help in depicting the validation.

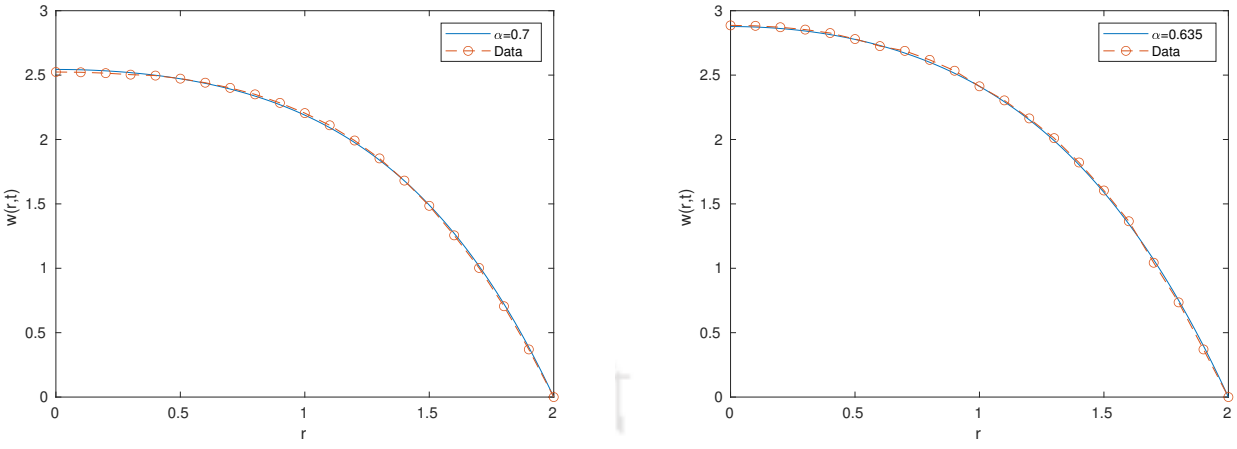

(a) (b)

Figure 5.7: Stenosed-artery blood flow for different α, with $R = 2.0$, $\epsilon = 1$, $\nu = 0.05$, $e = 0.8$, $\mu = 0.06$, $\rho = 0.08$, $P = 0.4$, $\sigma = \pi/2$ and $t = 0$: (a) for $M = 0.6$, (b) for $M = 0.2$.

Figure 5.7 corresponds to two different values of the magnetic number with $\sigma = \frac{\pi}{2}$, $R = 2$, $t = 0$, $\epsilon = 1.0$ and all the other parameters are as they are. Now, looking at Fig. 5.7(a) and 5.7(b), it can be observed that, with the aid of fractional order of the derivative, we successfully match the data fetched from the model by Singh et al. [59]. Hence, we establish the validation of our model by comparing it with the experimental data from existing literature.

Having validated our model against two established models, it can be inferred that the proposed model is suitable for studying various issues related to the MHD effect of blood flow in the stenosed artery.

5.5 Results and discussion

In order to identify the influence of different flow parameters on the blood velocity, we present the graphical illustrations, carried out by using the analytical solution (5.9) of the fractional model for different values of the parameters. In the treatment of several arterial diseases like atherosclerosis, which is mainly caused by forming stenosis in the arteries, the blood velocity $w(r,t)$ and the wall-shear stress play an important role. The focus is to influence the blood flow by applying magnetic field from outside. Here, we present the graphical illustrations for the blood velocity and wall-shear stress one by one, which are greatly influenced by the external magnetic field and the fractional order of the governing equation.

5.5.1 Velocity profile behaviour

As the stenosis in the arteries is caused due to the deposition of fatty substances like cholesterol, cellular waste product and lipoproteins inside the blood vessel, a possible remedy to circumvent those abnormalities is to carry out a surgery. But for some extreme cases, like for aged persons, having a surgery to treat the stenosis in the carotid artery etc., may be life-risking. For such situations, MHD effect of blood plays a crucial role: by applying external magnetic field, the blood velocity can be influenced, which is evident from Figs. 5.8−5.10.

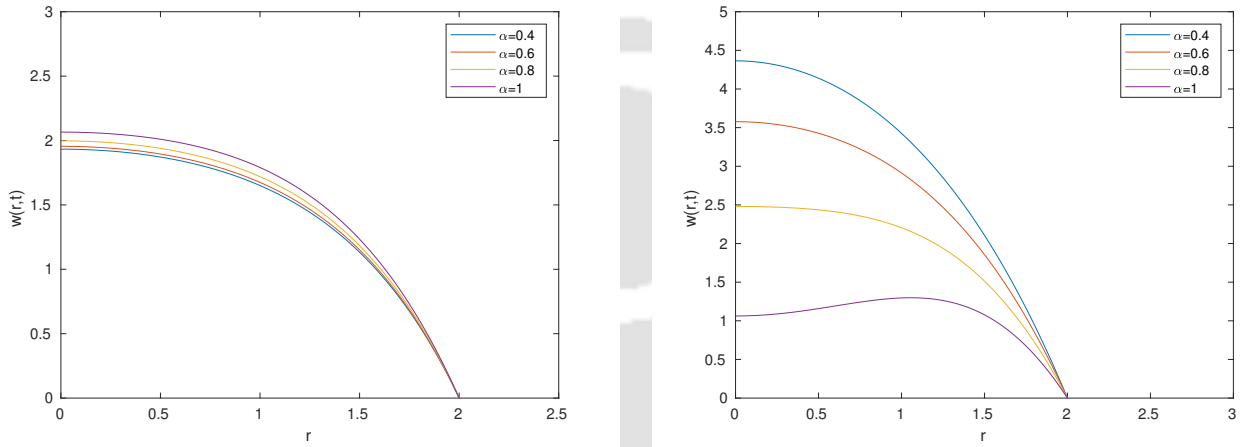

(a) (b)

Figure 5.8: Stenosed-artery blood flow for different α, with $R = 2.0$, $\epsilon = 1$, $\nu = 0.05$, $e = 0.8$, $\mu = 0.06$, $\rho = 0.08$, $P = 0.4$, $\sigma = \pi/2$ and $t = 0.1$: (a) for $M = 1$, (b) for $M = 0.1$.

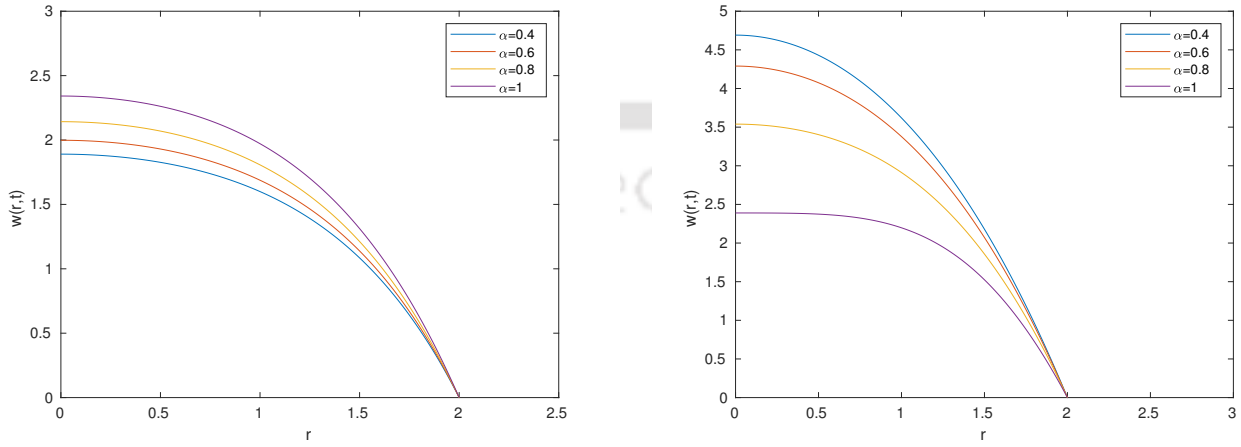

(a) (b)

Figure 5.9: Stenosed-artery blood flow for different α, with $R = 2.0$, $\epsilon = 1$, $\nu = 0.05$, $e = 0.8$, $\mu = 0.06$, $\rho = 0.08$, $P = 0.4$, $\sigma = \pi/2$ and $t = 0.3$: (a) for $M = 1$, (b) for $M = 0.1$.

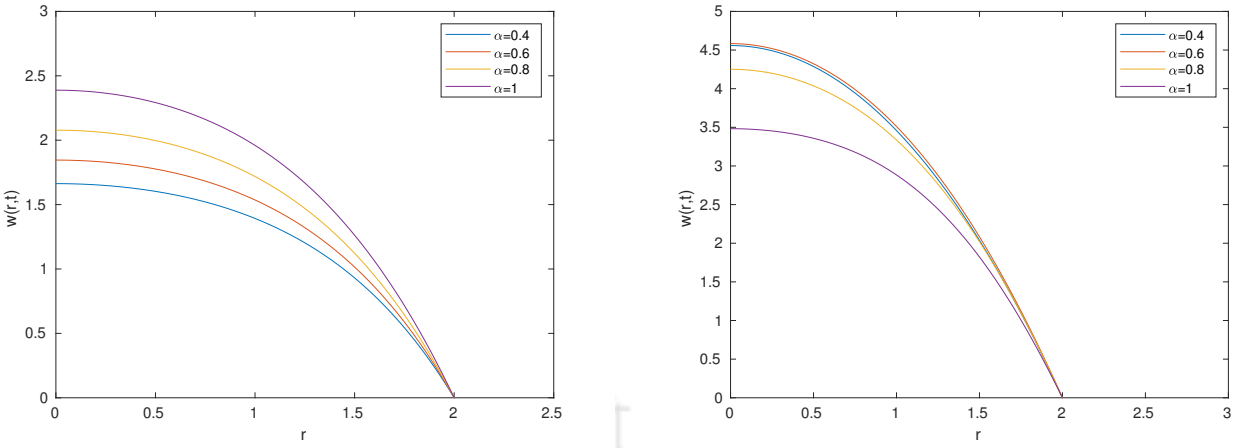

Figure 5.10: Stenosed-artery blood flow for different α, with $R = 2.0$, $\epsilon = 1$, $\nu = 0.05$, $e = 0.8$, $\mu = 0.06$, $\rho = 0.08$, $P = 0.4$, $\sigma = \pi/2$ and $t = 0.5$: (a) for $M = 1$, (b) for $M = 0.1$.

Figures 5.8–5.10 reveal that increasing the intensity of the magnetic field (in terms of magnetic number M) causes a diminution in blood velocity with the increment of the fractional-order of the derivative α, as the velocity profiles for $M = 1$ are much lower than those for $M = 0.1$. That is, the magnetic force regulates the velocity of blood flow in the deceased artery, which may be helpful in the treatment of cardiovascular deceases

One of the objectives is to examine whether it is possible to influence the blood velocity in the stenotic region in such a way that it helps getting rid of the stenosis, which is successfully achieved. By increasing or lowering the blood velocity in the stenotic region, we can create pressure on the stenosis wall, which, as a result, is hoped to help in dissolving the stenosis. As the fractional derivatives exhibit memory effect, the fractional models can provide supplemental information and some remarkable insights on the fluid behaviour with complex rheology as compared to the integer-order models. With the aid of the external magnetic field and the fractional derivative, we are going to capture the special characteristics of the blood flow.

From Figs. 5.8–5.10, it can be noticed that the blood flow profiles (velocity profiles) on the left-hand side (for $M = 1$) corresponding to the problem modelled by the integer-order model (IM) (Singh et al. [59]) is always above that of the proposed fractional model (FM). On the other hand, the profiles on the right-hand side (for $M = 0.1$) exhibit the opposite phenomenon, i.e., the profiles for IM always remain below those of FM. Hence, in a real-world situation, when we need the influenced velocity to be higher or lower than that of IM, we can prescribe the proposed fractional model which may help in dealing with a blood flow problem for a stenosed artery. It may be possible that the implementation of this model may allow recovery without any surgery.

5.5.2 Wall shear stress behaviour

Another important aspect, while treating the stenosed arteries, is the wall-shear stress at the stenosis wall. It actually helps in localizing the stenosis in the artery. Earlier, having control over the blood velocity by using the magnetic field and the fractional derivative, we proposed a procedure for a probable cure for the stenosis. Now, using the wall-shear stress, we can locate the exact position of the stenosis, and the utilization of the fractional derivative refines the procedure. Here, we present a few plots to shed some lights in this regard.

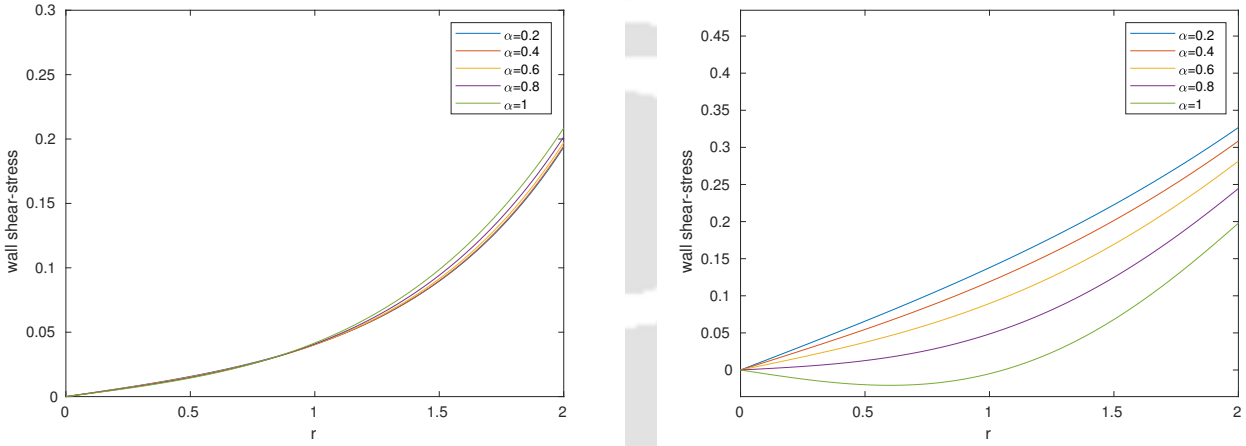

Figure 5.11: Fractional stenosed-artery blood flow for different α, with $R = 2.0$, $\epsilon = 1$, $\nu = 0.05$, $e = 0.8$, $\mu = 0.06$, $\rho = 0.08$, $P = 0.4$, $\sigma = \pi/2$ and $t = 0.1$: (a) for $M = 1$, (b) for $M = 0.1$.

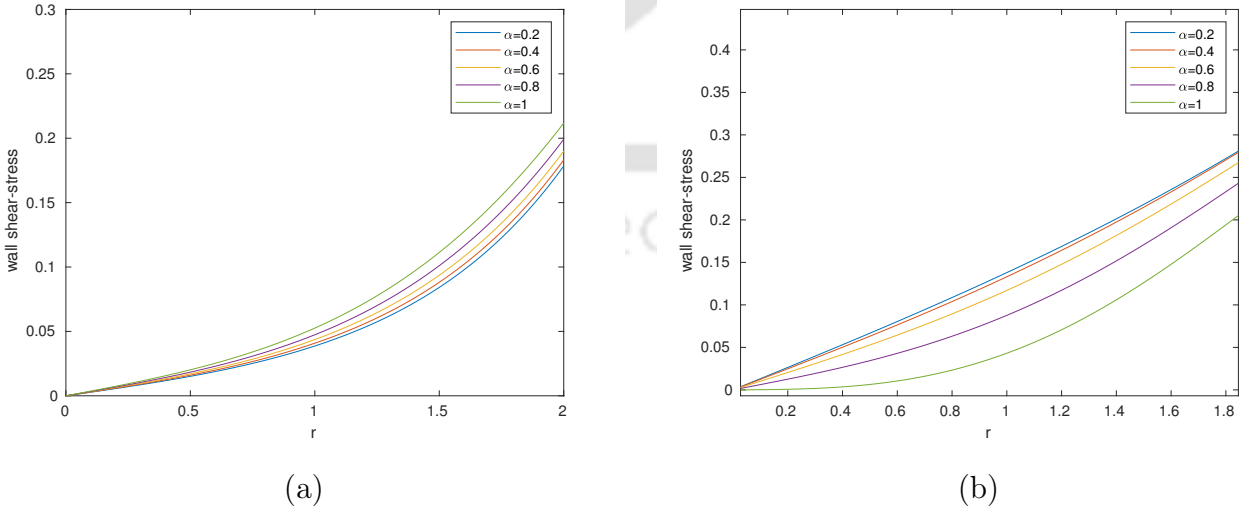

Figure 5.12: Fractional stenosed-artery blood flow for different α, with $R = 2.0$, $\epsilon = 1$, $\nu = 0.05$, $e = 0.8$, $\mu = 0.06$, $\rho = 0.08$, $P = 0.4$, $\sigma = \pi/2$ and $t = 0.3$: (a) for $M = 1$, (b) for $M = 0.1$.

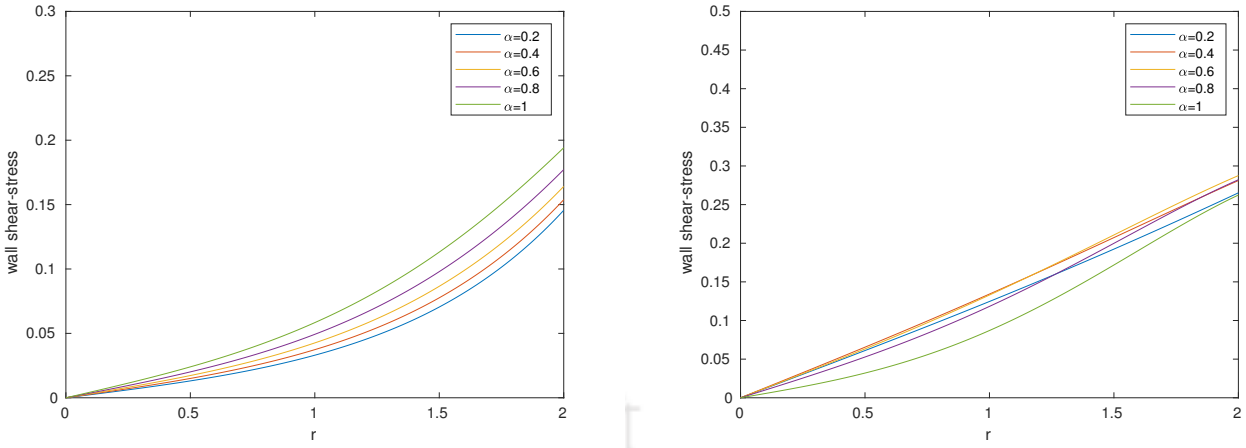

(a) (b)

Figure 5.13: Fractional stenosed-artery blood flow for different α, with $R = 2.0$, $\epsilon = 1$, $\nu = 0.05$, $e = 0.8$, $\mu = 0.06$, $\rho = 0.08$, $P = 0.4$, $\sigma = \pi/2$ and $t = 0.5$: (a) for $M = 1$, (b) for $M = 0.1$.

Looking at Figs. 5.11−5.13, it can be observed that, at $r = 2$, i.e., at the peak of the stenosis, the wall-shear stress is higher than at the other places as we increase the fractional order of the derivative α. In other words, we can say that starting from zero wall-stress, the place where we find the maximum wall-stress is the desired place to be identified.

The presence of the magnetic field at the stenotic throat decelerates the flow and subsequently, decreases the wall-shear stress as shown in Figs. 5.11−5.13: the profiles on the left (for $M = 1$) are much lower than those on the right (for $M = 0.1$). This implies that the wall-shear stress is also highly influenced by the external magnetic field which can be crucial in diagnosing the stenosis and providing a probable cure.

Like the velocity profiles, in Figs. 5.11−5.13, it can be observed that the wall-stress profiles follow the same pattern, i.e., for $M = 1$, the IM profile is above the FM profile, and for $M = 0.1$, the contrary happens. Hence, as the situation requires, we can prescribe both the cases having lower stress and higher stress region of the stenosis.

5.5.3 Magnetic field behaviour

Due to the bio-magnetic nature of blood, external magnetic field can be used to control abnormal blood circulation in the body that can lead to heart disease or even death. Now, we are going to exhibit the role of the magnetic field in influencing the blood flow in the stenosed artery.

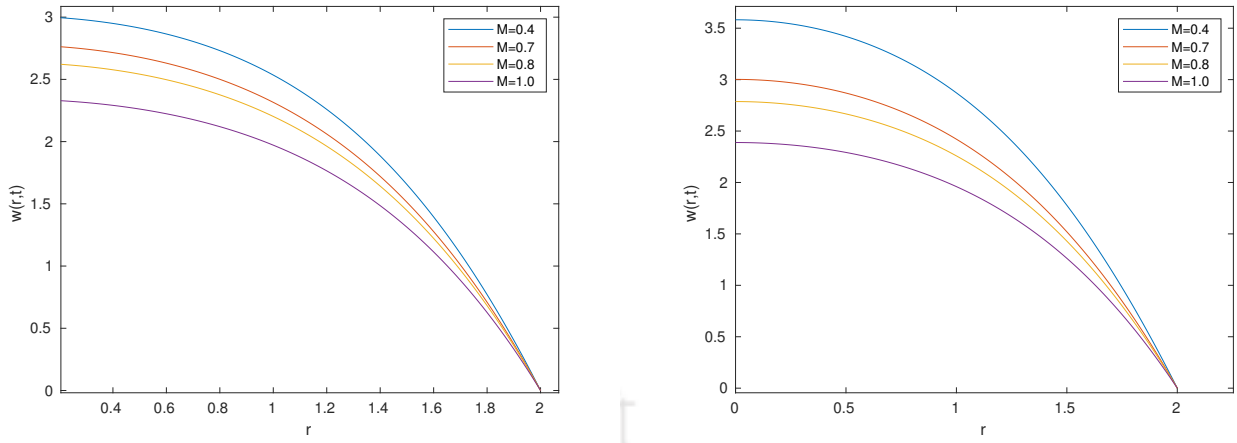

(a) (b)

Figure 5.14: Fractional stenosed-artery blood flow for different M, with $R = 2.0$, $\epsilon = 1$, $\nu = 0.05$, $e = 0.8$, $\mu = 0.06$, $\rho = 0.08$, $P = 0.4$, $\sigma = \pi/2$ and $\alpha = 1$: (a) for $t = 0.3$, (b) for $t = 0.5$.

As we apply the magnetic field in the transverse direction of the blood flow, the blood velocity should dip with an increment of the magnetic field. From Fig. 5.14, it can be easily observed that, as the magnetic number increases, the velocity of blood keeps decreasing. This happens since blood consists of magnetic particles like iron in the haemoglobin, which exhibits the ferromagnetic nature of the blood. Hence, the application of the external magnetic field can influence the blood velocity to a great extent. Figure 5.15 helps in having a clear view on how the magnetic field can influence the blood flow.

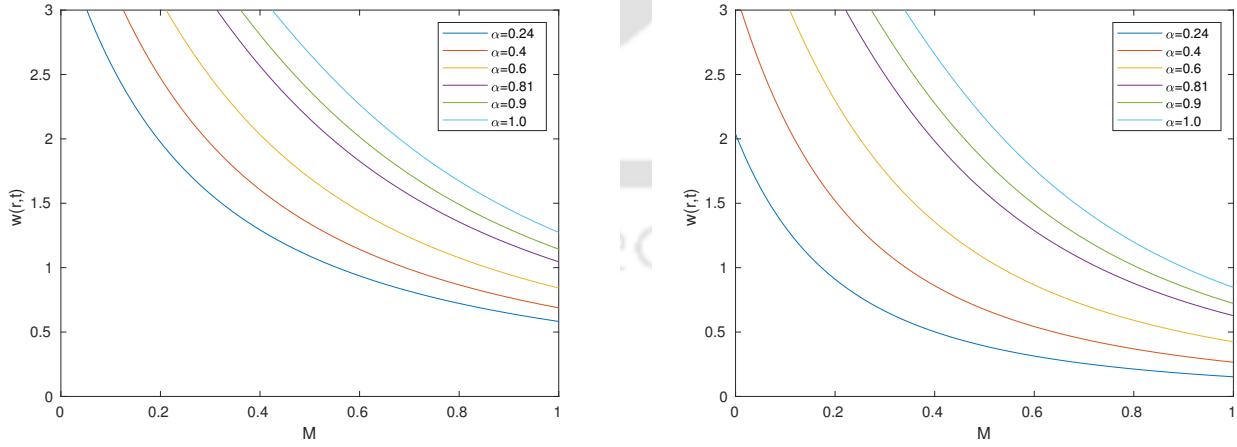

(a) (b)

Figure 5.15: Fractional stenosed-artery blood flow for different t, with different α, $R = 2.0$, $\epsilon = 1$, $\nu = 0.05$, $e = 0.8$, $\mu = 0.06$, $\rho = 0.08$, $P = 0.4$ and $\sigma = \pi/2$: (a) for $t = 0.8$, (b) for $t = 1$.

As we increase the magnetic number, which results in an increment in the external

magnetic field, the flow rate reduces. The plots in Fig. 5.15 ascertain the same. Now, this fact can be used in the treatment of the stenosis since, by influencing the blood velocity by applying external magnetic field, stress can be created on the tip of the stenosis, which as a result may help in getting rid of the stenosis.

However, we cannot consider arbitrary large values for the magnetic number since a large magnetic number corresponds to large magnetic intensity, which, on application to the human body, may very likely have adverse effects. Therefore, our aim is to develop a model with lower magnetic intensity, but which still serves our purpose. For that case, we need the help of a fractional model which helps us serve the same purpose but with a lower magnetic number. This can be explained via Fig. 5.16 from which it can be observed that, as we reduce the magnetic number (in other words, we reduce the external magnetic field intensity), the initial velocity becomes different, which can definitely be termed as a drawback of the integer-order model. Next, we are going to eliminate this

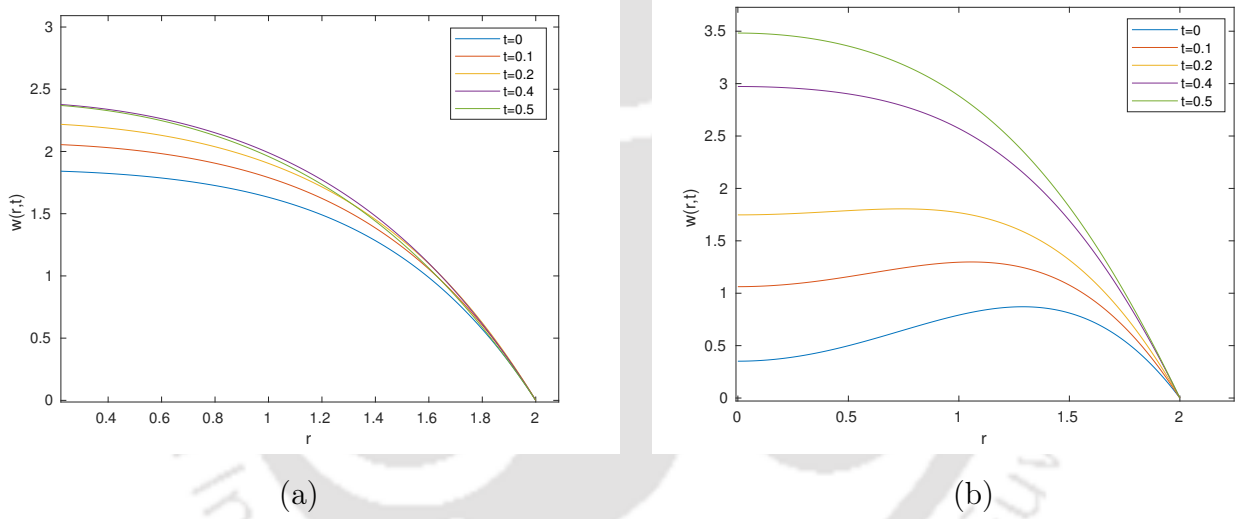

Figure 5.16: Fractional stenosed-artery blood flow for different t, with $R = 2.0$, $\epsilon = 1$, $\nu = 0.05$, $e = 0.8$, $\mu = 0.06$, $\rho = 0.08$, $P = 0.4$, $\sigma = \pi/2$: (a) for $M = 1$, (b) for $M = 0.1$.

error with the incorporation of the fractional order of the governing differential equation. Figure 5.17 elaborates the same, glancing through which, it can be observed that the initial condition (initial non-zero blood velocity) is successfully recovered by the fractional model on choosing $\alpha = 0.81$. Hence, where the integer-order model fails to recover the initial condition, the fractional-order model achieves that−definitely a benefit out of the proposed fractional model.

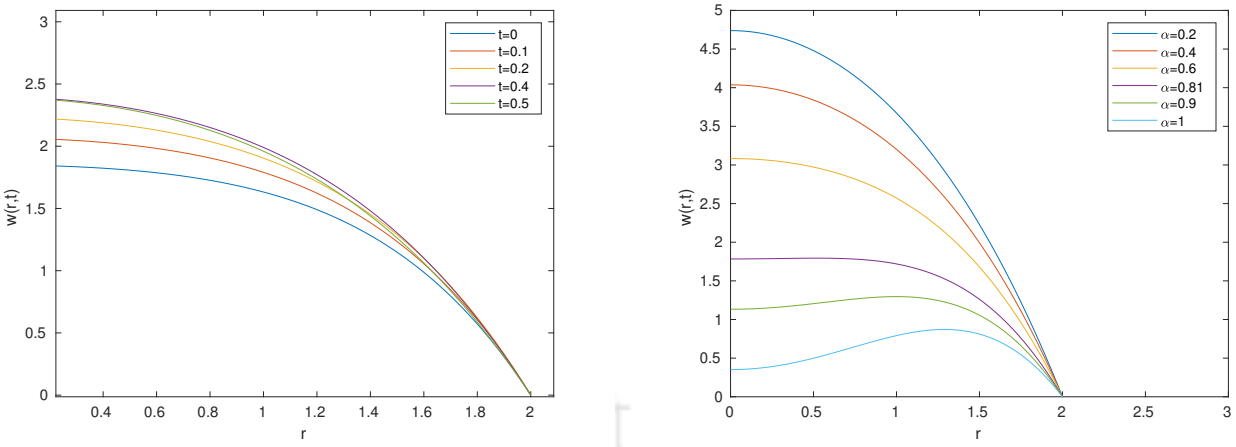

(a) (b)

Figure 5.17: Fractional stenosed-artery blood flow for different t and α, with $R = 2.0$, $\epsilon = 1$, $\nu = 0.05$, $e = 0.8$, $\mu = 0.06$, $\rho = 0.08$, $P = 0.4$, $\sigma = \pi/2$: (a) for $M = 1$, (b) for $M = 0.1$.

5.5.4 Experimental data approximation

In the earlier subsections, we studied the behaviours of various parameters which affect the flow in the stenosed artery. Here, we present one of the key features of the fractional model, viz., its ability to approximate the clinical or experimental data in a far better way than the integer-order model. To establish this fact, we next showcase a few plots.

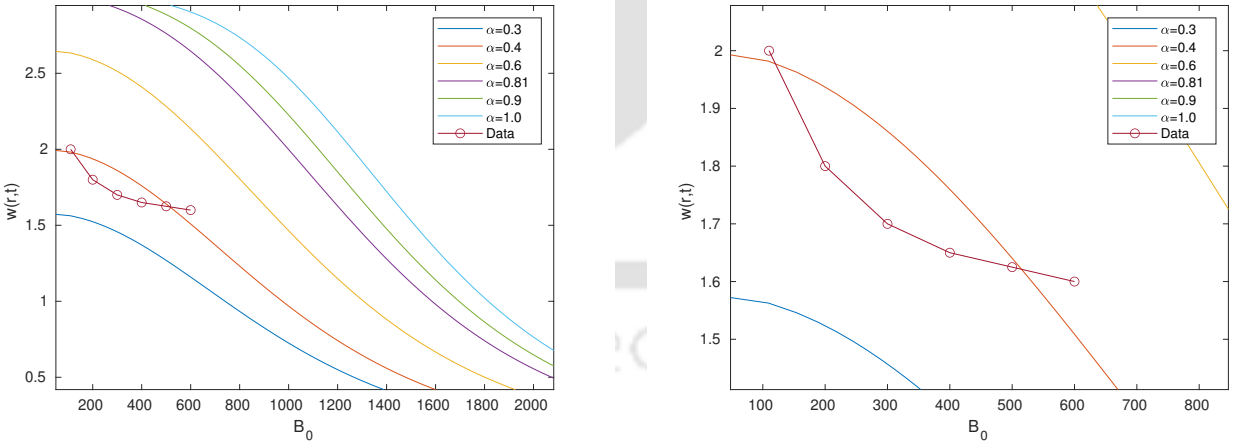

(a) (b)

Figure 5.18: Fractional stenosed-artery blood flow for different magnetic field intensity B_0 and different α, with $R = 2.0$, $\epsilon = 0$, $\nu = 0.05$, $e = 0.8$, $\mu = 0.06$, $\rho = 0.08$, $P = 0.4$, $\sigma = \pi/2$: (a) *standard plots*, (b) *amplified plots*.

For the graphical analysis, we render the data from the work of Sharma et al. [58], where the authors carried out an in-vitro experiment with artificial blood along with some mag-

netic particles in it to make it analogous to the real blood. In their investigation, they studied the effect of the external magnetic field on the blood flow without considering any stenosis in their model. To check whether our model is able to approximate their data or not, we take $\epsilon = 0$ to make our model analogous to their model.

Now, looking at Fig. 5.18, it can be seen that our solution is capable of catching the experimental data closely, whereas the integer-order solution ($\alpha = 1$) stays far away from the data. From those figures, we can prescribe that $\alpha = 0.4$ is the best choice for our model to meet the experimental data. Although we do not get the exact matching, still our model solution is able to get closer to the experimental data, and to the best of our knowledge, no researcher has ever taken this kind of study into their consideration along with the experimental data. One more observation from Fig. 5.18(a) is that the experimental data lies between the curves drawn for different fractional orders of the derivative. With the aid of this fractional order, we can now approximate a large class of experimental data taken from laboratory since, by varying this fractional order, we shall be able to approximate this data. Hence, we deem it appropriate that this unique feature not only unifies our model but also promises to be helpful in the future research in this direction.

5.6 Concluding remarks

As our aim was to broaden the study of Singh et al. [59], we considered the fractional version of their model. Our study facilitates the analytic solution for the fractional model and also the expression for the wall-shear stress on the stenosis wall. As the fractional derivatives generalize the integer-order ones, we have shown that our model also recovers the integer-order one by Singh et al. [59], both analytically and graphically (when $\alpha \to 1$). Imposing no restriction on the initial blood velocity to be zero, we have made our model more realistic, since blood in the arteries flows with some velocity. Later on, we validated our model against two established models available in literature. The graphical analysis carried out using the analytic solution of the fractional model shows that, having control over the magnetic number (in other words, magnetic field intensity) and the fractional order of the governing equation, it is possible to reach a probable cure for the stenosis in the arteries, when surgeries may be considered life-risking.

While the wall-shear stress helps in locating the stenosis, the fractional order of the differential equation enables us to recover the initial velocity for a lower magnetic number. In this context, the fractional order $\alpha = 0.81$ is found suitable, whereas the integer-order model fails to attain that.

The data approximation made by the fractional model not only helps in establishing the effectiveness of the model but also in approximating a large class of experimental data.

Research in this direction (modelling blood flow with the MHD effect in a stenosed artery by means of fractional derivative) has lacked this inclusion till date, which we deem it appropriate to claim that we have successfully established it.

On the other hand, there definitely appear a few limitations with respect to the present model. For instance, the fluid is considered to be Newtonian. It will be interesting to study the same by considering the fluid to be non-Newtonian. Further, we have not considered the effect of chemical reaction between the molecules of the blood and the temperature of the blood. It will be a significant development to be able to study the model by including the aspects of chemical reaction and temperature. Furthermore, we have taken the blood flow in the one-dimensional set-up which may be modelled in the two-dimensional set up to represent a more realistic scenario. These unexplored horizons are important to be investigated as one can hope that these may lead to much more accurate approximations which can outperform all the existing works. We are interested to address these issues in future; till then it is an open problem for all.

It may be noted that, even though this work is based on the work of Singh et al. [59], some errors in their work were noticed. Subsequently, these errors were rectified and our model was devised, based on the modified integer-order model.

6

Fractional model for ion diffusion in the extracellular microenvironment of the rat cerebellum

This chapter discusses a generalized version of the ion transport model presented by Nicholson and Phillips [44]. By the means of a fractional-order model, we establish that this phenomena can be captured in a far better way than the integer-order model. We obtain a fractional-order model by generalizing the integer-order derivative to study the transport process. The analytical solution appears to be of utmost importance in approximating the experimental data existing in the literature. We carry out graphical and tabular analysis, comparing our result with the existing ones which shows our model to be a better-suited one. We also prescribe the best possible value for the fractional derivative in reaching the best match with the experimental data.

6.1 Preliminaries

In this section, we outline a few developments on how the diffusion equations evolved over time for a complex porous medium like brain, and present some consequences in this regard. To define a complex medium, we require the concept of a certain reference scale. The ion diffusion takes place in the intervening places of cells having a dimension ranging from $0.01 - 0.04$ μm for most of the cases occurring at the microscopic level. At this stage, we may encounter free diffusion so that the actual ion concentration may vary substantially over a scale of such dimension, provided that the influence of the glycomolecules is not taken into account.

Now, to portray the advancement, we present a few latest improvements regarding the transport theory in a complex porous medium (Nicholson and Phillips [44]).

6.1.1 Fick's laws, tortuosity, porosity and averaging

Let us consider the concentration of a solute residing in the extracellular space to be C_0, representing the microscopic or interstitial concentration. If ∇C_0, i.e., the concentration gradient, subsists, then it can be analogous to the microscopic flux $\vec{J}$ according to Fick's first law as

$$\vec{J} = -D\nabla C_0, \tag{6.1}$$

where D represents the coefficient of diffusion of the solute.

The supporting boundary condition for the region remains so complicated that both the quantities C_0 and $\vec{J}$ change heterogeneously on a space of dimension d. To circumvent such an issue along with obtaining sufficiently smooth variables to deal with, the concept of volume average is taken into account (Whitaker [66]). Let us consider a tissue of volume V. There lies an extracellular phase of volume V_0 within this volume. Then the volume fraction or the porosity e of the tissue is defined by

$$e = \frac{V}{V_0}. \tag{6.2}$$

Following Nicholson and Phillips [44], the volume V, the porosity e and extracellular volume V_0 are considered to be constants for the tissue. It may, however, be noted that, in a more realistic scenario where concentration can influence the extracellular volume of the tissue, e and V_0 can be functions of both space and time variables while V remains as a set parameter.

Let us consider a variable ψ, which is associated with the extracellular phase only. It means that this variable has no impact on the non-extracellular phase. In other words, $\psi = 0$. Now, the volume average of such a variable may be defined as

$$< \psi > = \frac{1}{V}\int_{V_0} \psi d^3x, \tag{6.3}$$

where d^3x corresponds to the triple integral or the volume integral. This average is connected to the centroid of the volume V, and all the local co-ordinates can be elucidated in V with the reference of this point. It is to be mentioned that the centroid of V can reside in either the extracellular or non-extracellular phase. Therefore, $< \psi >$ remains smooth over the complete domain.

It is noteworthy that averaging takes care of the discontinuity of the variables by recasting them into continuous ones and therefore, resulting in an enhanced problem. Henceforth, the variables of Eq. (6.1) can be averaged by using a form of the averaging theorem (Gray et al. [19]) to obtain the macroscopic form of Fick's law as

$$< \vec{J} >= -D^*\nabla < C_0 >, \tag{6.4}$$

where, for an isotropic and homogeneous medium, we have

$$D^* = \frac{D}{\lambda^2},$$

with λ as the tortuosity, which is defined as the average hindrance of a complex medium relative to obstacle-free medium.

In many scenarios, we need to consider the volume average by taking into account only the extracellular phase; this is what an ion-selective micropipette measure associated with the concentration is. As an instance, such kind of average can be defined by

$$< \psi >_0 = \frac{1}{V_0} \int_{V_0} \psi d^3x. \tag{6.5}$$

Combining Eqs. (6.2), (6.3) and (6.5), one can write

$$< \psi > = e < \psi >_0 . \tag{6.6}$$

This helps in rewriting Eq. (6.4) in the following form:

$$< \vec{J} > = -eD^* \nabla < C_0 >_0, \tag{6.7}$$

where $< C_0 >_0$ refers to the quantity measured by an ion-selective micropipette.

Now, making use of the equation of conservation of mass within the interstitial space (Lehner [38]) and the volume averaging theorem (Gray et al. [19]), we finally reach Fick's second law:

$$D^* \nabla^2 < C_0 >_0 + \frac{< q >}{e} = \frac{\partial}{\partial t} < C_0 >_0, \tag{6.8}$$

with $< q >$ indicating an averaged quantity for the medium, commonly known as the averaged source density. In the work of Gardner-Medwin [16], C was introduced in place of the averaged term $< C_0 >_0$ for the aforementioned expression and Gardner-Medwin's J refers to the present $< \vec{J} >$.

Now for a simple medium, considering the newly introduced variable C in place of the quantity $< C_0 >_0$, and by using the concept of superposition, or application of the principle of reciprocity (Purves [50]), we estimate the solution of Eq. (6.8) by simply finding a solution for the following diffusion equation:

$$D^* \nabla^2 C + \frac{q}{e} = \frac{\partial C}{\partial t}. \tag{6.9}$$

6.1.2 Ionophoresis from a point source

Following Lehner [38], an ionophoretic electrode is driven by a constant ion source, which deals with approximating a point source. Now, using the spherical co-ordinates, Eq. (6.9)

can be recast in the following form:

$$\frac{D^*}{r}\frac{\partial^2(rC)}{\partial r^2}+\frac{QH(t)\delta(r)}{er^2}=\frac{\partial C}{\partial t}, \tag{6.10}$$

where r denotes the radial co-ordinate, $\delta(r)$ represents the well-known Dirac delta function and $H(t)$ indicates the unit-step function which is defined by $H(t)=1$ for $t>0$ and $H(t)=0$ for $t<0$. The Dirac delta function may be written in terms of the derivative of the function H with reference to the variable t. When this function is integrated with respect to t, $\delta(t)$ remains zero everywhere excluding $t=0$ where the function is unity (Jack et al. [27]). Here, Q represents the strength of the source, measured in mol.s^{-1}. Note that, when a source is added to the ionophoretic electrode, then we have

$$Q=\frac{In}{F}, \tag{6.11}$$

where n is the electrode's transport number, F denotes the Faraday's electrochemical equivalent and I is the electric current. With the aid of the following initial and boundary conditions:

$$\begin{cases} C(r,0)=0; \text{ for } r>0, \\ C(r,t)\to 0; \text{ as } r\to\infty, \end{cases} \tag{6.12}$$

along with a point source at the source electrode ($r=0$) of electric charge Q, the solution of Eq. (6.10) can be written as (following Crank [6])

$$C(r,t)=\frac{Q\lambda^2}{4\pi Der}\text{erfc}\left(\frac{r\lambda}{2\sqrt{Dt}}\right), \tag{6.13}$$

where the value of $D^*(=\frac{D}{\lambda^2})$ is substituted in the solution and erfc(.) denotes the complementary error function.

6.2 Fractional ionophoresis model and its analytical solution

6.2.1 Model description

In this section, we present a generalized version for ionophoresis in the extracellular space of the rat cerebellum, following the model of Nicholson and Phillips [44], by generalizing the governing partial differential equation (6.10). We generalize the time-partial derivative by adopting a suitable time-fractional derivative in (6.10) since the fractional models are capable of capturing more attributes of a physical phenomenon in comparison

to the integer-order ones. To be precise, we are going to utilize the Caputo time-fractional derivative to elaborate the diffusion process for ion transport in the extracellular microenvironments of the rat cerebellum.

As we wish to study the fractional version of the diffusion model given by Nicholson and Phillips [44], we present a generalized diffusion equation as

$$\frac{D^*}{r}\frac{\partial^2(rC)}{\partial r^2}+\frac{QH(t)\delta(r)}{er^2}=\frac{\partial^\alpha C}{\partial t^\alpha}, \tag{6.14}$$

where $0<\alpha\leq 1$ is the fractional order of the time derivative. Here, we utilize the Caputo time fractional derivative of order α, which is defined in Eqs. (1.4)−(1.6). All other parameters and the functions used in Eq. (6.14) hold exactly the same interpretation as in Eq. (6.10).

It may be noted that the spatial domain for the time-fractional partial differential equation is $0<r<\infty$. Due to this special form of the domain, Eq. (6.14) takes a simplified form as follows:

$$\frac{D^*}{r}\frac{\partial^2(rC)}{\partial r^2}=\frac{\partial^\alpha C}{\partial t^\alpha}. \tag{6.15}$$

As in Section 6.1, we define the Dirac delta function, which annihilates the second term of Eq. (6.14). Now, the resulting diffusion equation can be written as

$$D^*\frac{\partial^2 C}{\partial r^2}+\frac{2D^*}{r}\frac{\partial C}{\partial r}=\frac{\partial^\alpha C}{\partial t^\alpha}. \tag{6.16}$$

It can be noticed that, for the limiting case $\alpha\to 1$, Eq. (6.14) coincides with Eq. (6.10), i.e., both the models become identical. Hence, our model recovers the original model of Nicholson and Phillips [44] as a particular case. Now, it is of utmost importance to find an analytical solution to Eq. (6.14) to have a rigorous study via both graphical and numerical means.

Following Nicholson and Phillips [44], in our model also, we use the same initial and boundary conditions which are as follows:

$$\begin{cases} C(r,0)=0; \text{ for } r>0, \\ C(r,t)\to 0; \text{ as } r\to\infty, \end{cases}$$

along with a point source at the source electrode ($r=0$) of electric charge Q.

6.2.2 Analytical solution

Applying Laplace transform to both sides of Eq. (6.16), and using Eq. (1.16), we obtain

$$D^*\frac{d^2}{dr^2}\bar{C}(r,s)+\frac{2D^*}{r}\frac{d}{dr}\bar{C}(r,s)=s^\alpha\bar{C}(r,s)-s^{\alpha-1}C(r,0). \tag{6.17}$$

Making use of the initial condition $C(r,0)=0$, Eq. (6.17) gets converted to

$$D^*\frac{d^2}{dr^2}\bar{C}(r,s)+\frac{2D^*}{r}\frac{d}{dr}\bar{C}(r,s)=s^\alpha\bar{C}(r,s). \tag{6.18}$$

This equation can be rewritten, by using $R=\frac{r}{\sqrt{D^*}}$, as

$$\frac{d^2}{dR^2}\bar{C}(R,s)+\frac{2}{R}\frac{d}{dR}\bar{C}(R,s)=s^\alpha\bar{C}(R,s). \tag{6.19}$$

This equation may be solved by making the substitution $\bar{U}=\bar{C}R$ to obtain

$$\frac{d^2\bar{U}}{dR^2}-s^\alpha\bar{U}=0. \tag{6.20}$$

Now, the general solution of (6.19) can be written as

$$\bar{C}(r,s)=\frac{\sqrt{D}}{r\lambda}\left[A\,\exp\left(-\frac{r\lambda\sqrt{s^\alpha}}{\sqrt{D}}\right)+B\,\exp\left(\frac{r\lambda\sqrt{s^\alpha}}{\sqrt{D}}\right)\right], \tag{6.21}$$

where A, B are integration constants to be determined. Now, using the boundary condition in (6.12) and incorporating the source of charge Q at the source electrode, we obtain the solution for Eq. (6.18) as

$$\bar{C}(r,s)=\frac{Q\lambda^2}{4\pi eDr}\left(\frac{\exp\left(-\frac{r\lambda}{\sqrt{D}}\sqrt{s^\alpha}\right)}{s}\right). \tag{6.22}$$

To find the solution in the time domain, we need to find the inverse Laplace transform of Eq. (6.22). To do so, we follow the techniques developed earlier in Chapter 2 to get the solution in the following form:

$$C(r,t)=\frac{Q\lambda^2}{4\pi eDr}\left(\sum_{k=0}^{\infty}\frac{\left(-\frac{r\lambda}{\sqrt{D}}\right)^k}{k!}\frac{t^{-\frac{\alpha k}{2}}}{\Gamma\left(1-\frac{\alpha k}{2}\right)}\right), \tag{6.23}$$

which can further be recast in terms of a known function (closed form) as

$$C(r,t)=\frac{Q\lambda^2}{4\pi eDr}\left(\mathbb{W}\left(-\frac{\alpha}{2},1;-\frac{r\lambda}{\sqrt{Dt^\alpha}}\right)\right), \tag{6.24}$$

where $\mathbb{W}(\alpha,\alpha;.)$ is the Wright function of two parameters.

6.3 Model verification

The fractional model is considered here to elucidate the diffusion process in a more general sense by embedding the notion of the derivative from integer-order to fractional-order. As this model is a generalization of the model of Nicholson and Phillips [44], therefore, as a particular case, our proposed model should recover the original model. This is already established in Section 6.2, i.e., for the particular case $\alpha \to 1$, our model retrieves the original model of Nicholson and Phillips [44]. Now, we proceed to test whether the present solution follows the same path or not. In other words, for the particular case $\alpha \to 1$, it is to be checked whether our solution (6.24) recovers the solution for the original model or not.

Let us take $\alpha \to 1$ in Eq. (6.24). Then, the solution takes the form

$$C(r,t) = \frac{Q\lambda^2}{4\pi eDr}\left(\mathbb{W}\left(-\frac{1}{2},1;-\frac{r\lambda}{\sqrt{Dt}}\right)\right). \tag{6.25}$$

Now, we make use of some well-known relations from [48] listed below to obtain the relation between the Wright function and the complementary error function.
For a complex number Z, we have

a)
$$\Gamma(Z)\Gamma(1-Z) = \frac{\pi}{\sin(\pi Z)}; \quad \text{for } Z \neq 0, \pm 1, \pm 2, ..., \text{ and } 0 < \mathrm{Re}(Z) < 1,$$

b)
$$\Gamma(Z)\Gamma\left(Z+\frac{1}{2}\right) = \sqrt{\pi}2^{2Z-1}\Gamma(2Z); \quad \text{for } 2Z \neq 0, -1, -2, ...,$$

c)
$$\Gamma\left(n+\frac{1}{2}\right) = \frac{\sqrt{\pi}\ (2n)!}{2^{2n}\ n!}; \quad \text{for } n \in \mathbb{N}.$$

Next, after expanding the Wright function and then using the above-mentioned relations, we can write the solution (6.25) in the following form:

$$C(r,t) = \frac{Q\lambda^2}{4\pi Der}\mathrm{erfc}\left(\frac{r\lambda}{2\sqrt{Dt}}\right). \tag{6.26}$$

It can now be easily checked that both solutions (6.13) and (6.26) are exactly the same. Hence, we successfully recover not only the original model but its solution too.

Let us now strengthen our claim by means of graphical analysis. To serve our purpose, we need to select some appropriate values for the parameters and the constants used in the solution (6.24). Following Nicholson and Phillips [44], we choose the following values: the diffusion coefficient $D = 1.30 \times 10^{-9}$, the transport number of electrode $n = 0.40$, distance

between the electrodes $r = 114$, tortuosity $\lambda = 1.49$, volume fraction $e = 0.15$, time $t = 100$ and the values of the current $I = 180$, 140, and 100.

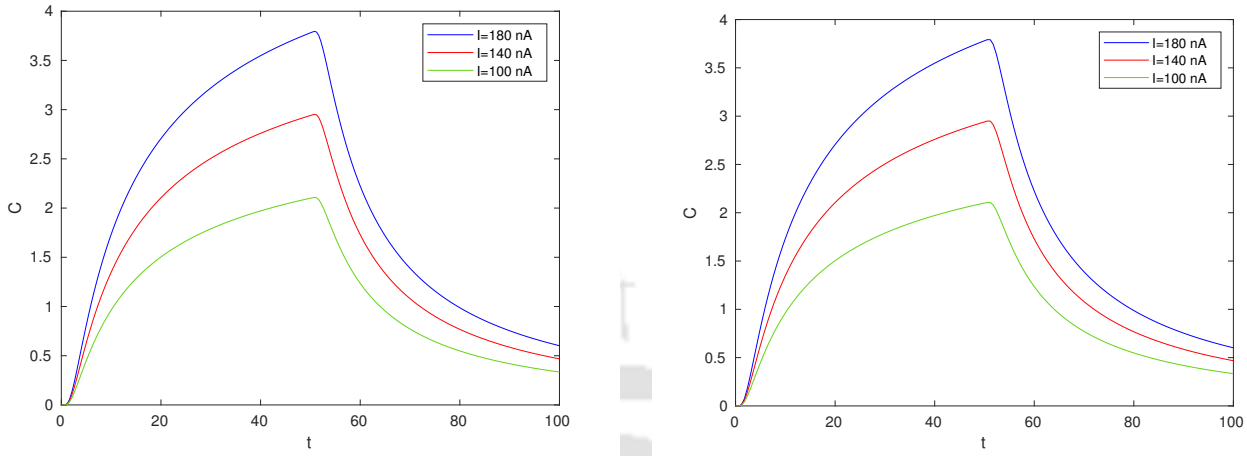

(a) (b)

Figure 6.1: Comparison of concentrations for different values of I for $D = 1.30 \times 10^{-9}$, $n = 0.40$, $r = 114$, $\lambda = 1.49$, $e = 0.15$ and $t = 100$: (a) *integer-order model based on [44],* (b) *fractional model with* $\alpha = 1$.

Then, we take a different set of values: $D = 1.06 \times 10^{-9} \mathrm{m}^2.\mathrm{s}^{-1}$, $n = 0.27$, $r = 85$ μm, $\lambda = 1.37$, $e = 0.13$, $t = 100$s and the values of the current $I = 90$nA, 60nA, and 30nA.

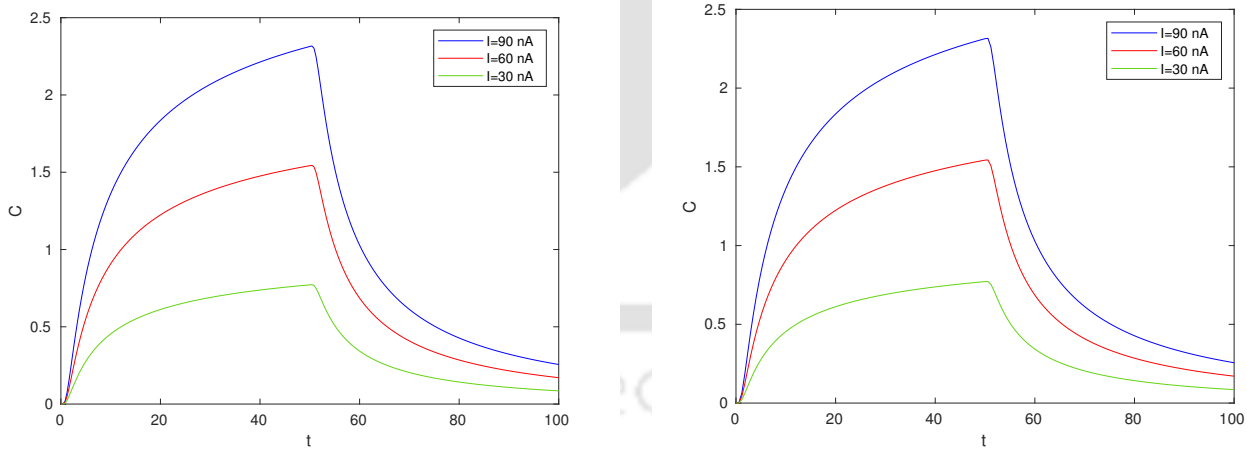

(a) (b)

Figure 6.2: Comparison of concentrations for different values of I for $D = 1.06 \times 10^{-9}$, $n = 0.27$, $r = 85$, $\lambda = 1.37$, $e = 0.13$ and $t = 100$: (a) *integer-order model based on [44],* (b) *fractional model with* $\alpha = 1$

Finally, we choose another set of values: $D = 0.79 \times 10^{-9}$, $n = 0.11$, $r = 108$, $\lambda = 1.75$, $e = 0.30$, $t = 100$ and the values of the current $I = 180$, 140, 100 and 60.

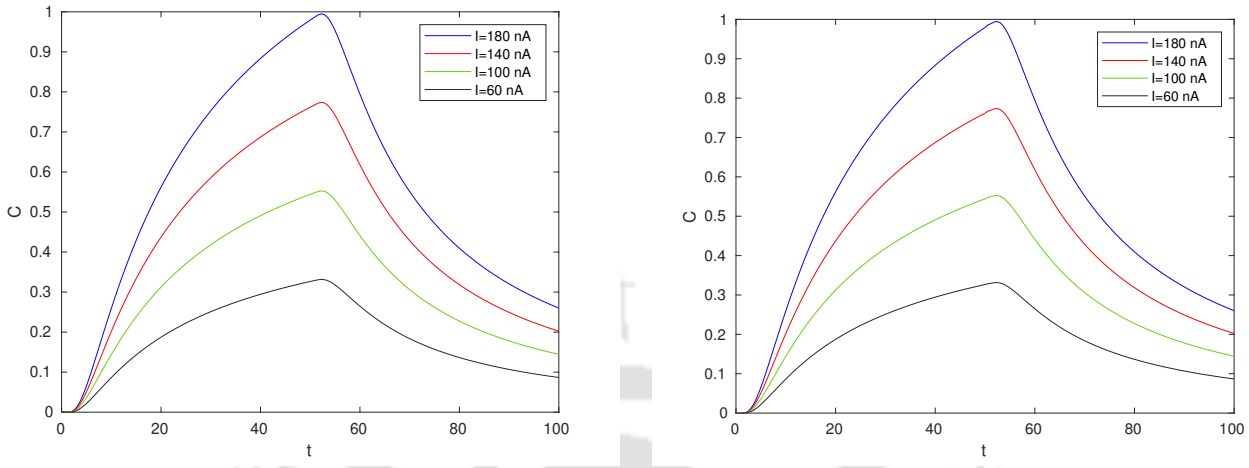

Figure 6.3: Comparison of concentrations for different values of I for $D = 0.79 \times 10^{-9}$, $n = 0.11$, $r = 108$, $\lambda = 1.75$, $e = 0.30$ and $t = 100$: (a) *integer-order,* (b) *fractional-order with* $\alpha = 1$.

Figures 6.1(a), 6.2(a), 6.3(a) correspond to the graphs drawn by using the integer-order model solution (6.13) while Figs. 6.1(b), 6.2(b), 6.3(b) correspond to the graphs plotted by using the fractional-order model solution (6.24) by taking the fractional-order $\alpha = 1$ for different values of the parameters and the constants. Now, by having a glance at the figures, it is quite clear that Figs. 6.1(a) and 6.1(b), 6.2(a) and 6.2(b), 6.3(a) and 6.3(b) match exactly with each other. Hence, we successfully show the graphical agreement too for both the models.

One point needs to be mentioned that, while plotting the solutions, the concentration curve corresponding to the falling phase caused by the deactivation of the source can be obtained by using Eq. (6.13) by simply summing up the concentration derived from a sink with strength $(-Q)$ which is activated at the closure of the pulse. To get the complete curve, we need the superposition of both the curves (Jaeger [28]). Exactly the same procedure is also followed for plotting the fractional model solution (6.24). It may be noted that the kink, as observed in the above figures, is the point where the activated source is taken away and thereafter the sink comes into play. In other words, the kink is produced where two curves meet: one for the activated source and the other for the sink (deactivated source).

6.4 Discussion: validation followed by results

This section deals with the validation of the proposed model with an available one in existing literature and then elaborating the plots and tables obtained from the fractional model.

6.4.1 Validation

Here, we exhibit how our model solution agrees with the existing experimental data taken from Nicholson and Phillips [44]. They conducted an experiment for ion transport in the microenvironments of the extracellular space of rat cerebellum taking different values for electric current, different spacing in the electrode, different values for the diffusion coefficient, various values for the tortuosity and volume fraction along with the transport number of the electrodes. They took female SD rats, commonly known as Sprague-Dawley rats or laboratory rats of weight $200-400$g for the experimental purpose. After the rats were anaesthetized, a pair of ionophoreric and ion-selective micro-electrodes were coupled together and placed in the cerebellum. The ionophoretic electrode was led by a constant current source, and the ion-selective electrode, containing two barrels, was used for capturing the ion signals. In this work, we incorporate their experimental data for elaborating the role of the fractional model in capturing this phenomenon in a better way.

Before proceeding further, let us elaborate the procedure we follow to validate our solution. Here, we primarily focus on having an exact matching of our model solution (6.24) with the experimental data drawn from the experiment carried out by Nicholson and Phillips [44]. When we do not get the exact matching, we aim to have a close estimate for our solution. To the best of our knowledge, no research has been carried out in this direction till date.

Here, we present a few plots to have a better understanding.

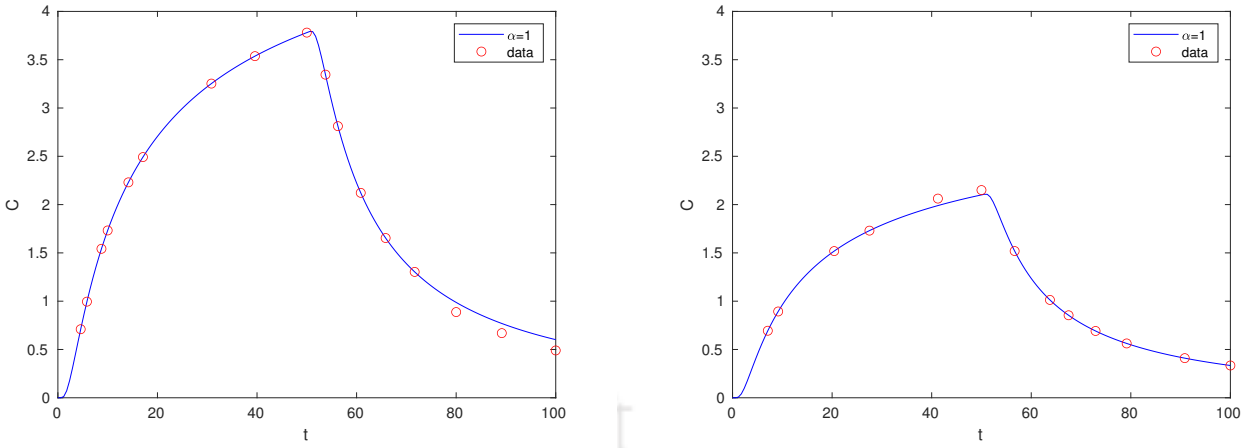

(a) (b)

Figure 6.4: Concentration curves along with experimental data for different values I, $\alpha = 1$ and $t = 100$: (a) for $I = 180.$, (b) for $I = 100$.

From Figs. 6.4(a) and 6.4(b), it can be observed that our solution graph exactly matches the experimental data except for a few points that we consider for the time being. Later on, we explain the reasons behind those unmatched points in the course of discussion. However, even for these points, we get a close estimate given by the analytical solution (6.24).

To make our claim a bit stronger, we present a few more plots in this regard.

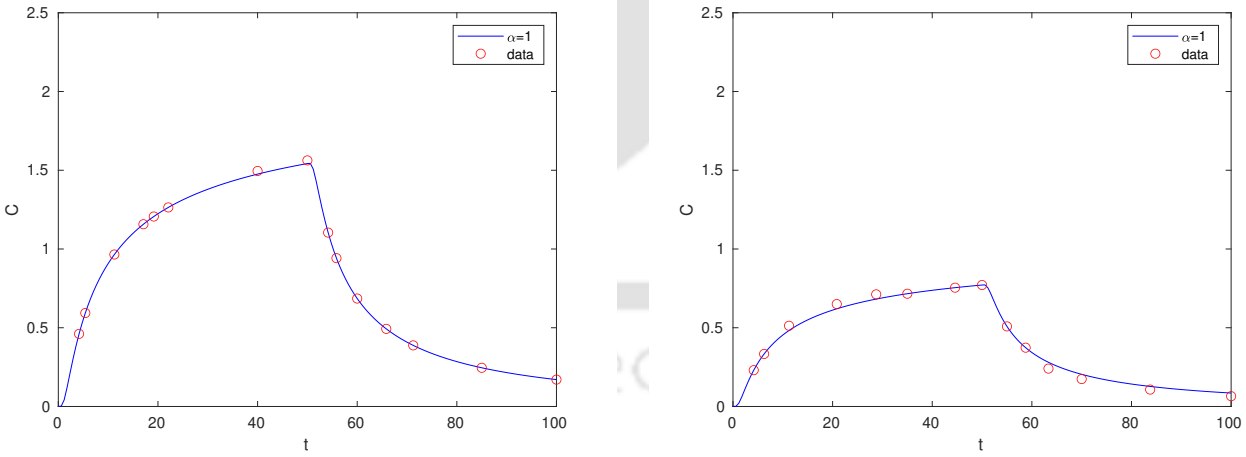

(a) (b)

Figure 6.5: Concentration curves along with experimental data for different values I, $\alpha = 1$ and $t = 100$: (a) for $I = 60$, (b) for $I = 30$.

Now, looking at Figs. 6.5(a) and 6.5(b), it can be noticed that we get almost the exact matching with the experimental data as we decrease the value of the current in the electrode. Hence, analysing Figs. 6.4 and 6.5, we can now infer that we have a suc-

cessful validation of our model against the existing experimental data (Nicholson and Phillips [44]).

Having achieved the validation, we can now consider our model to be suitable for studying different aspects related to ion transport in the extracellular microenvironments of the rat cerebellum.

6.4.2 Results

Now, we shift our focus to elaborating the graphs and data obtained from the proposed model, and test the applicability of the obtained solution by comparing with the existing literature (Nicholson and Phillips [44]). Here, we wish to apply the model solution (6.24) for a handful values for different parameters. Henceforth, we justify our best picked value for the pivotal parameter, i.e., the fractional order of the derivative.

Here, we present a few plots to show the effectiveness of our fractional-order model over the integer-order model by considering different fractional orders.

Case I:-

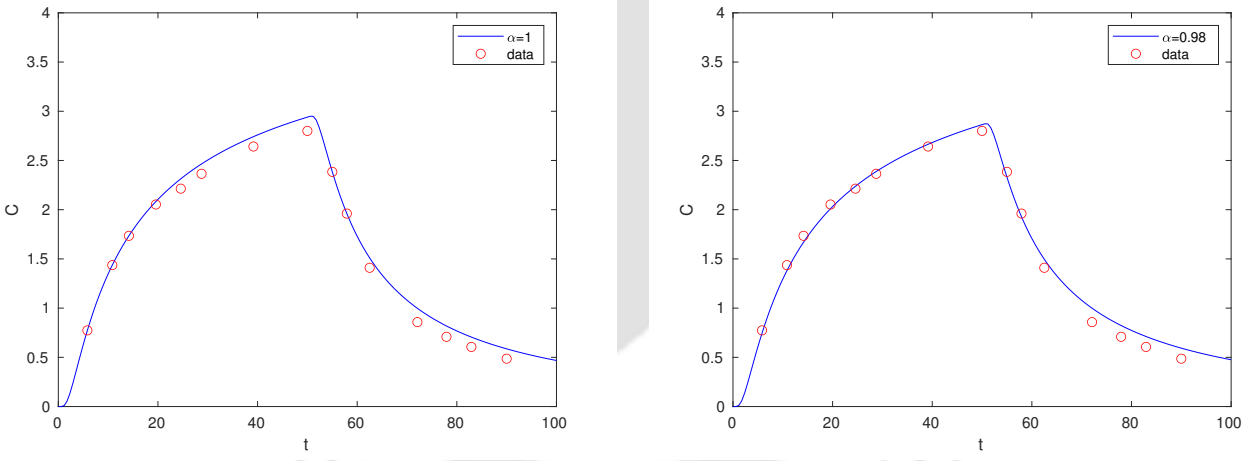

(a) (b)

Figure 6.6: Concentration curves along with experimental data for different values I, $\alpha = 1$ and $t = 100$: (a) for $\alpha = 1$, (b) for $\alpha = 0.98$.

Figures 6.6(a) and 6.6(b) correspond to the concentration curves drawn by using the values: $I = 140,\ D = 1.30 \times 10^{-9},\ n = 0.40,\ r = 114,\ \lambda = 1.49,\ e = 0.15$ with $\alpha = 1$ and $\alpha = 0.98$. It is worth mentioning that the fractional-order model for $\alpha = 0.98$ approximates the experimental data more accurately than that for the integer-order one (for $\alpha = 1$) as the difference between the analytical solution curve and the experimental data is more

evident for the integer-order case. Hence, for this case, we choose the best probable estimate for the fractional order to be $\alpha = 0.98$.

One point to note in this regard is that the concentration curves drawn from the analytical solution (6.24) in the rising phase, that means starting from the time $t = 0$ to $t = 50$s, have a good fit with the experimental data. Furthermore, for the falling phrases, i.e., starting from $t = 50$s to $t = 100$s, the concentration curves have estimated the experimental data adequately although the exact matching was not achieved. This variations are seen because of the mild distortions of the brain owing to the circulatory activities and breathing of the animals in between the successive ionophoretic measurements.

Next, we produce a tabular presentation, depicting how our fractional model, for the chosen $\alpha = 0.98$, closely captures the experimental data. Table 6.1 gives a clear representation.

Table 6.1: Analogy of concentration for $I = 140,\ D = 1.30 \times 10^{-9},\ n = 0.40,\ r = 114,\ \lambda = 1.49,\ e = 0.15$ with different α.

t	For $\alpha = 1$	For $\alpha = 0.98$	Experimental data
5.8824	0.7822	0.7534	0.753952
19.4118	2.0735	2.0012	2.0227
24.1176	2.2947	2.2193	2.21366
28.8235	2.4671	2.3902	2.3647
39.4118	2.7472	2.6697	2.64192
50	2.9404	2.864	2.80041
62.3529	1.5214	1.5073	1.41996

For a robust understanding, we consider a few more cases, which are exhibited next. To strengthen our observation, we consider $\alpha = 0.975,\ 0.985$ on either side of $\alpha = 0.98$.

Case II:-

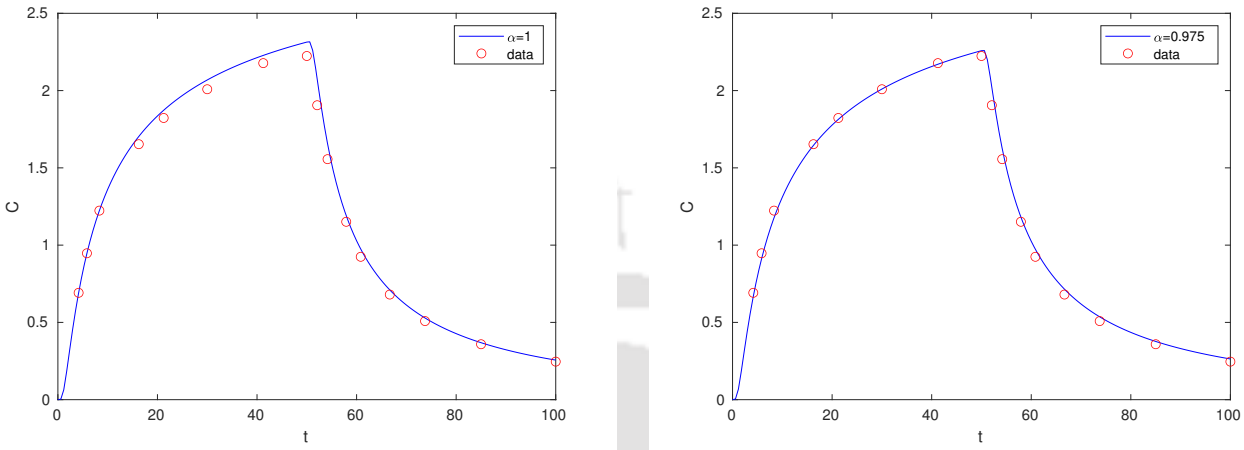

(a) (b)

Figure 6.7: Concentration curves along with experimental data for different values I, $\alpha = 1$ and $t = 100$: (a) for $\alpha = 1$, (b) for $\alpha = 0.975$.

Figures 6.7(a) and 6.7(b) correspond to the values of the parameters and constants: $I = 90,\ D = 1.06 \times 10^{-9},\ n = 0.27,\ r = 85,\ \lambda = 1.37,\ e = 0.13$ with $\alpha = 1$ and $\alpha = 0.975$. Analyzing the graphs, we can now prescribe the best probable fitting fractional order of the derivative to be $\alpha = 0.975$.

The representation in Table 6.2 signifies the role of the prescribed fractional order $\alpha = 0.975$ in capturing the experimental data to a great extent.

Table 6.2: Analogy of concentration for $I = 90,\ D = 1.06 \times 10^{-9},\ n = 0.27,\ r = 85,\ \lambda = 1.37,\ e = 0.13$ with different α.

t	For $\alpha = 1$	For $\alpha = 0.975$	Experimental data
8.2353	1.2142	1.1682	1.1812
16.4706	1.712	1.6542	1.6531
21.1765	1.8707	1.8117	1.8228
30	2.0687	2.0098	1.9987
41.1765	2.2268	2.1696	2.1776
50	2.3138	2.2582	2.2138
52.3529	2.0149	1.9637	1.8551
54.1176	1.6645	1.6326	1.5261
60.5882	0.9897	0.9877	0.9745

Case III:-

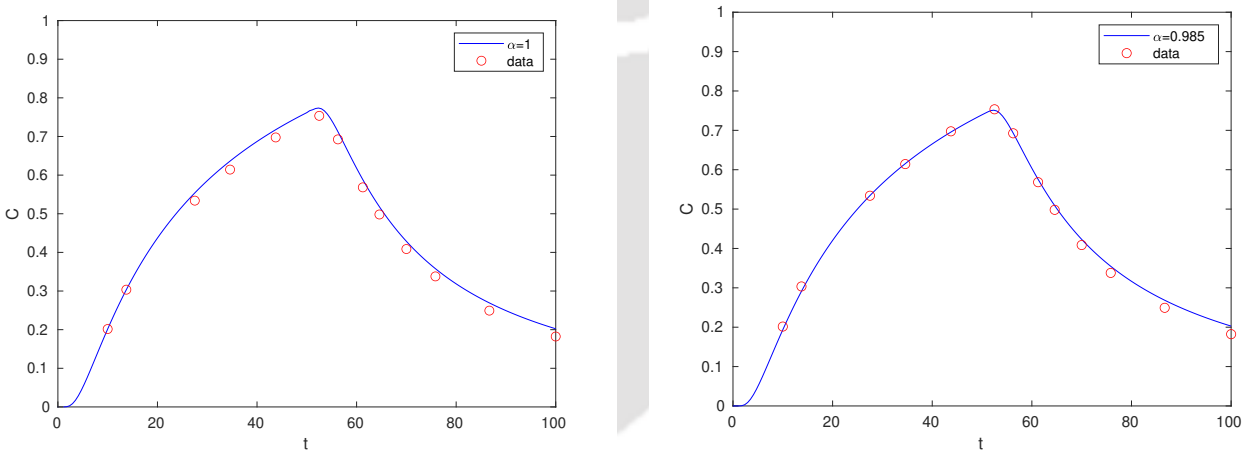

(a) (b)

Figure 6.8: Concentrations curve along with experimental data for different values I, $\alpha = 1$ and $t = 100$: (a) for $\alpha = 1$, (b) for $\alpha = 0.985$.

Figures 6.8(a) and 6.8(b) correspond to the values of the parameters and constants: $I = 140,\ D = 0.79 \times 10^{-9},\ n = 0.11,\ r = 108,\ \lambda = 1.75,\ e = 0.30$ with $\alpha = 1$ and $\alpha = 0.985$. For the best matching for the curve drawn by the analytical solution (6.24) to the experimental data, we can refer to $\alpha = 0.985$ as an appropriate fractional order.

Table 6.3 helps depicting the closeness of the fractional model solution for $\alpha = 0.985$ to the experimental data.

Table 6.3: Analogy of concentration for $I = 140,\ D = 0.79 \times 10^{-9},\ n = 0.11,\ r = 108,\ \lambda = 1.75,\ e = 0.30$ with different α.

t	For $\alpha = 1$	For $\alpha = 0.985$	Experimental data
5.8824	0.0759	0.0735	0.0725
27.6471	0.5559	0.5363	0.5339
34.7059	0.6376	0.6166	0.6143
43.5294	0.7158	0.694	0.6975
52.3529	0.7736	0.7512	0.7534
56.4706	0.707	0.6879	0.6924
61.1765	0.59	0.5772	0.5683

From Figs. 6.6−6.8 along with Tables 6.1−6.3, it can be observed that, while the integer-order model was unable to approximate the experimental data with much precision, our proposed fractional model successfully approximates the experimental data to a great extent, making this model impactful and worthy.

Nicholson and Phillips [44] carried out experiments to assert whether the diffusion of ions in the microenvironments was affected due to the ionophoretic current. Literature points toward some contrasting evidences in this context. Norman [46] and Lux et al. [39] showed that the electric field was too tiny to subsequently affect the migration of ions, except for the places which were very close to the extremity of the ionophoretic electrode. On the other hand, Trubatch et al. [62] established the opposite in their work.

Here, we consider two cases: first, by increasing (Figs. 6.6 and 6.8) and then by decreasing (Fig. 6.7) the current of the ionophoretic electrode. For both cases, we get the theoretical fit at each current strength with the experimental data, which Nicholson et al. [44] failed to achieve through their integer-order model solution (6.13). Here, we outperform their results by incorporating the fractional model. With the aid of this, we get the best matching in a few cases and the best probable approximation for the rest of the cases. For both types of cases, our model exhibits the best fit while approximating the experimental data by an analytical solution which, to the best of our knowledge, no research has ever depicted till date.

Another important aspect, drawn from our experiment, can be brought to notice in this regard. The generalization of the integer-order derivative in the model of Nicholson and Phillips [44] not only helps to have a better matching and approximations to the experimental (Nicholson and Phillips [44]) data by our model solution (6.13) but also helps approximate a wide class of experimental data taken from the laboratory, simply by choosing the arbitrary fractional order of the model appropriately. For the experimental data of Nicholson and Phillips [44], we find the fractional order of the derivative to be close to 1 (i.e., $\alpha = 0.975, 0.98,$ and 0.985) but not exactly 1, which provides the best

approximations to the experimental data (Nicholson and Phillips [44]) perfectly establishing the flexibility of the fractional-order models where integer-order ones fall short. Furthermore, this generalized model is capable of capturing a wide class of experimental data. The plots in Figs. 6.9 and 6.10 will definitely help in ascertaining this claim.

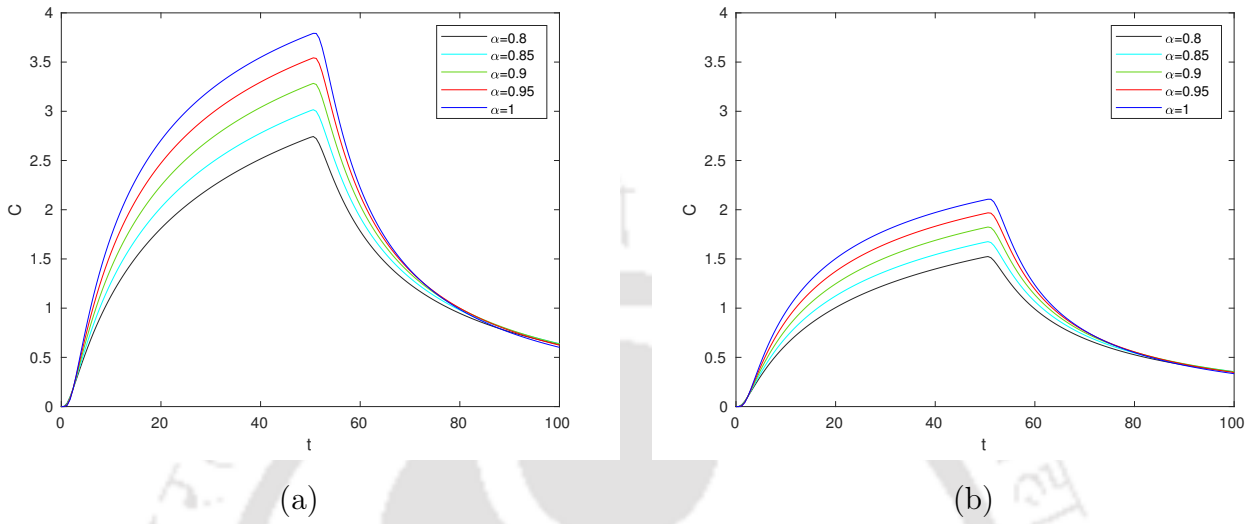

(a) (b)

Figure 6.9: Concentration curves for different values I, α and $t = 100$: (a) for $I = 180$, $r = 114$, (b) for $I = 100$, $r = 114$.

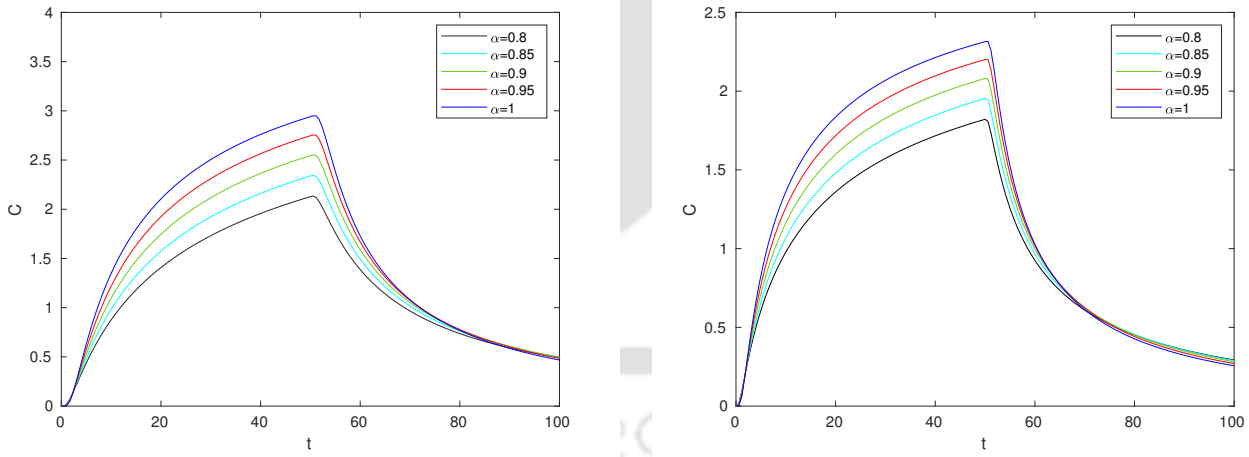

(a) (b)

Figure 6.10: Concentration curves for different values I, α and $t = 100$: (a) for $I = 140$, $r = 114$, (b) for $I = 90$, $r = 85$.

By observing Figs. 6.9 and 6.10, it can be followed that, by choosing an appropriate value for the fractional order α, it is possible to come nearer to the integer-order plot (corresponding to $\alpha = 1$) and also to move away from the integer-order plot. The most common trend for the experimental data taken from laboratory, available in Nicholson and Phillips [44], is to lie between the graphs presented in Figs. 6.9 and 6.10. Hence, we deem it appropriate to claim that, with the freedom given to the fractional order of the derivative in our proposed model, it is possible to approximate a wide class to experimental data, which, to the best of our knowledge, is quite new in the research of ion transport through analytical solution. Furthermore, we hope that this new attributes will be helpful in future research in this direction.

It may be noted that the main aim of the work carried out here is to get a better approximation to the experimental data via the fractional model, which is successfully acquired. Furthermore, it can be observed that, for all the figures, we vary the concentration C with respect to time t only. However, it may be useful if we shed some lights on the variation of the concentration C with respect to the radial distance r. In this direction, we present this fact through Fig. 6.11.

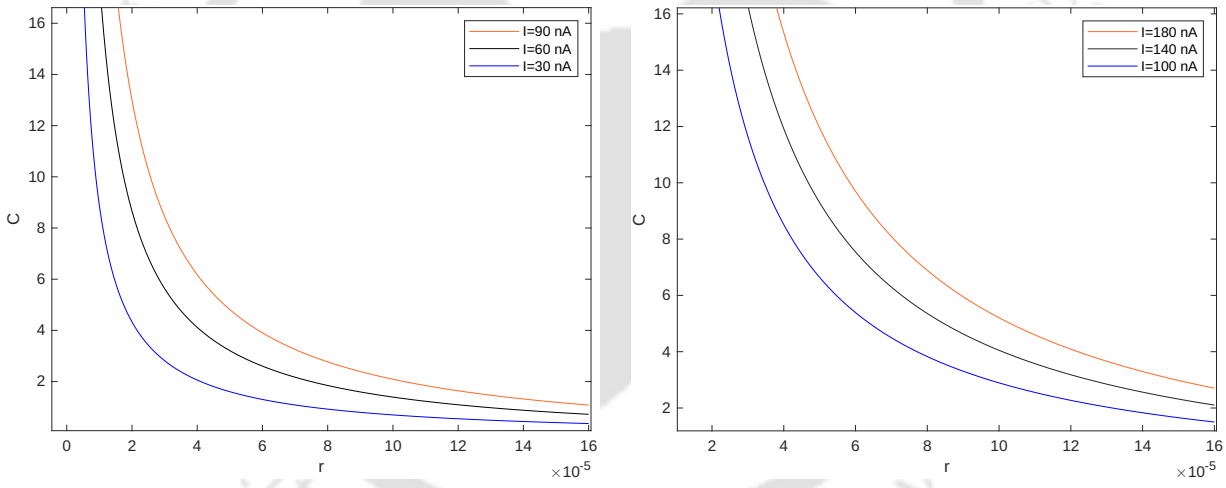

(a) (b)

Figure 6.11: Concentration C against r for various I with $t = 100$: (a) for $D = 1.06 \times 10^{-9}$, $n = 0.27$, $\lambda = 1.37$, $e = 0.13$, (b) for $D = 1.30 \times 10^{-9}$, $n = 0.40$, $\lambda = 1.49$, $e = 0.15$.

The profiles in Fig. 6.11 maintain the usual physical interpretation: as we move from the electrode (as r increases), the concentration decreases explaining the ion transport from one electrode to another. Therefore, our study also captures the same analogy for the concentration profile against the radial distance given by the distance between the electrodes, which can be noticed in earlier works [44, 45]. On this note, we conclude our discussion.

6.5 Concluding remarks

After making an appropriate introduction of the fractional ion transport model, which elucidates the ion transport in the extracellular space in the microenvironments of rat cerebellum, we have presented an analytical solution to our proposed model along with comparison of our results with the existing literature by means of graphical and numerical analysis. As a result of that, it has been found that our model is capable of recovering the original model with a more preciseness. Here, we achieve the accuracy of order 10^{-3} to 10^{-2} while approximating the experimental data by our model solution (6.24), in comparison with the solution provided by Nicholson and Phillips [44]. With the generalization of the derivative, it is shown that the inclusion of the fractional order of the derivative tremendously helped to get a close matching to the experimental data.

It is to be noted that Nicholson and Phillips [44] experimented with different values for the current of the electrode, whereas we have presented only those values for which they were unable to get the close match to the experimental data through their analytical solution. For the rest of the cases, our model exactly catches the same attributes as theirs. That is why we deem it appropriate to claim that our model generalizes their model.

On a general note, it can now be said that while integer-order models fall short in having a close estimate for the laboratory or experimental data or capturing some attributes, fractional models are the best fit for those cases. This work also justifies the same.

7 Conclusions and future scope

7.1 Conclusions

In this thesis, we study the mathematical modelling of a handful of problems arising in the biological science under the light of fractional calculus. As fractional models are best known for their outstanding capability of approximating a wide class of experimental or clinical data, here we pick up some problems, for which we establish the fractional models to be more efficient than their integer-order counterparts.

In this process, we first consider the fractional version of the conventional ESR model with the incorporation of non-zero uniform average blood velocity of the blood. An analytical solution is found to have an explicit analysis of the ESR test by varying different parameters and variables used therein. Followed by verification by means of both the explicit solution and graphical matching, we present some better-suited results in terms of graphical and tabular analysis. Furthermore, it is established that the inclusion of the non-zero uniform blood velocity leads to more accurate results than the earlier models available in literature. Later, we prescribe the most suitable value for the blood velocity along with the fractional-order of the derivative.

Next, we consider the same ESR model along with the concentration gradient of the blood nutrients. Here also, we first seek an analytical solution to gain a rigorous understanding of the different roles of the parameters and the variables. After having a two-step validation with the available experimental data, we present some interesting results with the aid of graphical and tabular analysis. Later on, to establish the credibility of the fractional model, we perform some data approximations by varying the newly introduced attribute, namely, the concentration gradient of blood nutrient. In the end, we also comment on the best suitable value for the concentration gradient.

Moving ahead, we take up a problem with the mathematical modelling of mass transport in brain cells. As an earlier integer-order model was detected with some major mathematical flaws, hence, we first eliminate those and obtain the corresponding desired

analytical solutions. After, a graphical representation of the obtained analytical solutions, we proceed for a data fitting for the experimental data taken from the laboratory, which motivates us to look for a better-suited fractional model. Hence, we present a fractional framework for the mass transport model to achieve those shortcomings which was intangible for the integer-order model.

Thereafter, we present a fractional approach to an integer-order model describing the MHD effect of blood flow in a stenosed artery. We obtain an analytical solution for the fractional governing equation and present an expression for the wall-shear stress too. After establishing a successful verification of our model with existing literature, we elucidate the obtained plots by using the analytic expression. We exhibit how fractional model is helpful for controlling the blood flow through a stenosed artery. We also present that the external magnetic field, along with the fractional order of the governing equation, plays a crucial role in the solution of the problem involving the treatment of stenosis. To showcase the reliability of the fractional models, we also perform some data approximation in the end.

Finally, we come up with a generalized version of the ion transport model in the extracellular microenvironment of the rat cerebellum. To have a rigorous analysis, we first solve the governing equation and obtain the analytical solution which appears to be of utmost importance in approximating the experimental data existing in literature. To establish the efficacy of our model, we carry out some graphical and tabular analysis. Having compared our result with the existing ones, we successfully establish the credibility of the underlying fractional model. We conclude our discussion by prescribing the best possible value for the fractional derivative to have the best match with the experimental data available in literature.

7.2 Future scope

In all the problems that are taken up, the order of the governing fractional differential equation is a parameter, i.e., it is a user-defined constant that belongs to $(0, 1]$. In future, we plan to address the following issues:

- to investigate the case when the frational order is a variable. As mentioned in da Sousa et al. [11], this modification may lead to some more efficient and interesting results.

- to investigate the existence, uniqueness and stability of the obtained solutions.

Till now we have used only the Caputo fractional derivative to model the real-life scenarios termed as the problems arising in the biological science. It will be an interesting endeavour to study these models under the light of newly developed ψ-Riemann-Liouville, ψ-Hilfer,

Caputo-Fabrizio derivatives, etc. As the theory for the above mentioned derivatives is still in progress, so it will be of utmost curiosity to apply them in real-world problems. In future, we wish to explore these new horizons and investigate whether we can come up with some more efficient modelling.

We may also utilize our knowledge garnered through the works in this thesis in other areas of science and engineering, say, open channel flow, electrical circuits, mathematical finance, underground contamination, etc.

References

[1] Abramowitz M, Stegun IA. *Handbook of Mathematical Functions with Formulas, Graphs, and Mathematical Tables*. US Government printing office, 1948.

[2] Aksnes DL, Egge JK. A theoretical model for nutrient uptake in phytoplankton. *Mar Ecol Prog Ser*. 1991;70(1):65-72.

[3] Bedell SE, Bush BT. Erythrocyte sedimentation rate. From folklore to facts. *Am J Med*. 1985;78(6):1001-1009.

[4] Brigden M. The erythrocyte sedimentation rate. Still a helpful test when used judiciously. *Postgrad Med*. 1998;103(5):257-274.

[5] Caputo M, Mainardi F. Linear models of dissipation in an elastic solid. *Riv Nuovo Cimento*. 1971;1(2):161-198.

[6] Crank J. *The Mathematics of Diffusion*. Oxford University Press, Oxford, UK, 1979.

[7] da Sousa JVC, de Oliveira EC, Magna LA. Fractional calculus and the ESR test. *AIMS Math*. 2017;2(4):692–705.

[8] da Sousa JVC, dos Santos MN, Magna LA, de Oliveira EC. Validation of a fractional model for erythrocyte sedimentation rate. *Comput Appl Math*. 2018;37:6903-19.

[9] da Sousa JVC, de Oliveira EC. On the ψ-Hilfer fractional derivative. *Commun Nonlinear Sci Numer Simulat*. 2018;60:72-91.

[10] da Sousa JVC, de Oliveira EC. Leibniz type rule: ψ-Hilfer fractional operator. *Commun Nonlinear Sci Numer Simulat*. 2019;77:305-311.

[11] da Sousa JVC, dos Santos MN, da Costa E, Magna LA, de Oliveira EC. A new approach to the validation of an ESR fractional model. *Comput Appl Math*. 2021;40(3):1-20.

[12] Das S. *Functional Fractional Calculus*. Berlin, Springer, 2011.

[13] Darras A, Peikert K, Rabe A, Yaya F, Simionato G, John T, Dasanna AK, Buvalyy S, Geisel J, Hermann A, Fedosov DA. Acanthocyte sedimentation rate as a diagnostic biomarker for neuroacanthocytosis syndromes: experimental evidence and physical justification. *Cell*. 2021;10(4):788.

[14] Debnath L, Bhatta D. *Integral Transforms and Their Applications*. Chapman and Hall/CRC, Boca Raton, Florida, USA, 2016.

[15] Fåhraeus R. The suspension stability of the blood. *Physiol Rev*. 1929;9(2):241-274.

[16] Gardner-Medwin AR. Membrane transport and solute migration affecting the brain cell microenvironment. *Neurosci Res Prog Bull*. 1980;18:208-226.

[17] Gholampour S, Balasundaram H, Thiyagarajan P, Droessler J. A mathematical framework for the dynamic interaction of pulsatile blood, brain, and cerebrospinal fluid. *Comput Methods Programs Biomed*. 2023;231:107209.

[18] Gorenflo R, Mainardi F. *Fractional Calculus: Integral and Differential Equations of Fractional Order*. Springer Vienna, 1997.

[19] Gray WG, Lee PCY. On the theorems for local volume averaging of multiphase systems. *Int J Multiph Flow*. 1977;3(4):333-340.

[20] Grote J, Süsskind R, Vaupel P. Oxygen diffusivity in tumor tissue (DS-carcinosarcoma) under temperature conditions within the range of 20–40 C. *Pflügers Archiv*. 1977;372(1):37-42.

[21] Grzybowski A, Sak J. Edmund Biernacki (1866-1911): Discoverer of the erythrocyte sedimentation rate. On the 100th anniversary of his death. *Clin Dermatol*. 2011;29(6):697-703.

[22] Grzybowski A, Sak JJ. Who discovered the erythrocyte sedimentation rate? *J Rheumatol*. 2011;38(7):1521-1522.

[23] Haik Y, Pai V, Chen CJ. *Biomagnetic Fluid Dynamics at Interfaces*. Cambridge University Press, Cambridge, 1999.

[24] Harris EJ, Burn GP. The transfer of sodium and potassium ions between muscle and the surrounding medium. *Trans Faraday Soc*. 1949;45:508-528.

[25] Hilfer R. *Applications of Fractional Calculus in Physics*. World Scientific Publishing Company, London, 2000.

[26] Hrabe J, Hrabětová S, Segeth K. A model of effective diffusion and tortuosity in the extracellular space of the brain. *Biophys J.* 2004;87(3):1606-1617.

[27] Jack JJB, Noble D, Tsien RW. *Electric Current Flow in Excitable Cells.* Clarendon Press, Oxford, UK, 1975.

[28] Jaeger JC. *Diffusion from Constrictions. In Studies in Physiology: Presented to John C. Eccles.* Springer Berlin, Heidelberg, Germany, 1965.

[29] Jain M, Sharma GC, Singh R. Diffusion-reaction model for mass transportation in brain tissues. *Jnanabha.* 2008;38:77-84.

[30] Jain M, Sharma GC, Singh A. Mathematical analysis of MHD flow of blood in very narrow capillaries. *Int J Eng Tran B.* 2009;(22):307-315.

[31] Kangle H, van Genuchten MT, Renduo Z. Exact solutions for one-dimensional transport with asymptotic scale-dependent dispersion. *Appl Math Model.* 1996;20(4):298-308.

[32] Keynes RD. The ionic fluxes in frog muscle. *Proc R Soc Lond B Biol Sci.* 1954;142(908):359-382.

[33] Khanafer K, Vafai K, Kangarlu A. Computational modeling of cerebral diffusion-application to Stroke imaging. *Magn Reson Imaging.* 2003;21(6):651-661.

[34] Kilbas AA, Srivastava HM, Trujillo, JJ. *Theory and Applications of Fractional Differential Equations.* North-Holland Mathematics Series, Elsevier Inc, 2006.

[35] Kucharz EJ. The forgotten contribution of Dr. Edmund Faustyn Biernacki (1866-1911) to the discovery of the erythrocyte sedimentation rate. *J Lab Clin Med.* 1988;112(2):279-80.

[36] Kucharz E. Edmund Biernacki and the erythrocyte sedimentation rate. *Lancet.* 1987;329(8534):696.

[37] Kushner I. The acute phase response: An overview. *Meth Enzymol.* 1988;163:373-383.

[38] Lehner FK. On the validity of Fick's law for transient diffusion through a porous medium. *Chem Engng Sci.* 1979;34(6):821-825.

[39] Lux HD, Neher E. The equilibration time course of $[K+]_0$ in cat cortex. *Exp Brain Res.* 1973;17:190-205.

[40] Mainardi F, Carpinteri A. *Fractals and Fractional Calculus in Continuum Mechanics*. Springer, 1997.

[41] Mainardi F, Pagnini G. The Wright functions as solutions of the time-fractional diffusion equation. *Appl Math Comput*. 2003;141(1):51-62.

[42] Meidani AN, Hasan M. Mathematical and physical modelling of bubble growth due to ultrasound. *Appl Math Model*. 2004;28(4):333-351.

[43] Miller KS, Ross B. *An Introduction to the Fractional Calculus and Fractional Differential Equations*. Willey, New York, 1993.

[44] Nicholson C, Phillips JM. Ion difusion modifed by tortuosity and volume fraction in the extracellular micro-environment of the rat cerebellum. *J Physiol*. 1981;321:225-57.

[45] Nicholson C. Difusion and related transport mechanisms in brain tissue. *Rep Prog Phys*. 2001;64(7):815-84.

[46] Norman RS. Diffusional spread of iontophoretically injected ions. *J Theor Biol*. 1975;52(1):159-162.

[47] Oldham K, Spanier J. *The Fractional Calculus Theory and Applications of Differentiation and Integration to Arbitrary Order*. Elsevier, Amsterdam, 1974.

[48] Podlubny I. *Fractional Differential Equations, Mathematics in Science and Engineering*. Academic Press, San Diego, USA, 1999.

[49] Puri AN, Kuo CY, Chapman RS. Turbulent diffusion of mass in circular pipe flow. *Appl Math Model*. 1983;7(2):135-138.

[50] Purves RD. The time course of cellular responses to iontophoretically applied drugs. *J Theor Biol*. 1977;65(2):327-344.

[51] Ray L, Iliff JJ, Heys JJ. Analysis of convective and diffusive transport in the brain interstitium. *Fluids Barriers CNS*. 2019;16(1):1-18.

[52] Samko SG, Kilbas AA, Marichev OI. *Fractional Integrals and Derivatives: Theory and Applications*. Gordon and Breach Science Publisher, Amsterdam, 1993.

[53] Schirmer WN, Lisboa HD, Moreira R, Rosolen JM. Modeling volatile organic compounds (voc's) adsorption onto cupstacked carbon nanotubes (cscnt) using the linear driving force model. *Acta Sci Technol*. 2010;32(2):159-166.

[54] Shah NA, Vieru D, Fetecau C. Effects of the fractional order and magnetic field on the blood flow in cylindrical domains. *J Magn Magn Mater*. 2016;409:10-19.

[55] Sharan M, Popel AS. A compartmental model for oxygen transport in brain microcirculation in the presence of blood substitutes. *J Theor Biol*. 2002;216(4):479-500.

[56] Sharma GC, Jain M, Saral RN. A mathematical model for concentration of blood affecting erythrocyte sedimentation. *Comput Biol Med*. 1996;26(1):1-7.

[57] Sharma GC, Jain M. A computational solution of mathematical model for oxygen transport in peripheral nerve. *Comput Biol Med*. 2004;34(7):633-645.

[58] Sharma S, Singh U, Katiyar VK. Magnetic field effect on flow parameters of blood along with magnetic particles in a cylindrical tube. *J Magn Magn Mater*. 2015;377:395-401.

[59] Singh R, Sharma GC, Jain M. Mathematical modeling of blood flow in a stenosed artery under MHD effect through porous medium. *Int J Eng*. 2010;23(3):243-252.

[60] Somjen GG. Extracellular potassium in the mammalian central nervous system. *Annu Rev Physiol*. 1979;41(1):159-177.

[61] Tannenbaum AR, Georgiou T, Deasy J, Norton L. Control and the analysis of cancer growth models. *Interpolation and Realization Theory with Applications to Control Theory: In Honor of Joe Ball*. 2019;343-353.

[62] Trubatch J, Van Harreveld A. Spread of iontophoretically injected ions in a tissue. *J Theor Biol*. 1972;36(2):355-366.

[63] Varshney G, Katiyar V, Kumar S. Effect of magnetic field on the blood flow in artery having multiple stenosis: a numerical study. *Int J Eng Sci Technol*. 2010;2(2):967-82.

[64] Westergren AL. Studies of the suspension stability of the blood. *Acta Medica Scandinavica*. 1921;54:247.

[65] Westergren A. The technique of the red cell sedimentation reaction. *Am Rev Tuberc*. 1926;14(1):94-101.

[66] Whitaker S. Advances in theory of fluid motion in porous media. *Ind Eng Chem*. 1969;61(12):14-28.

[67] Zubik-Kowal B. An algorithm for partial functional differential equations modeling tumor growth. *Appl Math Comput*. 2018;321:85-92.

List of Publications

Journal articles: Published/Accepted

- Abhijit Shit, Swaroop Nandan Bora (2022), ESR fractional model with non-zero uniform average blood velocity. **Computational and Applied Mathematics**, 41 (8):354, 1-15, DOI:10.1007/s40314-022-02072-1
- Abhijit Shit, Swaroop Nandan Bora (2024), Incorporation of concentration gradient of blood nutrients in Erythrocyte Sedimentation Rate fractional model with non-zero uniform average blood velocity. **Mathematical Methods in the Applied Sciences**, 47(12):10334-10350, DOI:10.1002/mma.10125
- Abhijit Shit, Swaroop Nandan Bora (2024), Fractional model for blood flow in a stenosed artery under MHD effect through a porous medium. (**Accepted** in **International Journal of Applied Mechanics**), DOI:10.1142/S1758825124501011
- Abhijit Shit, Swaroop Nandan Bora (2024), Mass transport in brain cells: integer-order and fractional-order modelling. (**Accepted** in **Physica Scripta** on November 25, 2024), DOI:10.1088/1402-4896/ad97ee

Journal article: Communicated

- Abhijit Shit, Swaroop Nandan Bora, Fractional model for ion diffusion in the extracellular microenvironment of the rat cerebellum. (Under Review)